

OFF-GAS ANALYSIS FOR CONTROLLING SEQUENTIALLY OPERATED WASTEWATER TREATMENT PROCESSES

Lies Vervaeet

Student number: 01905921

Promotor: prof. dr. ir. Eveline Volcke

Tutor: dr. ir. Laurence Strubbe & dr. Paula Carrera Fernández

Master's Dissertation submitted to Ghent University in partial fulfilment of the requirements for the degree of master of Bioscience Engineering: Environmental Technology.

Academic year: 2023 - 2024

De auteur en promotor geven de toelating deze scriptie voor consultatie beschikbaar te stellen en delen ervan te kopiëren voor persoonlijk gebruik. Elk ander gebruik valt onder de beperkingen van het auteursrecht, in het bijzonder met betrekking tot de verplichting uitdrukkelijk de bron te vermelden bij het aanhalen van resultaten uit deze scriptie.

The author and promoter give the permission to use this thesis for consultation and to copy parts of it for personal use. Every other use is subject to the copyright laws, more specifically the source must be extensively specified when using results from this thesis.

Gent, May 31, 2024

The author,

The promotor,

Lies Vervaet

prof. dr. ir. Eveline Volcke

The tutors,

dr. ir. Laurence Strubbe

dr. Paula Carrera Fernández

ACKNOWLEDGMENTS

First, I would like to express my gratitude to my promotor, Professor Eveline Volcke. Your passion for wastewater treatment has intensified my interest and inspired me to explore the possibilities within this field further. Your insightful feedback during our progress meetings and your questions have elevated my work to a higher level, encouraging me to delve deeper. Thank you for your support and guidance.

I am also thankful to my tutor, Laurence Strubbe, for the support and feedback throughout my thesis. Despite the distance from Switzerland, your willingness to stay involved and provide quick responses to my questions was very appreciated.

A thank you goes to my other tutor, Paula Carrera Fernández, for our conversations during the second semester. These discussions challenged me to rethink parts of my research, leading to interesting insights.

To Emile, my boyfriend, thank you for being my bright source of positivity and for your support and understanding during this hectic year.

Finally, I would like to dedicate this thesis to my parents. Papa, thank you for being my rock these past five years. I truly do not know where I would be today without your constant support and encouragement. Mama, no words can describe how much I wish you were still with me to give me your thoughtful advice that always helped to reassure me. This thesis is written with you close in my heart and memory. Dit is voor jullie.

CONTENTS

Contents	iv
Abstract	v
Samenvatting	vii
Introduction	xiii
1 Literature review	1
1.1 Biological wastewater treatment systems	1
1.1.1 A brief history	1
1.1.2 Bioconversions	2
1.1.3 Continuous wastewater treatment systems	3
1.1.3.1 Operation	3
1.1.3.2 Continuous reactor configurations	3
1.1.3.3 Process control	4
1.1.4 Sequencing batch reactors	5
1.1.4.1 Operation	5
1.1.4.2 Process control	7
1.1.4.3 Full-scale application	12
1.1.5 Aerobic granular sludge	13
1.2 Gas-liquid mass transfer	15
1.2.1 General principles and physical background	15
1.2.2 Oxygen mass transfer	18
1.2.2.1 Aeration system characteristics	18
1.2.2.2 Oxygen uptake rate	20
1.2.3 Carbon dioxide mass transfer	21
1.3 Applications of off-gas analysis	25
1.3.1 Off-gas analysis: advantages and challenges	25
1.3.2 Monitoring of aeration characteristics	26
1.3.3 Monitoring of greenhouse gas emissions	27
1.3.4 Monitoring of influent composition and reactor conversions	27
1.3.5 Potential of process control with off-gas analysis	27
1.4 Conclusions literature review	29
1.5 Thesis objectives	30
2 Materials and Methods	31
2.1 System under study	31
2.1.1 Influent composition	31
2.1.2 Sequencing batch reactor cycle	31
2.2 Model description	33
2.3 Research outline	33
2.3.1 Reference case: model validation and process performance	33
2.3.2 Detecting the end of nitrification: strategy validation	33
2.3.3 Closed loop analysis	34
2.3.4 Influence of influent characteristics on detection strategy robustness	35
2.3.4.1 Constant influent conditions	35
2.3.4.2 Dynamic influent conditions	35
2.3.5 Detecting the end of denitrification: strategy development	36

3	Results and discussion	37
3.1	Reference case: model validation and process performance	37
3.2	Detecting the end of nitrification: strategy validation	40
3.3	Closed loop analysis	45
3.3.1	Closed loop implementation and strategy adaptation	45
3.3.2	Open loop versus closed loop: benefits	49
3.4	Influence of influent characteristics on detection strategy robustness	50
3.4.1	Constant influent conditions	50
3.4.2	Dynamic influent conditions	55
3.5	Detecting the end of denitrification: strategy development	57
4	Conclusions and perspectives	61
	Bibliography	65
	Appendix A Influent composition	77
	Appendix B Model description	79
	Appendix C Results and discussion: extra figures	89

ABSTRACT

The wastewater treatment sector continuously aims to minimize operating costs by optimizing treatment time and reducing energy consumption. Efficient control of the treatment processes is an important factor in achieving this objective.

This thesis delves into the control of a sequencing batch reactor (SBR) for biological wastewater treatment. Typically, SBR operation is controlled through liquid-phase measurements of pollutants such as ammonium and phosphate, or indirect parameters such as pH and dissolved oxygen. However, literature suggests that analysing compounds in the off-gas (e.g. oxygen and carbon dioxide) could also provide insights into biological processes in the reactor. Consequently, off-gas analysis emerges as a potential complement to or substitute for liquid-phase measurements for efficient control of SBRs.

In this context, this thesis explored the potential of off-gas analysis for process control in an SBR. The control of both the aerobic and the anoxic phase was assessed through modelling and simulation in Matlab/Simulink. A strategy to detect the end of nitrification based on the analysis of the oxygen and carbon dioxide off-gas concentrations was validated and adapted. The detection strategy was then applied to actually control the aerobic phase length following nitrification endpoint detection. This resulted in reductions in the aerobic phase length and thus energy savings in the treatment of municipal wastewater with a constant composition. However, the strategy did not show fully robust when testing a wider range of influent compositions and a dynamic influent. Further research is required in order to adapt the detection strategy to cope with variable conditions.

Furthermore, a detection strategy was developed to identify the end of denitrification in the anoxic phase. Relative changes in carbon dioxide and nitrogen off-gas concentrations could be linked to the end of denitrification, marking a first step in developing a strategy to control the length of the anoxic phase.

Overall, this thesis demonstrated the potential of off-gas analysis for controlling sequentially operated processes in the aerobic and anoxic phase. The study yielded valuable insights and revealed options and bottlenecks for the practical implementation of off-gas analysis for biological wastewater treatment control.

SAMENVATTING

De waterzuiveringssector streeft steeds naar minimale operationele kosten door de behandelings-tijd van het afvalwater te optimaliseren en het energieverbruik te verminderen. Efficiënte controle van de zuiveringsprocessen is een belangrijke factor om dit doel te bereiken.

Deze thesis focust op de controle van sequential batch reactoren (SBR), een mogelijke configuratie om afvalwater biologisch te behandelen. Processen in een SBR worden vaak gecontroleerd door het monitoren van verontreinigingen (bv. fosfaat of ammonium) of indirecte parameters (bv. pH of opgeloste zuurstof) in de vloeistoffase. Literatuur toont echter aan dat concentraties in de off-gas (gasstroom die de reactor verlaat) gelinkt kunnen worden aan biologische processen in de vloeistoffase. Hierdoor zou analyse van de off-gas fase aangewend kunnen worden om biologische processen te controleren, dit als aanvulling of ter vervanging van metingen in de vloeistoffase.

In deze thesis werd het potentieel van off-gas analyse om processen in een SBR te controleren onderzocht. De controle van zowel de aerobe als anoxische fase werd onderzocht aan de hand van modellering in Matlab/Simulink. Een detectiestrategie gebaseerd op de meting van zuurstof en koolstofdioxide concentraties in de off-gas werd gevalideerd en aangepast om het einde van nitrificatie te detecteren. Vervolgens werd deze detectiestrategie toegepast om de lengte van de aerobe fase te sturen door deze te beëindigen bij het detecteren van het einde van nitrificatie. De tijdsduur van de aerobe fase werd zo sterk gereduceerd wat resulteerde in verminderde energieconsumptie bij de behandeling van huishoudelijk afvalwater met een constante samenstelling. Echter, de detectiestrategie was niet volledig robuust voor een reeks van verschillende constante influentsamenstellingen en een dynamische influent. Dit gaf aan dat verder onderzoek noodzakelijk is om de strategie aan te passen aan meer variabele omstandigheden.

Verder werd een detectiestrategie ontwikkeld om het einde van denitrificatie in de anoxische fase te identificeren. Veranderingen in de koolstofdioxide en stikstof off-gas concentraties werden gekoppeld aan het einde van het denitrificatieproces. Zo werd een eerste stap gezet in de ontwikkeling van een strategie om de lengte van de anoxische fase te controleren.

Deze thesis toonde het potentieel van off-gas analyse aan om processen in de aerobe en anoxische fase van een SBR te controleren. Het onderzoek leverde waardevolle inzichten op en suggereerde ook verdere onderzoeksmogelijkheden om off-gas analyse in de praktijk te implementeren in de toekomst.

SYMBOLS

a	transfer area per volume of liquid [$\text{m}^2 \cdot \text{m}^{-3}$]
A	area [m^2]
C_{AG}	concentration in the gas bulk phase [$\text{g} \cdot \text{m}^{-3}$]
C_{AGi}	gas concentration in the gas-liquid interface [$\text{g} \cdot \text{m}^{-3}$]
C_{AL}	concentration in the liquid bulk phase [$\text{g} \cdot \text{m}^{-3}$]
C_{ALi}	liquid concentration in the gas-liquid interface [$\text{g} \cdot \text{m}^{-3}$]
C_{AL}^*	saturation concentration in the bulk liquid phase [$\text{g} \cdot \text{m}^{-3}$]
C_i	concentration of compound i [$\text{g} \cdot \text{m}^{-3}$]
C_i^*	saturation concentration of compound i [$\text{g} \cdot \text{m}^{-3}$]
D_i	diffusivity of compound i [$\text{m}^2 \cdot \text{s}^{-1}$]
F	fouling factor [–]
H_i	Henry's law constant for compound i [$(\text{g} \cdot \text{m}^{-3}\text{-gas}/\text{g} \cdot \text{m}^{-3}\text{-liquid})$]
k_G	gas-phase mass transfer coefficient [$\text{m} \cdot \text{h}^{-1}$]
k_L	liquid-phase mass transfer coefficient [$\text{m} \cdot \text{h}^{-1}$]
K_L	overall liquid-phase mass transfer coefficient [$\text{m} \cdot \text{h}^{-1}$]
$k_L a_i$	volumetric mass transfer coefficient of compound i [h^{-1}]
K	equilibrium constant [$\text{mol} \cdot \text{m}^{-3}$]
M_i	molecular weight of compound i [$\text{g} \cdot \text{mol}^{-1}$]
P	power [kW]
p_{atm}^G	atmospheric pressure [Pa]
$q_{A,G}$	rate of mass transfer through the gas phase [$\text{g} \cdot \text{m}^{-3} \cdot \text{h}^{-1}$]
$q_{A,L}$	rate of mass transfer through the liquid phase [$\text{g} \cdot \text{m}^{-3} \cdot \text{h}^{-1}$]
q_A	overall liquid-gas mass transfer rate [$\text{g} \cdot \text{m}^{-3} \cdot \text{h}^{-1}$]
Q	volume flow rate [$\text{m}^3 \cdot \text{h}^{-1}$]

T	temperature [°C]
V	volume [m ³]
W	mass flow rate [g.h ⁻¹]
x_i	molar fraction of compound i [-]
α	alpha factor [-]

ABBREVIATIONS

AE	aeration efficiency
AEN	aeration energy
AGS	aerobic granular sludge
AOB	ammonium oxidizing bacteria
COD	chemical oxygen demand
CPR	carbon dioxide production rate
CSTR	continuous stirred tank reactor
CTR	carbon dioxide transfer rate
DO	dissolved oxygen
NOB	nitrite oxidizing bacteria
OHO	ordinary heterotrophic organisms
ORP	oxidation reduction potential
OTE	oxygen transfer efficiency
OTR	oxygen transfer rate
OUR	oxygen uptake rate
PAO	phosphate accumulating organisms
PHA	polyhydroxylalkanoate
PP	polyphosphate
SBR	sequencing batch reactor
sOTR	standard oxygen transfer rate
SRT	sludge retention time
VFA	volatile fatty acids
VER	volume exchange ratio

INTRODUCTION

Wastewater treatment plays a critical role in safeguarding aquatic ecosystems against eutrophication and harmful compounds, and protecting human health. Achieving this requires compliance with stringent effluent criteria through a combination of treatment methods including biological, physical and chemical processes.

In a biological treatment process, microorganisms degrade pollutants in the influent, converting them into compounds safe for release into the environment. The most common biological process is the activated sludge process, predominantly operated within continuous flow reactors or sequencing batch reactors (SBRs). Maintaining optimal conditions (aerobic/ anoxic/ anaerobic) for the biomass is crucial for efficient pollutant removal. Moreover, minimizing operational costs by optimizing treatment duration and energy usage is important, particularly during aerobic processes. Aeration energy constitutes a significant part of the overall energy consumption during treatment, making up 45 to 75 % of the total energy costs (Rosso et al., 2008).

These requirements can be met by efficient control of the treatment plant. Control involves continuous assessment of some system parameters (e.g. ammonium concentration, pH) to evaluate system performance and to adjust the process if necessary, such as by changing the aeration rate. Nowadays, such measurements mostly occur in the liquid phase. These liquid measurement sensors demand frequent maintenance due to their exposure to liquid-phase pollutants. This maintenance is crucial to have accurate measurements, given the substantial effect of efficient control on operation and costs.

A possible alternative for liquid-phase measurements is monitoring the off-gas flow from wastewater treatment plants. This is the gas flow that leaves the reactor, primarily consisting of the remaining aeration flow supplied during the aerobic phases. Literature suggests that analysing oxygen and carbon dioxide concentrations in the off-gas stream could provide insights into biological processes occurring in the liquid phase (Hellinga et al., 1996; Leu et al., 2010; Baeten et al., 2021). As off-gas measurement technology will become more prevalent in the coming years to monitor greenhouse gasses, incorporating additional measurements of oxygen and carbon dioxide concentrations would only be a limited extra investment.

This thesis explores the potential of off-gas measurements as a complement to or a substitute for liquid-phase measurements to monitor and control biological wastewater treatment processes in an SBR. More specifically, it is investigated whether variations in the oxygen and carbon dioxide off-gas profiles can be linked to the end of nitrification in aerobic phases and the end of denitrification in anoxic phases. Throughout the study, emphasis will be mostly placed on detecting the end of nitrification, which would allow to define the end of aeration accurately, thereby minimizing unnecessary aeration energy losses.

The thesis starts with a literature review in Chapter 1. First, the characteristics of biological wastewater treatment in continuous flow reactors and SBRs are discussed, followed by an overview of off-gas analysis fundamentals and applications in wastewater treatment. Chapter 2 explains the model setup for simulating SBR operation together with the off-gas flow. Additionally, the different steps in this thesis to assess the feasibility of off-gas analysis for control purposes are outlined. Chapter 3 presents the results together with a thorough discussion. Finally, Chapter 4 provides conclusions and recommendations for further research.

1. LITERATURE REVIEW

In this chapter, biological wastewater treatment systems and the application of gas-liquid mass transfer principles during this treatment are discussed. The operation and process control of both continuous systems and sequencing batch reactors are studied in Section 1.1. Section 1.2 introduces the fundamental principles of gas-liquid mass transfer, with a detailed discussion on oxygen and carbon dioxide mass transfer. The applications of off-gas analysis are addressed in Section 1.3. Section 1.4 concludes this literature review and Section 1.5 defines the objectives for this thesis.

1.1 Biological wastewater treatment systems

1.1.1 A brief history

Effective wastewater treatment is important for safeguarding public health and preserving an optimal environment. Already in ancient Roman times, there was a recognition of the health risks and nuisance associated with wastewater, leading to the development of an extensive sewer network across the Empire (Chen et al., 2020). However, in most historical periods, wastewater was not dealt with. It took until the 19th century, when large cities began to emerge due to the Industrial Revolution, that sewage systems were gradually implemented in response to pressing hygiene issues and disease outbreaks (Nathanson and Ambulkar, 2023). Initially, wastewater was only collected and discharged in nearby water bodies. Given the high levels of pollution in this untreated wastewater, research into wastewater treatment methods also started toward the end of the 19th century (Lofrano and Brown, 2010).

Numerous treatment methods were developed and tested. Anaerobic systems, such as septic tanks, gained popularity in the late 19th century and early 20th century (Lofrano and Brown, 2010). However, their efficiency was limited. The first research into aeration in order to enhance treatment commenced in 1882. It was hypothesized that oxygen might mitigate odours associated with anaerobic conditions (Alleman and Prakasam, 1983). In the initial years, aeration did not yield substantial improvements. It was only when Ardern and Lockett, two students in Manchester, retained the flocculant solids in the tank for a longer duration rather than discarding them after 1 cycle, that higher efficiencies were obtained (Alleman and Prakasam, 1983). This marked the beginning of the well-known activated sludge process.

Ardern and Lockett's experiments were conducted using a fill-and-draw approach, which is still applied in SBRs (Orhon, 2015). However, as treatment facilities grew in size following the discovery of the activated sludge process, there was a rapid shift toward continuous operation.

In the beginning of the 20th century, knowledge and tools for process control were limited, and batch-wise operation required significant operator attention involving for example valve switching and precise timing. Hence, continuous operation was preferred. Consequently, all large municipal treatment plants were constructed in a continuous configuration at that time (Irvine et al., 1983).

In the subsequent years, continuous treatment methods were further developed, while batch-wise operations were somewhat forgotten. It was during the 1970s that environmental concerns gained attention, leading governments to formulate policies (Kurrer and Lipcaneanu, 2023). These stricter effluent regulations placed pressure on both industries and researchers to enhance continuous processes or explore alternative treatment techniques. Consequently, the traditional fill-and-draw systems were looked into again. Irvine and Busch (1979) stated that batch-wise operation was now a viable alternative due to the availability of improved process control technologies such as motorized valves, electronic timers, sensors etc. The periodic operation of sequencing batch reactors offered several advantages over the conventional activated sludge process, as will be explained in Section 1.1.4.3. In the following decades, research increasingly focused on batch-wise operated treatment, and nowadays, this treatment technique is frequently employed in industrial applications such as the pharmaceutical, chemical and textile sector (Rania and Singha, 2020), as well as in municipal treatment plants.

1.1.2 Bioconversions

During biological wastewater treatment, pollutant removal is performed by microorganisms. These mostly exist as activated sludge flocs, which is the most conventional form in wastewater treatment. These microorganisms are specialized in the removal of organic matter (expressed in chemical oxygen demand (COD)), nitrogen or phosphorus. A summary of the biological reactions is given in Table 1.1. It has to be noted this is a schematic overview, the stoichiometry is thus not correct.

Organic matter is degraded both in the aerobic and anoxic phase, with O_2 or NO_3^- as electron acceptor, respectively. In the influent, nitrogen primarily exists in the form of ammonium, which undergoes a transformation into nitrate during the aerobic phase through the process of nitrification. In the subsequent anoxic phase, the nitrate is converted into nitrogen gas (N_2). Phosphorus is removed by the phosphate-storing PAO. During the anaerobic phase, phosphate is released due to the breakdown of intracellular polyphosphate (PP). The energy released during this breakdown is used for storing volatile fatty acids (VFAs) in the form of intracellular polyhydroxylalkanoates (PHAs). In the subsequent aerobic and anoxic phases, these PHAs serve as an energy source for growth and the resupply of PP. As growth occurs, more PP becomes necessary, leading to the uptake of more phosphate than what was initially released in the anaerobic phase. By wasting part of the PAO biomass, phosphate removal is facilitated from the reactor (Mino et al., 1998).

1. Literature review

Table 1.1: Overview of reactions during biological treatment under aerobic, anoxic and anaerobic conditions. The groups of microorganisms responsible for the reaction are given in the last column: ordinary heterotrophic organisms (OHO), ammonium oxidizing bacteria (AOB), nitrite oxidizing bacteria (NOB) and phosphate accumulating organisms (PAO) (Metcalf & Eddy et al., 2014; Lopez-Vazquez et al., 2020a; Yuan et al., 2012). Abbreviations: polyhydroxylalkanoate (PHA), polyphosphate (PP) and volatile fatty acids (VFA).

Aerobic		
<i>Function</i>	<i>Reaction</i>	<i>Group</i>
Organic matter removal	$\text{COD} + \text{O}_2 + \text{nutrients} \longrightarrow \text{CO}_2 + \text{biomass} + \text{other end products}$	OHO
Nitrification	$\text{NH}_4^+ + \text{O}_2 + \text{CO}_2 \longrightarrow \text{NO}_3^- + \text{H}^+ + \text{H}_2\text{O} + \text{biomass}$	AOB & NOB
Phosphate uptake	$\text{PO}_4^{3-} + \text{O}_2 + \text{PHA}_{\text{intracellular}} \longrightarrow \text{PP}_{\text{intracellular}} + \text{biomass}$	PAO
Anoxic		
<i>Function</i>	<i>Reaction</i>	<i>Group</i>
Denitrification	$\text{NO}_3^- + \text{COD} \longrightarrow \text{N}_2 + \text{CO}_2 + \text{H}_2\text{O} + \text{biomass}$	OHO
Phosphate uptake & denitrification	$\text{PO}_4^{3-} + \text{NO}_3^- + \text{PHA}_{\text{intracellular}} \longrightarrow \text{PP}_{\text{intracellular}} + \text{biomass}$	PAO
Anaerobic		
<i>Function</i>	<i>Reaction</i>	<i>Group</i>
Phosphate release	$\text{VFA}_{\text{bulk liquid}} + \text{PP}_{\text{intracellular}} \longrightarrow \text{PO}_4^{3-}_{\text{bulk liquid}} + \text{PHA}_{\text{intracellular}}$	PAO

1.1.3 Continuous wastewater treatment systems

1.1.3.1 Operation

A continuous flow reactor is characterized by a continuous flow of influent and effluent respectively in and out of the system while maintaining a constant volume (Bukhtiyarova et al., 2023). The continuous flow within the reactor can be classified by different hydraulic regimes: the continuous stirred tank reactor (CSTR), the plug flow reactor or the dispersed flow reactor (Von Sperling, 2002). In a CSTR, it is assumed that the contents of the tank are perfectly mixed, so the effluent concentrations are the same as those inside the tank. This differs in a plug flow reactor, where the flow is segmented into 'plugs', each with its own concentration. Within each plug there is internal mixing, but not between different plugs, causing concentrations in a plug flow reactor to vary depending on their position in the reactor (Mettler Toledo, sd). While a CSTR and plug flow reactor represent idealized cases of the hydraulic regime, a disperse flow model is a more generic representation that aligns better with reality. However, when characterizing a continuous flow reactor, designers prefer the idealized regimes as they simplify calculations.

1.1.3.2 Continuous reactor configurations

The necessary environmental conditions for the biological reactions are created by the use of a series of tanks (Grady Jr et al., 2011). Various configurations can occur, depending on the specific nutrient removal requirements. These configurations involve different sequences of anaerobic,

anoxic and aerobic conditions, as well as diverse recycling strategies. Three main configurations are given below:

- **MLE (modified Ludzak-Ettinger)** - This configuration is applied when only nitrogen has to be removed. It includes one anoxic tank and one aerobic tank; with a recirculation flow from the aerobic to the anoxic tank to ensure effective removal of nitrate formed in the aerobic tank (Ekama and Wentzel, 2020; Grady Jr et al., 2011).
- **Phoredox (A/O)** - This configuration is applied when only phosphorus has to be removed. An anaerobic tank is followed by an aerobic tank (Lopez-Vazquez et al., 2020a).
- **Anaerobic/anoxic/oxic (A²/O)** - This configuration is applied when both nitrogen and phosphorus have to be removed. It involves a sequence of an anaerobic, anoxic and aerobic tank, with a recirculation flow from the aerobic to the anoxic tank for nitrate removal. The lay-out of the A²/O configuration can be seen in Figure 1.1 (Lopez-Vazquez et al., 2020a).

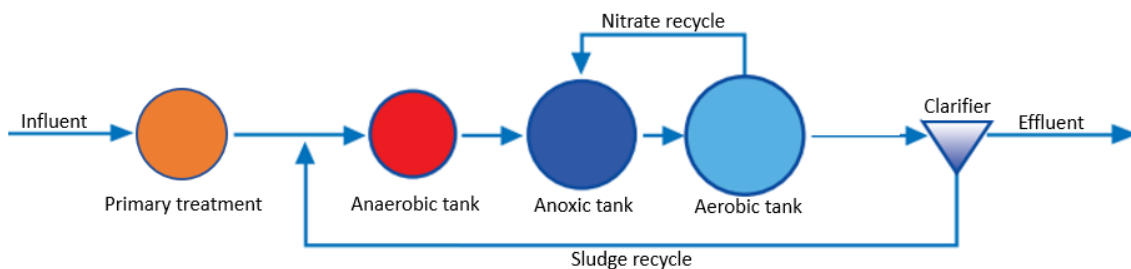


Figure 1.1: Continuous flow configuration for COD removal, nitrification/denitrification and enhanced phosphorus removal (A²/O) - adapted from Lopez-Vazquez et al. (2020a).

Before the influent enters the tanks, it passes often through a primary settler where part of the particulate COD is removed. This lowers the energy demand for subsequent organic matter removal. However, attention has to be paid that sufficient COD is still present for the denitrification process (Patziger et al., 2016). Before discharge of the effluent, there is also a secondary settler to allow the suspended activated sludge to settle and to clarify the stream. The settled sludge is partially recycled back into the reactor (in the anaerobic or anoxic tank (Grady Jr et al., 2011)) to maintain the biomass quantity in the system, while the other part is wasted. This wastage should be accurately controlled to preserve a good substrate to microorganism ratio in the tanks (Pitman, 1991; Ma et al., 2006).

1.1.3.3 Process control

In order to effectively manage variations in influent composition and quantity while maintaining a high-quality effluent, several control strategies are typically implemented. One of the most commonly applied control strategies is for maintaining the level of dissolved oxygen by aeration. An optimal dissolved oxygen (DO) level is essential for the activity of microorganisms in the aerobic tank. However, since aeration consumes a significant amount of energy, the DO level

should not be higher than required. Therefore aeration control can be applied by a predetermined setpoint of the DO or an adjusting setpoint based on a continuous measurement of the ammonium load in the aerobic tank (Vilanova et al., 2011; Newhart et al., 2020).

The degree of denitrification in the anoxic tank can be controlled by the internal recirculation flow of nitrate or external COD addition (Vilanova et al., 2011). The degree of nitrate recirculation can be determined based on nitrate measurements at the outlet of the anoxic zone and a specified setpoint. A limiting factor of denitrification can be the absence of biodegradable COD, therefore external COD can be added if nitrate measurements exceed the desired levels (Yuan et al., 2002).

1.1.4 Sequencing batch reactors

1.1.4.1 Operation

The sequencing batch reactor (SBR) is a fill-and-draw biological system employed in wastewater treatment. In this system, wastewater is introduced into a single reactor, where all reactions (aerobic, anoxic and anaerobic) as well as settling, occur during a certain time period (Morgenroth and Wilderer, 1998). To be able to process wastewater in a continuous way, two or more reactors can be used in parallel (Shammas and Wang, 2009). All reactions are similar to continuous flow treatment as described in Section 1.1.2, except they occur sequentially over time rather than space.

A time cycle of the SBR is typically divided in 5 phases: fill, reaction, settling, draw and idle (Figure 1.2) (Arora et al., 1985). Figure 1.2 makes a distinction between sludge wastage and the drawing of treated water during the draw phase. The duration of all phases can either be fixed or adjusted according to varying loading conditions or effluent requirements.

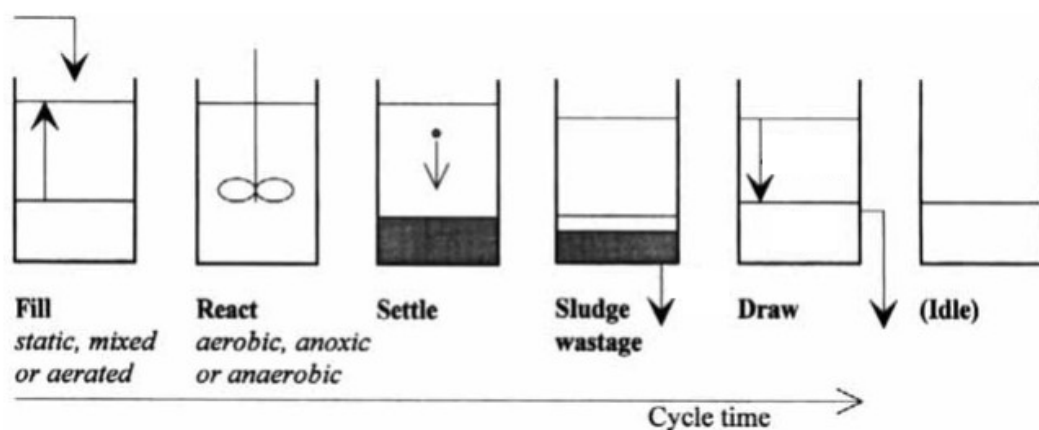


Figure 1.2: Phases in an SBR cycle - adapted from Morgenroth and Wilderer (1998)

Fill phase

In the fill phase, raw wastewater is introduced into the reactor, usually alongside a volume of water and biomass remaining from the previous cycle. There are three methods of filling (Dutta and Sarkar, 2015):

- **Static fill:** influent wastewater is fed without mixing or aeration. It creates a high food-to-microorganism ratio, promoting the growth of PAO.
- **Mixed fill:** influent wastewater is mixed with the remaining biomass, without aeration. This creates anoxic conditions suitable for denitrification of nitrate in the residual water from the previous cycle.
- **Aerated fill:** influent wastewater is mixed with the remaining biomass and aeration is applied. This stimulates nitrification and COD removal, aerobic biological reactions.

Reaction phase

The reaction phase is an extension of the fill phase, where the biochemical conversions initiated during filling are completed. The specific reactions are controlled by aeration, creating anaerobic, anoxic or aerobic conditions (Alattabi et al., 2017). Turning aeration on and off, provides the appropriate conditions for nitrification, denitrification and phosphorus removal (Singh and Srivastava, 2011).

Originally, the approach for efficient nitrogen, phosphate and COD removal involves a single cycle of an anaerobic phase, followed by an aerobic phase and ended with an anoxic phase (Freitas et al., 2009; Liu et al., 2020). However, challenges arise when dealing with high influent nitrogen concentrations (i.e. low COD/N), which demand a large amount of organic matter during denitrification. Often, the rapidly biodegradable COD is depleted during the anaerobic and aerobic phases, resulting in a shortage of COD in the anoxic phase and, consequently, high nitrate concentrations in the effluent (Puig et al., 2004). External COD addition during the anoxic phase is a potential solution for this issue, although it comes with a significant operational cost. Therefore, an alternative sequence is frequently used: after the anaerobic phase, the aerobic and anoxic phases are alternated with additional feeding during the anoxic phase (Lin and Jing, 2001). During this additional feeding, the carbon sources needed for denitrification of nitrate formed in the aerobic period, are provided in the following anoxic period (Guo et al., 2007).

Settling phase

In the settling phase sludge is allowed to settle for a predefined period (Artan et al., 2001). This quiescent settling yields better effluent quality compared to continuous treatment, where settling is hindered by a continuous in- and outflow (Dutta and Sarkar, 2015).

Draw phase

During the draw phase, the clear supernatant in the tank is discharged. Not all clarified effluent is drawn, some remains in the reactor for the next cycle to convert the remaining nitrate during denitrification (Shammas and Wang, 2009). The percentage of drawn effluent to the total effluent volume in the reactor is defined as the volume exchange ratio (VER). Additionally, excess sludge is removed during this phase (Singh and Srivastava, 2011).

Idle phase

The idle phase is defined as the period between the ending of the draw phase and the beginning of the fill phase of the next cycle (Morgenroth and Wilderer, 1998). This time period is necessary, either when wastewater is not readily available or to facilitate a smooth operation of multiple reactors.

1.1.4.2 Process control

To obtain a good effluent quality and reduce power consumption, efficient control of the different phase lengths during the operation of an SBR plant is important. SBRs were reintroduced in the 1970s, as mentioned in Section 1.1.1, attributed to the improvements in automation technology. During that period, the prevalent approach was fixed-time control, where the duration of each phase is predetermined based on the average influent characteristics and the wastewater treatment system. However, with the ongoing advancements in instrumentation, control and automation, real-time control has become a viable option nowadays (Yang et al., 2010). An overview of these control strategies can be seen in Figure 1.3.

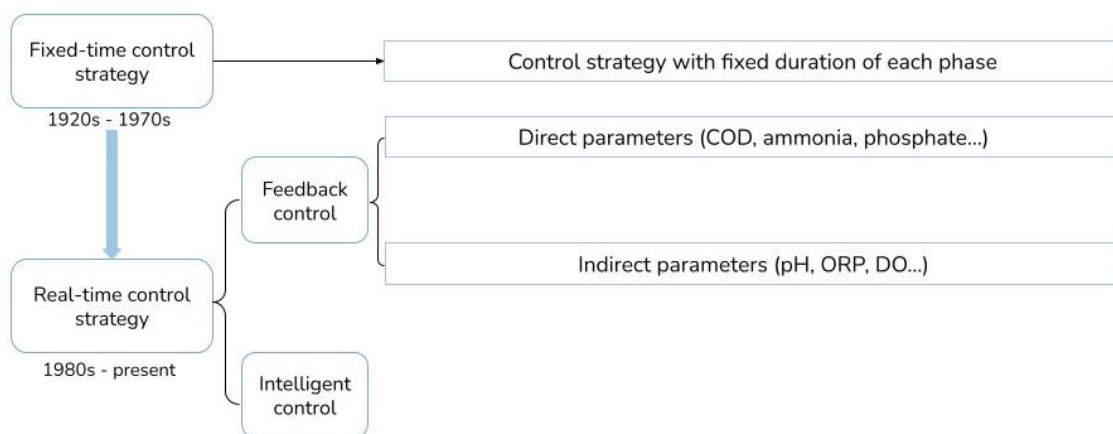


Figure 1.3: History of development control strategies - adapted from Yang et al. (2010)

As implied by its name, fixed-time control is incapable to take into account fluctuations in influent quality and quantity as the length of the phases remain constant throughout plant operation (Yang et al., 2010). Consequently, real-time control could become the preferred option. Based on real-time measurements of the influent/effluent quality or quantity, it becomes feasible to adapt the phase lengths if necessary (Schilling et al., 1996). With real-time control, operators

can achieve significant energy and time savings in comparison to fixed-time control (Won and Ra, 2011).

Among the real-time control options, there exist multiple control strategies. Figure 1.3 depicts two of them: feedback control and intelligent control. Feedback control is more common, but the emergence of AI has increased research into intelligent control (Yang et al., 2010). Intelligent control is able to reproduce characteristics of human intelligence: the system can adapt itself and learn from additional information, it can cope with high uncertainty and process large amounts of data (Koutsoukous and Antsaklis, 2000). Furthermore, intelligent control is able to work with symbolic, vague, or incomplete data, which is often the case in wastewater treatment plants (Manesis et al., 1998). The review paper of Wang et al. (2023) states that some intelligent models have been successfully applied in an experimental setting. However, in the field intelligent control is not commonly applied. The application of intelligent control is limited by for example its big data demand for machine learning, poor model reproducibility and lack of standardization and comparison at the moment. In addition, they have a high cost and require a lot of technical knowledge (Fox and Clifford, 2018).

Feedback real-time control is more often applied (Zanetti et al., 2012; Paul et al., 1998; Fatone et al., 2008; Fox and Clifford, 2018). This control strategy can be classified based on the sensor measurements, distinguishing between direct and indirect control. In the case of direct control, pollutant concentrations (COD, ammonium, phosphate, nitrate etc.) are directly measured in the liquid phase. Control decisions are mostly made by considering the absolute values of these variables. However, these direct sensors have a high cost, complex operation and require frequent maintenance (Yang et al., 2010). The other option is indirect control, where variables related to the pollutants are assessed. Profiles of these indirect measurements can reveal fluctuations in biological processes (Zanetti et al., 2012). Examples of such variables are pH, oxidation reduction potential (ORP), DO and conductivity (Andreottola et al., 2001). Indirect feedback control primarily relies on relative changes in the profile of these variables, thereby avoiding the issue of unreliable absolute values (Pavšelj et al., 2001). Moreover, these indirect sensors are easier to use, robust and inexpensive compared to direct sensors (Dries, 2016; Olsson et al., 2005).

Below, a discussion follows about the profiles of these indirect variables, how they are related to the biological processes and how they can be used for control. Phase length control in an SBR is often based on the endpoints of nitrogen removal (nitrification and denitrification), as this is a key part of wastewater treatment (Li et al., 2019). Figure 1.4 provides a schematic overview of the considered variables for a cycle with initial feeding before the anaerobic phase and additional feeding in the anoxic phase as explained in Section 1.1.4.1.

pH

The pH shows clear variations during the different operating phases of an SBR (Figure 1.4). At the start of the anaerobic phase a decline in pH is observed, attributed to phosphate release by the PAO and hydrolysis of organic matter (Comeau et al., 1987; Li et al., 2008). The pH stabilizes towards the end of the anaerobic phase when the phosphate release ceases. The start

of the aerobic phase is marked by a turning point in the pH profile. Initially, the pH rises due to CO₂-stripping as a consequence of aeration. When the rate of nitrification increases, the pH begins to decrease, primarily due to the release of protons during the nitrification process. The end of nitrification (all ammonia is converted into nitrate) is indicated by the so-called ammonia valley in the pH profile: the pH starts to increase again. This increase is not often explained in literature, as it is still not fully understood (Al-Ghusain et al., 1994). It may be associated with for example ongoing ammonification of organic matter (Hong et al., 2012; Al-Ghusain et al., 1994) or CO₂-stripping (Kim et al., 2004).

Figure 1.4 illustrates a scenario with low phosphate concentrations in the influent: phosphate uptake in the aerobic phase will be finished before the end of nitrification. Phosphate uptake has an increasing effect on the pH: when the wastewater has a high phosphate concentration, no pH decrease will be observed during nitrification. An ammonia valley is then not visible, only a change in the slope of the rising profile (Spagni et al., 2001). If the rate of nitrification is higher than the rate of phosphate uptake, an ammonia valley will be clearly visible.

At the start of the anoxic phase, the pH initially decreases, possibly due to the additional feeding. However, it quickly rises as denitrification starts, attributed to the production of alkalinity (Li et al., 2008). As denitrification ends, the pH profile decreases again: this is the nitrate apex. When all nitrate is removed at the end of denitrification, the system evolves to an anaerobic environment, where heterotrophic microorganisms will produce acids from the remaining organic matter during fermentation, which explains the pH decrease in the profile (Yang et al., 2010).

DO

During the anaerobic and anoxic phases, no oxygen is supplied to the system, so the profile of dissolved oxygen is only applicable during aerobic conditions. At the end of nitrification, the system requires less oxygen. Therefore, a breakthrough in the oxygen concentration is visible on the profile of Figure 1.4 which is indicated as the DO breakpoint (Yang et al., 2010). Note this is only valid when a fixed flow rate of oxygen is supplied, when dissolved oxygen is controlled by a setpoint this breakthrough does not occur.

ORP

The ORP serves as a measure for the degree of the oxidizing or reducing conditions within a system and is expressed in millivolts (mV) (Myers, 2019). A positive ORP value signifies oxidizing conditions, while a negative value indicates reducing conditions. The presence of oxidizing agents such as O₂, MnO₂, NO₃⁻ or NO₂⁻ contributes positively to the ORP, whereas reducing compounds such as NH₄⁺ or sulfides will influence it negatively (Meijer, 2004).

In the plot in Figure 1.4, the ORP initially decreases during the anaerobic phase as reducing conditions occur. At the start of the aerobic phase, a turning point is visible, coinciding with an increase in ORP. With the start of aeration, oxygen (an oxidizing compound) is introduced, the system undergoes a shift towards oxidizing conditions. The production of nitrate during nitrification also starts. Variations in oxygen levels have a substantial effect on the ORP. At the

end of nitrification, the oxygen concentration in the system increases suddenly, which is reflected by an increase in the ORP profile, termed the ammonia elbow (Plisson-Saune et al., 1996).

When the anoxic phase starts, the ORP starts to decrease, signaling the absence of oxygen and the decrease of nitrate as an oxidizing substance due to denitrification (Li et al., 2008). The end of denitrification is indicated by the nitrate knee as can be seen in Figure 1.4. Here, the ORP decreases more rapidly as the system transitions into a reducing environment. In anaerobic conditions, the activity of sulfate-reducing microorganisms, which produce sulfides, starts. Before, during anoxic conditions, nitrate was an inhibitor for this activity (Puig Broch, 2008; Plisson-Saune et al., 1996).

Conductivity

Conductivity (in Siemens per meter - S/m) is not shown in Figure 1.4 but is sometimes also used for indirect control. Spagni et al. (2001) indicates that conductivity is especially a good indicator during the anaerobic phase for phosphate release. The conductivity will increase until phosphate release ceases. During nitrification and denitrification multiple variables influence conductivity, therefore it is here difficult to distinguish changes in the profile (Spagni et al., 2001; Kim et al., 2007).

The profiles of the discussed indirect variables (pH, DO & ORP) can be used to control the wastewater treatment plant as a replacement or addition to control with direct variables (ammonium, nitrate, phosphate etc.). This is mostly done by a mathematical translation of relative changes in the profile. The ammonia valley and nitrate apex in the pH-profile are a local minimum and maximum respectively, so the first derivative will be zero. The ammonia elbow and nitrate knee of the ORP profile and the DO breakpoint are inflections points as the profile changes concavity (Khan Academy, 2023), so the second derivative of the profile should be zero at these points. Figure 1.5 shows an example of a possible control strategy for the length of the aerobic and anoxic phase based on the pH profile. To have a more reliable control, different control strategies can be applied simultaneously (Yang et al., 2010; Olsson et al., 2005).

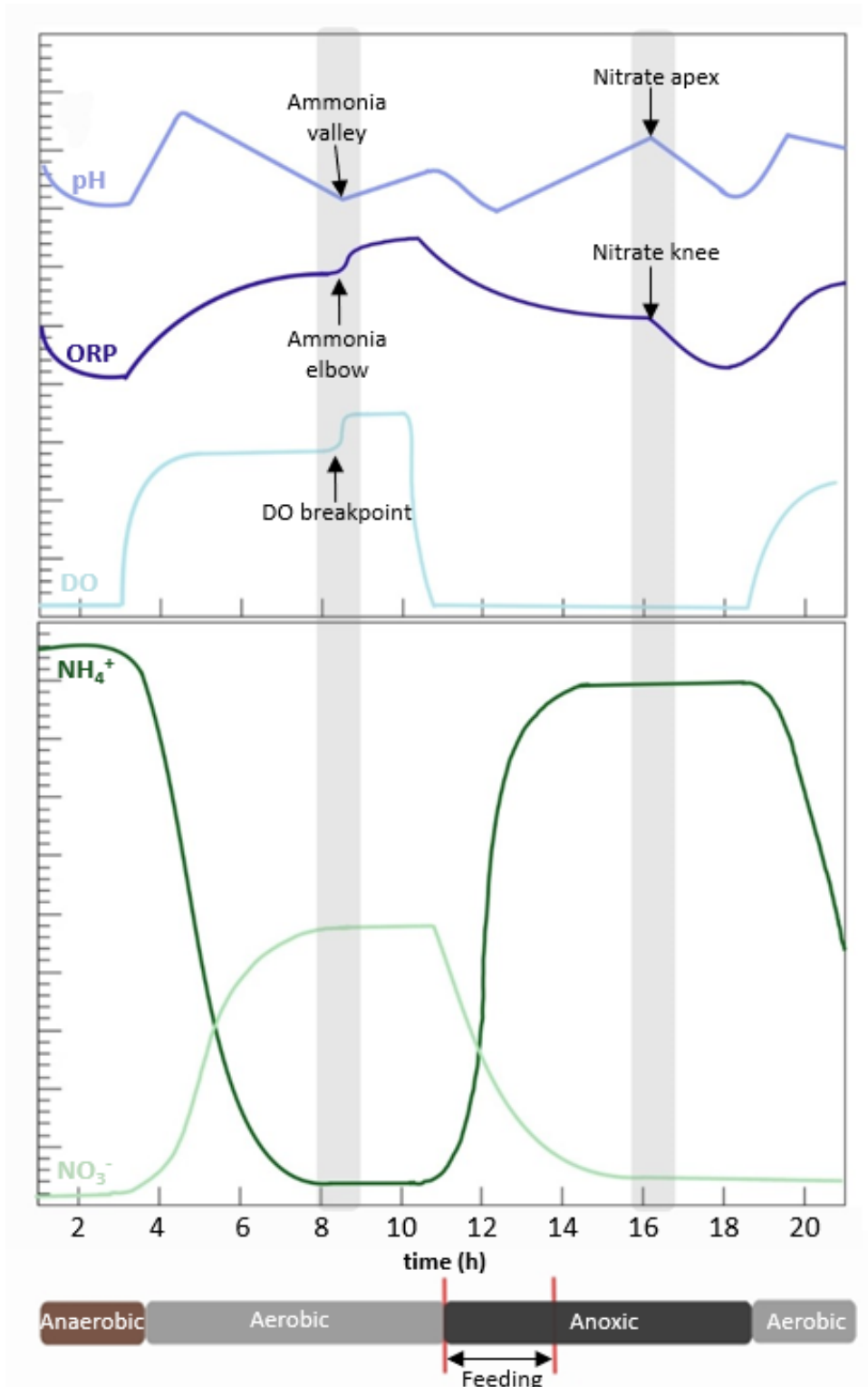


Figure 1.4: Schematic profiles of NH_4^+ and NO_3^- (lower graph) and corresponding pH, ORP and DO profiles (upper graph) during the operation of an SBR with additional feeding at the start of the anoxic phase. The two light grey vertical lines indicate the end of nitrification and denitrification, respectively. The beam below the graphs shows the anaerobic phase (brown), aerobic phases (light grey) and anoxic phase (dark grey) related to the time. The initial feeding occurred before the indicated anaerobic phase - adapted from Li et al. (2008)

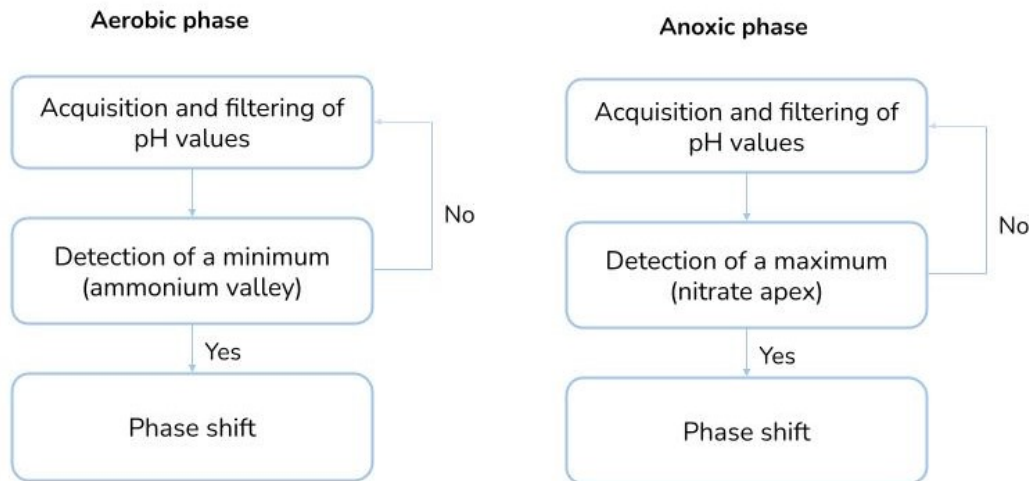


Figure 1.5: Control strategy for phase length during the aerobic and anoxic phase based on pH profile - adapted from Casellas et al. (2006)

1.1.4.3 Full-scale application

Sequencing batch reactors are applied small-scale and large-scale for the treatment of both municipal and industrial wastewater. Examples of existing full-scale applications of SBRs are:

- **Wine and brewery wastewater:** the wastewater is heavily polluted by organic matter. There is a high seasonal variability in the load and flow, the high operation flexibility of an SBR is therefore a good option (Mace and Mata-Alvarez, 2002).
- **Landfill leachate:** the flow and load of this wastewater is again highly variable, which makes the use of an SBR a viable solution (Mace and Mata-Alvarez, 2002).
- **Municipal treatment for small communities:** the limited footprint and limited pumping equipment of an SBR makes this type of treatment a good option for small rural communities that are not connected onto the main sewage network (Eloy water, 2022; Schleypen et al., 1997).

It has to be noted that continuous flow reactors are more common, mainly because, in the past, operating SBRs was considered overly complex. Section 1.1.1 highlights that operation and control of an SBR requires sophisticated controls, involving numerous automated switches and valves, especially when dealing with parallel tanks (Al-Rekabi et al., 2007; EPA, 1999). Consequently, treatment plants built in the past century, especially those handling high flowrates, tended to prefer continuous flow reactors (EPA, 1999; Shammas and Wang, 2009). Nowadays, there is again a growing interest in the application of SBRs driven by the need to reduce the footprint and energy consumption while complying with stringent effluent regulations (Vivienne, 2023). Furthermore, the current availability of advanced control equipment allows for operational flexibility in the application of SBRs (Cassidy et al., 2000; Miao et al., 2014).

A continuous flow reactor must maintain a constant volume, it is thus difficult to extend the reaction time of the system. However, an SBR, operating with a single tank, can lengthen the reaction phase if necessary (Mirbagheri et al., 2017). Additionally, an SBR exhibits better resilience against peak flows or loadings, without major degradation in effluent quality (Arora et al., 1985). Applying an SBR offers the additional benefit of reducing the required footprint (De Bruin et al., 2004). A continuous flow reactor requires multiple tanks and settlers as explained in Section 1.1.3, while an SBR operates with one tank for all phases, including settling. Furthermore, SBRs exhibit lower energy consumption, attributed to the reduced pumping capacity needed for the singular-tank operation and the absence of sludge recycling (Muzaffar et al., 2022; EPA, 1999).

1.1.5 Aerobic granular sludge

An important aspect in the research field of wastewater treatment nowadays, is the increase in treatment capacity. One approach to achieve this is by increasing the biomass concentration in the system. This method of capacity increase is limited in both SBRs and continuous flow reactors which use flocculated activated sludge. Due to poor settling characteristics of these flocs, a large increase of the settler surface area becomes necessary when the biomass is increased (De Bruin et al., 2004).

An alternative strategy to increase the biomass concentration is aerobic granular sludge (AGS), mostly applied in SBRs (Adav et al., 2008). It could thus be seen as a special case of SBR operation. These are dense, structured granules with a high settling velocity. The granules are characterized by a layered structure due to an oxygen gradient over the granule: an aerobic outer layer with an anoxic inner layer and anaerobic core. This implies that aerobic nitrifying organisms in the outer layer can coexist with denitrifying organisms in the anoxic layer. A visual representation of the intersection of a granule with the layered structure can be seen in Figure 1.6. The coexistence of the different organisms in a granule implies that simultaneous removal of nitrogen, phosphorus and COD from the wastewater is possible (Pronk et al., 2015; Adav et al., 2008). By controlling the aeration rate, the dissolved oxygen concentration is adjusted during the aeration phase. This will influence the ratio between nitrification and denitrification, which is dependent on the oxygen penetration in the granule. If denitrification in the aerobic phase is insufficient, the aeration phase can be followed by a shortened anoxic phase by turning the aeration off. For phosphate release, feeding under anaerobic conditions must be sufficiently long. In the aerobic phase, phosphate will be taken up. Furthermore, due to the fast settling characteristics of the granules, simultaneous filling and discharge is possible (Pronk et al., 2020). Figure 1.7 illustrates a typical SBR cycle with aerobic granular sludge without an anoxic phase.

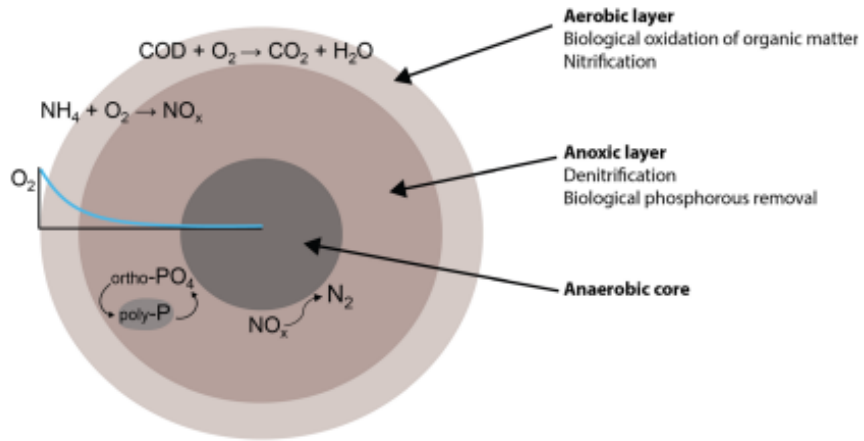


Figure 1.6: Visual representation of an AGS granule with biochemical processes taking place in the different layers - (Wilén et al., 2018)

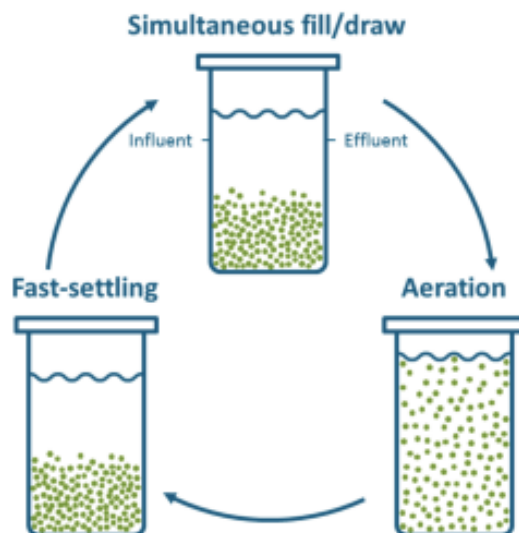


Figure 1.7: SBR cycle with aerobic granular sludge - (Pronk et al., 2020)

1.2 Gas-liquid mass transfer

1.2.1 General principles and physical background

Mass transfer is a fundamental process that occurs when a concentration gradient is present in a system. In essence, it involves the migration of a compound from regions of high concentration to regions of lower concentration, driven by this gradient (Dutta, 2007). This phenomenon is essential to explain various processes in scientific and engineering contexts. A common form of mass transfer is gas-liquid transfer, where a compound is exchanged between the gas and liquid phase. This interchange is categorized based on the direction of transfer: absorption, when a compound moves from the gas phase to the liquid phase, and stripping, when the transfer occurs in the opposite direction (Treyball, 1980).

Gas-liquid mass transfer plays a pivotal role in the context of wastewater treatment where the exchange of gases and dissolved substances is of high importance for the ongoing biological processes. A few examples of gas-liquid transfer processes during wastewater treatment are (Amaral et al., 2019):

- **Aeration for oxygen supply:** air bubbles containing a high concentration of oxygen are introduced into the liquid medium characterized by lower oxygen levels. Oxygen transfer from the gas bubbles to the bulk liquid will occur.
- **Carbon dioxide production during biological respiration:** as microorganisms consume organic matter, a byproduct of this metabolic activity is carbon dioxide. This carbon dioxide will transfer from the microorganisms in the liquid phase to the gas phase, to leave the installation.
- **Production of greenhouse gases:** during the biological processes, greenhouses gases such as methane and nitrous oxide are produced. These gases transfer to the gas phase, contributing to their release into the environment.

One of the prominent theories used to understand gas-liquid mass transfer is the two-film theory (Lewis and Whitman, 1924). It is based on the formation of a mass transfer boundary layer between two phases. In this theory it is assumed that all mass transfer occurs by molecular diffusion in the boundary layer at steady state. The bulk phases beyond this layer are so well-mixed, that there is no concentration gradient here (Taylor and Krishna, 1993; Dutta, 2007). In Figure 1.8 the concentration profile of compound A can be seen. The concentration of A in the bulk gas phase, C_{AG} , is higher than the concentration of A in the bulk liquid phase, C_{AL} , diffusion of compound A to the liquid phase will thus occur. It is transferred from the bulk gas phase to the gas-liquid interface and from the gas-liquid interface to the bulk liquid phase. The rates of mass transfer through the gas and liquid boundary layers, $q_{A,G}$ and $q_{A,L}$ ($\text{g}\cdot\text{m}^{-3}\cdot\text{h}^{-1}$), respectively, are proportional with the concentration gradient (driving force) between the specific bulk phase and the gas-liquid interface and proportional with the transfer area per volume of liquid (Doran, 2013):

$$q_{A,G} = k_G \cdot a \cdot (C_{AG} - C_{AGi}) \quad (1.1)$$

$$q_{A,L} = k_L \cdot a \cdot (C_{ALi} - C_{AL}) \quad (1.2)$$

The proportionality factors k_G and k_L represent the gas-phase and liquid-phase mass transfer coefficients ($\text{m}\cdot\text{h}^{-1}$), respectively. a denotes the transfer area per volume of liquid ($\text{m}^2\cdot\text{m}^{-3}$). The difference terms express the concentration gradients between the bulk phases and the interface: C_{AG} and C_{AL} are the gas and liquid concentrations in the bulk phases ($\text{g}\cdot\text{m}^{-3}$), while C_{AGi} and C_{ALi} are the gas and liquid concentrations at the gas-liquid interface ($\text{g}\cdot\text{m}^{-3}$).

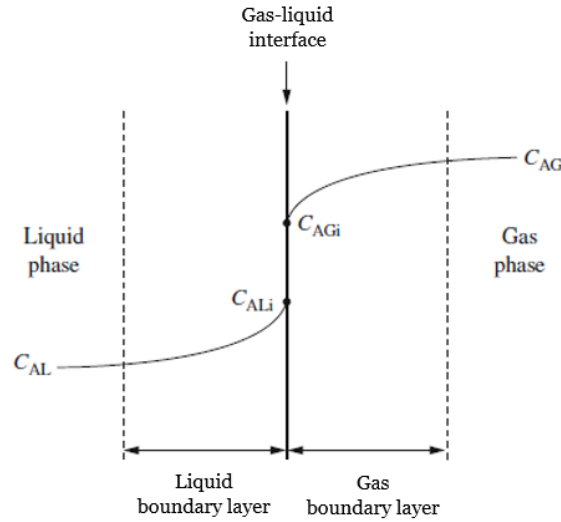


Figure 1.8: Concentration profile of compound A during gas-liquid mass transfer - adapted from Doran (2013)

The gas and liquid concentration at the interface (C_{ALi} and C_{AGi}) are in equilibrium according to the two-film theory, so their relation can be expressed by Henry's law (Villadsen et al., 2011):

$$C_{AGi} = H_A \cdot C_{ALi} \quad (1.3)$$

in which H_A denotes Henry's law constant ($\text{g}\cdot\text{m}^{-3}\text{-gas}/\text{g}\cdot\text{m}^{-3}\text{-liquid}$). As the interface concentrations C_{AGi} and C_{ALi} are not directly measurable, it is often easier to consider the overall liquid-gas mass transfer rate from the bulk liquid phase to the bulk gas phase, q_A ($\text{g}\cdot\text{m}^{-3}\cdot\text{h}^{-1}$):

$$q_A = K_L a \cdot (C_{AL}^* - C_{AL}) \quad (1.4)$$

with K_L ($\text{m}\cdot\text{h}^{-1}$) an overall mass transfer coefficient and C_{AL}^* the saturation concentration in the bulk liquid phase which is in equilibrium with the bulk gas-phase concentration ($\text{g}\cdot\text{m}^{-3}$). This equilibrium relation can again be expressed by Henry's law:

$$C_{AL}^* = \frac{C_{AG}}{H_A} \quad (1.5)$$

The difference between the saturation concentration and the actual concentration in the liquid phase determines the driving force of the mass transfer. If the driving force is positive, mass transfer from the gas phase to the liquid phase will occur (absorption), if the driving force is negative, transfer will take place from the liquid phase to the gas phase (stripping) (Treyball, 1980).

It is further assumed that there is steady state mass transfer in the system, i.e. there is no accumulation of components at the interphase. Under these conditions the overall mass transfer rate will be equal to the separately considered liquid or gas mass transfer rates:

$$q_A = q_{A,G} = q_{A,L} \quad (1.6)$$

The overall liquid-phase mass transfer coefficient K_L can be calculated based on the mass transfer coefficients in the gas and liquid phase (Morrison, 2021; Villadsen et al., 2011). First, Eq. 1.4 is rewritten:

$$\frac{1}{K_L a} = \frac{C_{AL}^* - C_{AL}}{q_A} = \frac{C_{AL}^* - C_{ALi} + C_{ALi} - C_{AL}}{q_A} \quad (1.7)$$

$$\frac{1}{K_L a} = \frac{(C_{AL}^* - C_{ALi})}{q_A} + \frac{(C_{ALi} - C_{AL})}{q_A} \quad (1.8)$$

Now, substitution of C_{ALi} and C_{AL}^* by Eq. 1.3 and 1.5 respectively, results in:

$$\frac{1}{K_L a} = \frac{(\frac{C_{AG}}{H_A} - \frac{C_{AGi}}{H_A})}{q_A} + \frac{(C_{ALi} - C_{AL})}{q_A} \quad (1.9)$$

Considering q_A equals $q_{A,G}$ and $q_{A,L}$ (Eq. 1.6) and further substitution by Eq. 1.1 and Eq. 1.2, one obtains:

$$\frac{1}{K_L a} = \frac{1}{H_A} \cdot \frac{(C_{AG} - C_{AGi})}{q_{A,G}} + \frac{(C_{ALi} - C_{AL})}{q_{A,L}} \quad (1.10)$$

$$\frac{1}{K_L a} = \frac{1}{H_A} \cdot \frac{1}{k_G a} + \frac{1}{k_L a} \quad (1.11)$$

$$\frac{1}{K_L} = \frac{1}{H_A \cdot k_G} + \frac{1}{k_L} \quad (1.12)$$

Poorly soluble gases, such as O_2 and CH_4 , are characterized by a high H_A value and k_G is much larger than k_L (Villadsen et al., 2011). The first term on the right-hand side of Eq. 1.12 will then be negligible. As a result, the overall mass transfer coefficient K_L will be almost equal to k_L for compounds poorly soluble in the liquid phase. In contrast, for very soluble compounds, such as N_2O (Baeten et al., 2020), k_L is large compared to k_G and K_L can then be approximated by k_G .

Eq.1.4 can be rewritten as:

$$q_A = k_L a \cdot (C_{AL}^* - C_{AL}) \quad (1.13)$$

As the mass transfer coefficient k_L and the transfer area a are both dependent on many factors (bubble size and number, medium composition, stirrer speed etc.), they are difficult to measure. Therefore, they are usually described as one term $k_L a$, the volumetric mass transfer coefficient (h^{-1}) (Amaral et al., 2019).

1.2.2 Oxygen mass transfer

Oxygen mass transfer is an important gas-liquid mass transfer process in the biological treatment of wastewater. Since oxygen is poorly soluble, maintaining a high level of dissolved oxygen in the water poses a challenge (Rosso et al., 2020). Despite this difficulty, achieving an adequate level of oxygen is essential, as microorganisms in the activated sludge use oxygen as electron acceptor during the aerobic processes for growth and metabolic production (Amerlinck et al., 2016). Given that aeration is one of the most energy consuming processes during wastewater treatment, a good understanding of the oxygen transfer process is valuable for optimizing aeration and facilitating comparisons between different technologies (Rosso et al., 2008).

1.2.2.1 Aeration system characteristics

Most of the parameters to characterize an aeration system can be calculated for both clean water and process water conditions.

Clean water conditions

An aeration device manufacturer will often mention the values in clean water to facilitate comparison between different devices.

The first parameter is the oxygen transfer rate (OTR), defined as the amount of oxygen an aeration system can supply per unit of time, regardless its efficiency ($\text{gO}_2 \cdot \text{h}^{-1}$) (Garcia-Ochoa et al., 2010; Rosso et al., 2020). The oxygen mass transfer rate can be modelled by the two-film theory as described in Section 1.2.1 (Rosso et al., 2018):

$$OTR = k_L a_{(O_2)} \cdot (C_{O_2, L}^* - C_{O_2, L}) \cdot V \quad (1.14)$$

where $k_L a_{(O_2)}$ represents the overall liquid mass transfer coefficient of oxygen (h^{-1}), $C_{O_2, L}^*$ the dissolved oxygen concentration in the water at saturation ($\text{gO}_2 \cdot \text{m}^{-3}$), $C_{O_2, L}$ the dissolved oxygen concentration ($\text{gO}_2 \cdot \text{m}^{-3}$) and V the volume of water (m^3).

To compare even better between aeration devices independently from the environment, standard conditions are often used in the calculations. Then it is assumed there is no fouling, the dissolved

oxygen concentration in the water is zero, the water temperature is 20 °C and there is a standard atmospheric pressure of 1 atm (Mueller et al., 2002). At standard conditions the OTR (expressed as the standard oxygen transfer rate (sOTR)) is:

$$sOTR = k_L a_{(O_2), 20} \cdot (C_{O_2, L, 20}^* - C_{O_2, L}) \cdot V \quad (1.15)$$

Another parameter is the oxygen transfer efficiency (OTE) or the fraction of the mass flow of oxygen supplied to the treatment system which is actually dissolved into the water (Mueller et al., 2002). This parameter allows comparison between different aeration devices and is calculated as follows (Rosso et al., 2020):

$$OTE = \frac{C_{O_2, G-in} Q_{in} - C_{O_2, G-out} Q_{out}}{C_{O_2, G-in} Q_{in}} \quad (1.16)$$

where $C_{O_2, G-in}$ represents the oxygen concentration of the entering air flow into the system ($\text{g}\cdot\text{m}^{-3}$), $C_{O_2, G-out}$ the outgoing oxygen concentration of the air flow out of the system ($\text{g}\cdot\text{m}^{-3}$) and Q_{in} and Q_{out} the gas volume flow in and out of the wastewater treatment system, respectively ($\text{m}^3\cdot\text{h}^{-1}$).

The OTE can also be expressed in terms of the OTR, with W_{O_2} the oxygen mass flow rate fed by the aeration system ($\text{gO}_2\cdot\text{h}^{-1}$):

$$OTE = \frac{OTR}{W_{O_2}} \quad (1.17)$$

Lastly, the aeration efficiency (AE), defined as the ratio of the oxygen transfer rate to the power consumed by the aeration system (gO_2/kWh), is derived from the OTR with P the power needed by the aeration system (kW) (Rosso et al., 2020):

$$AE = \frac{OTR}{P} \quad (1.18)$$

Process water conditions

For operators of wastewater treatment, site-specific information is important. With sufficient information about the process water and environment the values of OTR, OTE and AE can be calculated under process conditions, taking into account the effects of the wastewater composition.

The calculation of the OTR under process conditions at a temperature T (°C) is as follows, with several correction factors (Amerlinck et al., 2016; Rosso et al., 2018):

$$OTR = \alpha \cdot F \cdot k_L a_{20, (O_2)} \cdot \theta^{(T-20)} \cdot (\beta \cdot \tau \cdot \Omega \cdot C_{O_2, L, 20}^* - C_{O_2, L}) \cdot V \quad (1.19)$$

The influence of the contaminants in the wastewater on the oxygen transfer rate are partly integrated in the alpha factor (α). This alpha factor is often defined as the ratio of the process water to clean water mass transfer coefficient (Schwarz et al., 2022):

$$\alpha = \frac{k_{La(O_2, \text{process water})}}{k_{La(O_2, \text{clean water})}} \quad (1.20)$$

Predicting the alpha factor is very difficult as both the clean water ($k_{La(O_2, \text{clean water})}$) and the process water mass transfer coefficient ($k_{La(O_2, \text{process water})}$) rely on many factors (e.g. air flow rate, turbulence, surface area). The $k_{La(O_2, \text{process water})}$ differs from $k_{La(O_2, \text{clean water})}$ due to two groups of influences: the composition of the process water (e.g. surfactants) and the aeration device aging process (e.g. fouling and clogging) (Stenstrom and Gilbert, 1981; Gillot and Héduit, 2008).

Furthermore, F in Eq. 1.19 represents the fouling factor, which indicates the ratio between the mass transfer coefficient (k_{La}) of a new aeration system under process conditions and the k_{La} of an aeration system that is already used for some time. θ is the Arrhenius temperature coefficient, β is a correction factor for dissolved solids and can be approximated by the ratio of the saturated dissolved oxygen concentration under process conditions to the one under clean water conditions, τ is a correction factor for the temperature and Ω is a correction factor for the atmospheric pressure. The mass transfer coefficient $k_{La_{20}}$ determined under standard clean water conditions is thus adapted for process conditions by the alpha factor, fouling factor and a temperature coefficient. The saturated dissolved oxygen concentration $C_{O_2, L, 20}^*$ is also adapted for temperature, pressure and process conditions. The $k_{La(O_2), 20}$ and $C_{O_2, L, 20}^*$ can be derived from literature. A value for $k_{La(O_2), 20}$ can also be given by the manufacturer of the aeration device, often determined in an experimental set-up with a chemical, physical or biological method (Ochoa and Gómez, 2009). The OTE and AE under process conditions can be calculated with the OTR calculated in Eq. 1.19.

1.2.2.2 Oxygen uptake rate

Concerning oxygen, the activity of the microorganisms in the activated sludge can be quantified through the oxygen uptake rate (OUR), representing the amount of oxygen consumed by the microorganisms per time unit. A value for OUR ($\text{gO}_2 \cdot \text{h}^{-1}$) can be derived with an oxygen mass balance in the liquid system (Pittoors et al., 2014):

$$V \cdot \frac{dC_{O_2, L}}{dt} = OTR - OUR = k_{La(O_2)} \cdot (C_{O_2, L}^* - C_{O_2, L}) \cdot V - q_{O_2} \cdot X \quad (1.21)$$

with q_{O_2} the specific oxygen uptake rate by the microorganisms ($\text{gO}_2 \cdot \text{h}^{-1} \cdot \text{g}^{-1}$) and X the biomass in the system (g). To calculate OUR, the oxygen mass transfer rate and accumulation of dissolved oxygen must be measured.

An alternative to determine the OUR, without knowing the OTR, is by shutting down aeration after some period. Eq. 1.21 then reduces to (Spanjers and Vanrollegem, 2020):

$$\frac{dC_{O_2, L}}{dt} = -OUR = -q_{O_2} \cdot X \quad (1.22)$$

By measuring the decrease in dissolved oxygen as a function of time when there is no aeration, the OUR can be calculated. If the amount of biomass is known, the specific oxygen uptake rate q_{O_2} can be determined as well.

1.2.3 Carbon dioxide mass transfer

Carbon dioxide is produced by microorganisms in the activated sludge when they break down organic matter for growth due to the oxidation of part of the substrate (Lijklema, 1971). By the principle of gas-liquid mass transfer, this CO_2 will be stripped from the liquid phase to the gas phase. Similar to how the OUR by microorganisms can be determined based on the OTR in Eq. 1.21 (Subsection 1.2.2.2), the carbon dioxide production rate (CPR) can be related to the carbon dioxide transfer rate (CTR) between the gas and liquid phase.

The CTR ($gCO_2 \cdot h^{-1}$) can be calculated analogously to Eq. 1.14 (Contreras, 2007):

$$CTR = k_{La(CO_2)} \cdot (C_{CO_2, L}^* - C_{CO_2, L}) \cdot V \quad (1.23)$$

with $k_{La(CO_2)}$ the overall liquid mass transfer coefficient for carbon dioxide (h^{-1}), $C_{CO_2, L}^*$ the dissolved carbon dioxide concentration in the water at saturation ($gCO_2 \cdot m^{-3}$), $C_{CO_2, L}$ the actual dissolved carbon dioxide concentration in the water ($gCO_2 \cdot m^{-3}$) and V the volume (m^3) of water. As the produced carbon dioxide is stripped, the saturation concentration will be lower than the actual concentration.

The $k_{La(CO_2)}$ can be determined experimentally, analogous to $k_{La(O_2)}$. Both Contreras (2007) and Hill (2006) were for example able to determine the $k_{La(CO_2)}$ during experimental set-ups for stripping. The $k_{La(CO_2)}$ could be calculated based on measurements of the total inorganic carbon concentration in the liquid medium, the pH level and the air flow rate over time. Another method to calculate the $k_{La(CO_2)}$ is based on the $k_{La(O_2)}$, which is mostly already known for the used aeration device in the reactor (Khoo et al., 2016):

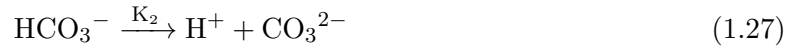
$$k_{La(CO_2)} = k_{La(O_2)} \sqrt{\frac{D_{O_2}}{D_{CO_2}}} \quad (1.24)$$

with D_{O_2} the diffusivity of oxygen ($m^2 \cdot s^{-1}$) and D_{CO_2} the diffusivity of carbon dioxide ($m^2 \cdot s^{-1}$). The diffusivities of oxygen and carbon dioxide in pure water at 20 °C are $2 \cdot 10^{-9} m^2 \cdot s^{-1}$ (Xing et al., 2014) and $2.1 \cdot 10^{-9} m^2 \cdot s^{-1}$, respectively (Li et al., 2021). In process water these values will be lower (Jamnongwong et al., 2010).

The calculation of the CPR is not as straightforward as the determination of the OUR based on the oxygen mass balance. This is because carbon dioxide in the liquid medium is involved in several reversible reactions. Inorganic carbon in the liquid phase can appear in different species (free carbon dioxide ($\text{CO}_{2\text{aq}}$), carbonic acid (H_2CO_3), the bicarbonate ion (HCO_3^-) and the carbonate ion (CO_3^{2-})) (Spérandio and Paul, 1997; Hill, 2006). The ratio of $\text{CO}_{2\text{aq}}$ to H_2CO_3 is high under most conditions (independent of pH or ionic strength changes) (Contreras, 2007; Pratt et al., 2003):



Therefore, these two species are mostly expressed as one, H_2CO_3^* . The dissolved CO_2 in the liquid is in equilibrium with bicarbonate and carbonate:



K_1 and K_2 represent the equilibrium constants with a value of $4.5 \cdot 10^{-7}$ and $4.7 \cdot 10^{-11}$, respectively (Kalff, 2002). These constants can be calculated (Husemann et al., 2021):

$$K_1 = \frac{[\text{HCO}_3^-] \cdot [\text{H}^+]}{[\text{H}_2\text{CO}_3^*]} = \frac{[\text{HCO}_3^-] \cdot 10^{-\text{pH}}}{[\text{H}_2\text{CO}_3^*]} \quad (1.28)$$

$$K_2 = \frac{[\text{CO}_3^{2-}] \cdot [\text{H}^+]}{[\text{HCO}_3^-]} = \frac{[\text{CO}_3^{2-}] \cdot 10^{-\text{pH}}}{[\text{HCO}_3^-]} \quad (1.29)$$

The pH in a biological system is mostly between 6 and 9 (Kalff, 2002). At this pH the dissociation of HCO_3^- into CO_3^{2-} (reaction 1.27) is negligible which can also be seen in Figure 1.9. The graph represents the percentual portions of the inorganic carbon species in function of the pH in a system. A schematic overview of reactions 1.25 - 1.27 with the predominant carbon species in a biological environment can be seen in Figure 1.10.

The predominant inorganic carbon species within the pH range of 6 to 9, are H_2CO_3^* (free carbon dioxide and carbonic acid) and HCO_3^- (bicarbonate), as can be seen in Figure 1.9 and Figure 1.10. At a pH of 6.3, half of the carbon dioxide exists in the bicarbonate form (Spérandio and Paul, 1997). At a constant pH, the system will be in equilibrium and the concentration of free carbon dioxide, which can transfer to the gas phase, will not change. However, the equilibrium of these reactions is greatly affected by a change in pH, an increase in pH results in the conversion of more H_2CO_3^* to HCO_3^- . This leads to less free carbon dioxide in the liquid phase and thus less stripping to the gas phase. When the pH decreases, the reverse is true (Leu et al., 2010). A change in pH can be the result of the biological reactions in the liquid phase (nitrification, denitrification). However, a shift in the equilibrium can also be the result of a change in the alkalinity concentration of the influent (Lijklema, 1969). The concentration of carbonate and bicarbonate ions primarily determine the alkalinity of the influent (Weissenbacher et al., 2007; Bozorg-Haddad et al., 2021). These equilibrium reactions also explain the name often used for this equilibrium system: *the bicarbonate buffer system* as the system will try to counteract a pH shift by reaching a new equilibrium.

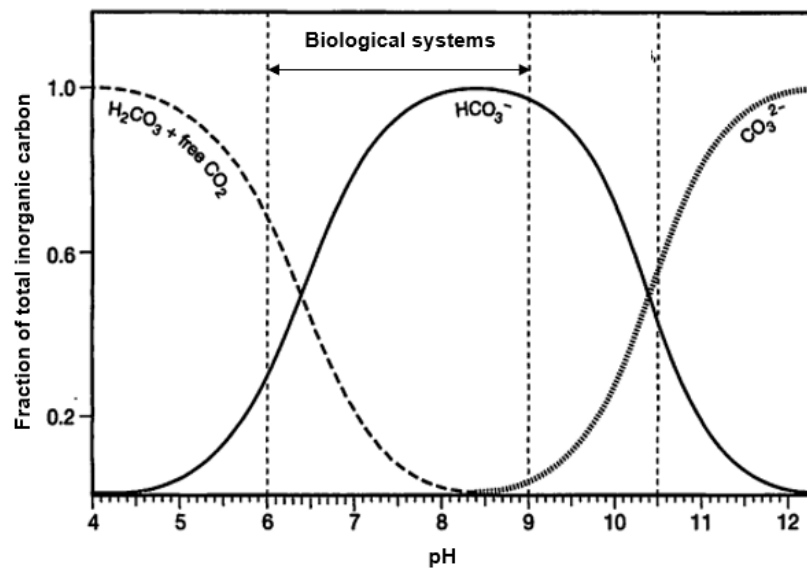


Figure 1.9: Distribution of the various inorganic carbon species as a percentage of the total inorganic carbon in function of the pH ($pK_1 = 6.3$ & $pK_2 = 10.4$) - adapted from Kalff (2002)

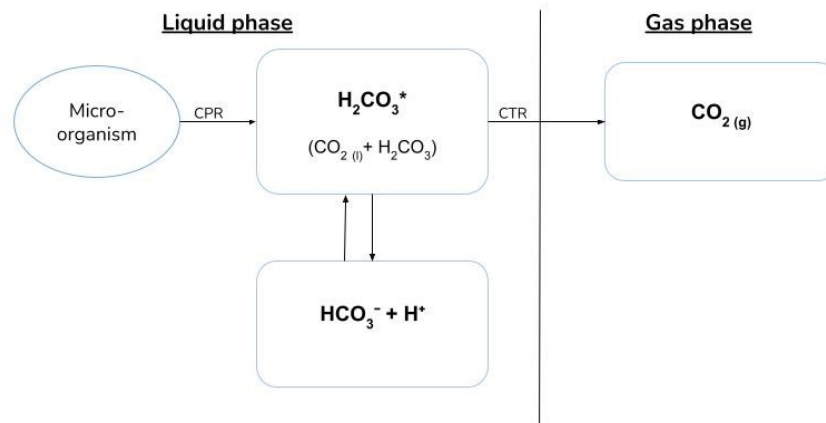


Figure 1.10: Schematic overview of the inorganic carbon species in a biological system - adapted from Spérandio and Paul (1997)

Overall, changes of the CO_2 concentration in the off-gas after carbon dioxide mass transfer, can be due to changes in the carbon dioxide production rate by the microorganisms and/or by changes in the equilibrium of the inorganic carbon species due to a pH shift. To be able to apply Eq. 1.23 to calculate the transfer to the gas phase, the liquid free CO_2 concentration has to be known. Therefore, the following carbon dioxide mass balance is considered in the liquid phase (Weissenbacher et al., 2007):

$$V \cdot \frac{dC_{CO_2,L}}{dt} = CPR - CTR - r_F \cdot M_{CO_2} \quad (1.30)$$

With M_{CO_2} ($g \cdot mol^{-1}$) the molecular weight of CO_2 and r_F ($mol \cdot h^{-1}$) the rate at which $H_2CO_3^*$ is converted to HCO_3^- or HCO_3^- is converted to $H_2CO_3^*$ if the system is not in equilibrium

yet. The calculation of this rate is shown below. k_1 and k_{-1} are the kinetic rate constants of reaction 1.31 in s^{-1} and $m^3 \cdot g^{-1} \cdot s^{-1}$ respectively (Spérandio and Paul, 1997):



$$r_F = k_1 \cdot [H_2CO_3^*] - k_{-1} \cdot [HCO_3^-][H^+] \quad (1.32)$$

At equilibrium rate r_F will be zero, but with a change of pH this rate can influence the mass balance.

The CTR can be measured with off-gas analysis based on the carbon dioxide concentration in the supplied air flow of the aeration device and the off-gas (Weissenbacher et al., 2007; Frahm et al., 2002). However, as indicated by the mass balance in Eq. 1.30, this CTR cannot be directly linked with the production of carbon dioxide (CPR) by microorganisms. A change in pH can also lead to a change in the CTR without a change in the production of carbon dioxide. To be able to link changes in the off-gas carbon dioxide to the liquid phase biological processes, the CTR has to be corrected, which has proven to be challenging. Weissenbacher et al. (2007) developed a model to correct the CO_2 off-gas data for pH shifts in the liquid medium or changes in alkalinity of the influent. Standard on-line pH measurements and periodical off-line alkalinity titration of the influent were performed to estimate the influence of the equilibrium reactions on the off-gas concentration of CO_2 (Weissenbacher et al., 2007). Pratt et al. (2003) developed a model, where a TOGA sensor (combination of titration and off-gas analysis) is used to determine the CTR by off-gas analysis and the hydrogen production rate by titration to estimate the pH of the liquid medium. However, this sensor is rather expensive, and thus less used in practice.

To be able to characterize the biological activity of a system, it is often desired to determine the CPR besides the OUR as the CPR is also able to characterize activity during the anoxic and anaerobic phase as well, when oxygen is not the electron acceptor (Pratt et al., 2003). It has to be noted in order to measure carbon dioxide in the off-gas during the anoxic or anaerobic phase, a gas flow is necessary. Pratt et al. (2003) used for example an inert argon stream to facilitate this.

1.3 Applications of off-gas analysis

Analysis of the off-gas from a wastewater treatment plant can have an added value for the operation and control of the system. Compounds such as oxygen, carbon dioxide, methane or nitrous oxide can be measured in the off-gas. These measurements provide information about processes in the liquid phase, the aeration efficiency, the carbon footprint or can help with process control.

1.3.1 Off-gas analysis: advantages and challenges

Measurements in the gas phase offer several advantages compared to liquid-phase measurements. The sample pre-treatment is simpler, no chemical reagents are needed, the investment cost for measuring is lower and less maintenance is required (Schuchardt et al., 2005; Hellinga et al., 1996). Furthermore, a measurement in the liquid phase is a point measurement while a gas sample is well-mixed and thus relatively more representative for the whole reactor (Mears et al., 2017).

Adequate sampling can still be challenging. It is easiest when the treatment plant is covered, measuring the ventilation air is then sufficient. However when the system is open to air, the use of a gas hood or the measurement of the downwind gas plume is required (Chandran et al., 2016). In open continuous plants, an off-gas sampler is less common due to the spatial concentration gradients over the basin caused by the water flow which leads to varying off-gas concentrations at different sampling locations. This explains why off-gas analysis is more applied in sequentially operated plants such as an SBR, as there is no continuous feeding, there are no spatial gradients. This implies less spatial differentiation in the off-gas composition and only one sampling point is representative for the entire reactor (Baeten et al., 2021). The difference between off-gas measuring in a continuous operated reactor and sequentially operated reactor is visually represented in Figure 1.11.

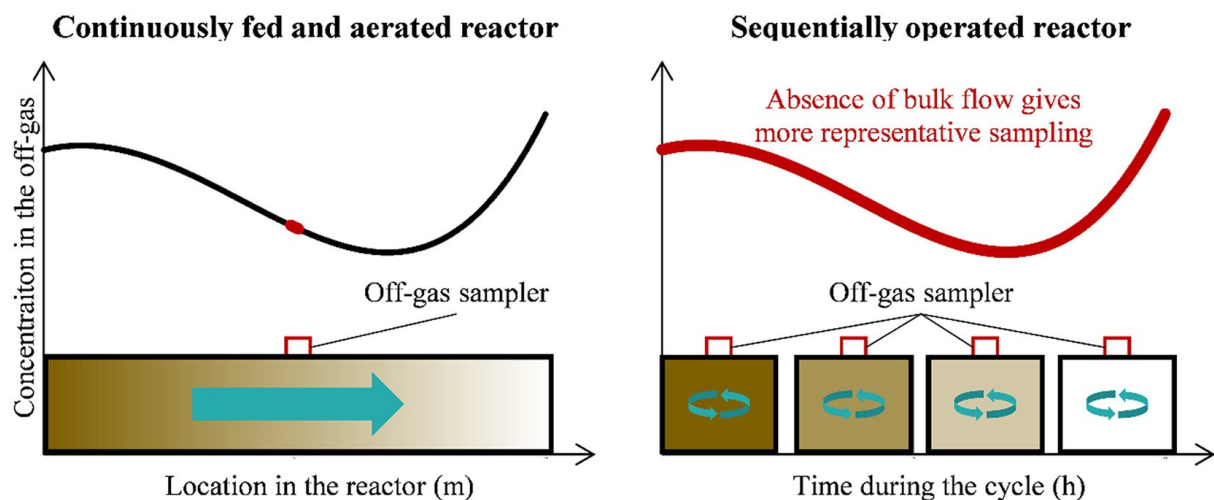


Figure 1.11: Off-gas analysis with one sampler in a continuously fed and aerated reactor (left) and sequentially operated reactor (right) - (Baeten et al., 2021)

1.3.2 Monitoring of aeration characteristics

As aeration consumes a lot of energy and the oxygen transfer from the gas phase to the liquid phase is often a limiting factor, it is important to have adequate information about the performance of the aeration system (Amerlinck et al., 2016). In section 1.2.2, the theoretical principles of the oxygen transfer rate (OTR) and efficiency (OTE) were described. These can be applied in practice by measuring the off-gas oxygen concentration.

The most common technique to measure the OTR is described by Redmon et al. (1983). A gas-phase mass balance is made over the reactor by measuring the O_2 concentration in the supplied air flow ($C_{O_2,air}$) and off-gas ($C_{O_2,off-gas}$):

$$V \cdot \frac{dC_{O_2,G}}{dt} = Q \cdot C_{O_2,air} - Q \cdot C_{O_2,off-gas} - OTR \quad (1.33)$$

With Q the air flow rate ($m^3 \cdot h^{-1}$), assumed to be constant. If steady state is assumed, the OTR can easily be derived. When the oxygen mass flow rate (W_{O_2}) is calculated, the OTE is also known. If the OTR is known, the oxygen uptake rate can be calculated based on equation 1.21 (Leu et al., 2009).

Several articles used off-gas measurements as a technique to retrieve information about aeration characteristics:

- Groves et al. (1992) used off-gas analysis to determine the influence of several aeration device characteristics (type, layout, age etc.) on oxygen transfer efficiency. By keeping all factors but one constant in every experiment, the influence of each factor on the oxygen transfer efficiency could be determined.
- Amerlinck et al. (2016) conducted an off-gas measuring campaign to obtain information on the performance and behaviour of an aeration system related to the OTE. The retrieved data could be used to improve model prediction of aeration performance.
- Leu et al. (2009) did research in fine-pore diffusers that are often used for aeration. These diffusers have fouling problems, which cause a decline in aeration performance. Regular cleaning of the diffusers is necessary to avoid too much extra energy costs. To be able to determine the frequency of cleaning, they used off-gas measuring to obtain a profile of the OTE over time. Based on the decrease and increase of the OTE the frequency and intensity of cleaning could be determined.
- Baeten et al. (2021) observed a gradual improvement of the oxygen transfer efficiency over time in an off-gas study in an aerobic granular sludge reactor. The increase was attributed to the degradation of soluble biodegradable organics over the aeration phase. This principle is also explained in Strubbe et al. (2023).

1.3.3 Monitoring of greenhouse gas emissions

Wastewater treatment can be an important source of anthropogenic greenhouse gas emissions (Yoshida et al., 2014). The most important greenhouse gases produced during wastewater treatment are methane (CH_4) and nitrous oxide (N_2O). Methane is formed during anaerobic degradation of the organic matter, while nitrous oxide can be produced during the nitrification and denitrification process (Campos et al., 2016; Daelman et al., 2012). It is important to be able to identify the amount of emissions as these two greenhouse gases have a high global warming potential, with N_2O having a GWP-100 of 273 and CH_4 a GWP-100 of 27 (IPCC, 2021). By measuring their concentration in the off-gas it is possible to determine the carbon footprint of an installation (Chandran et al., 2016) and subsequently, to take adequate measures.

Although CO_2 is produced during microbial degradation of organic matter, it is not considered as a greenhouse gas in wastewater treatment by the IPCC, as it is assumed to be biogenic. Biogenic means that the CO_2 was drawn from the atmosphere during the growth of the organic matter (Gupta and Singh, 2012). Only carbon dioxide indirectly produced by burning fossil fuels for generating energy for the treatment plant is considered as a greenhouse gas contribution (Daelman et al., 2012).

1.3.4 Monitoring of influent composition and reactor conversions

During aerobic COD removal O_2 is consumed and CO_2 is produced. Also during nitrification and phosphate uptake O_2 is consumed and during denitrification CO_2 will be produced (Table 1.1, Section 1.1.3). As O_2 and CO_2 are gaseous soluble compounds, their profiles in the off-gas are an indirect representation of the biological processes in the liquid phase (Baeten et al., 2021; Hellinga et al., 1996).

Hellinga et al. (1996) demonstrated that calculating the RQ-value (ratio of the carbon production rate and oxygen consumption rate) with off-gas measurements of O_2 and CO_2 , could be a good indicator for the chemical oxygen demand to total organic carbon (COD/TOC) ratio of the waste in the influent. Analogously, Baeten et al. (2021) could show that the CO_2 emitted per kg catabolized COD corresponded to the COD/TOC ratio in a reactor with balanced nitrification and denitrification.

Leu et al. (2010) showed that the nitrification performance of the activated sludge process could be estimated by measuring the O_2 and CO_2 in the off-gas. For this, the relationships between OTR, OUR, CTR, CPR and nitrification performance were investigated. The ratio of CTR to OTR could indicate the relative rates of heterotrophic and nitrifier activity.

1.3.5 Potential of process control with off-gas analysis

As measurements of the O_2 or CO_2 concentration in the off-gas can tell something about the biological reactions in the liquid phase, these measurements could be used for control of the treatment plant.

Limited literature is available on this topic. What can be found is mostly applied on continuous plants (Hellings et al., 1996; Leu et al., 2010), but as indicated in Baeten et al. (2021) off-gas analysis (and thus control) is more easily applicable in sequentially operated plants. Furthermore, as an SBR operates in the transient state, changes in the concentration profile of the off-gas will be visible. This implies that breakpoint control in the gas-phase similar to the principle of indirect control in the liquid phase (discussed in Section 1.1.4.2) could be possible.

In the future, the monitoring (and control) of greenhouse gases will become more important in the view of climate change. Therefore, off-gas analysis equipment will have to be installed regardless. As the equipment will be already present, control based on off-gas analysis could easily be applied as an additional control system for the wastewater treatment plant.

1.4 Conclusions literature review

Continuous flow reactors and sequencing batch reactors are both well-established systems for biological wastewater treatment. These two systems involve similar reactions by microorganisms to remove organic matter (COD), nitrogen and phosphorus.

Control is an important aspect of the operation of a wastewater treatment plant, especially for minimizing the energy-intensive aeration. As the continuous flow reactor operates in a steady state under mixed conditions, control based on a (fixed) setpoint is often applied. However, as a sequencing batch reactor operates in a transient state, dynamic profiles of pollutants in the liquid phase (e.g. ammonium or phosphate) can be used for direct control. Furthermore, indirect real-time control strategies, involving the measurement of pH, ORP and DO, are an inexpensive and robust option for control of SBRs, as relative changes in the profile of these variables can indicate the end of a removal process.

Off-gas analysis has multiple applications in a wastewater treatment plant by taking into account the principles of gas-liquid mass transfer (e.g. monitoring of aeration characteristics, influent composition or greenhouse gas emissions). The indirect control strategies in the liquid phase of a sequencing batch reactor could be complemented or maybe even replaced by measuring in the off-gas due to different advantages related to the latter. Monitoring biological reactions in the liquid phase by measuring oxygen and carbon dioxide in the off-gas is possible, as suggested by Hellinga et al. (1996) and Leu et al. (2009). However, as described in this literature review, research on how to put these principles into practice is limited.

1.5 Thesis objectives

In the remaining chapters of this thesis, the potential of off-gas analysis to monitor and control biological processes in an SBR reactor will be investigated through model simulations.

As it is often preferred to minimize aeration during operation, the initial focus is on controlling the aerobic phase by detection of the end of nitrification through off-gas analysis. If the aerobic phase can be ended at the end of nitrification, energy and time are saved while reaching a sufficiently low ammonium concentration. A method for detecting the end of nitrification through off-gas analysis was already proposed by a former thesis student at the BioCo Research Group, Wouter Michiels. He was able to link the end of nitrification with relative changes in the oxygen and carbon dioxide off-gas profiles. However, the method was only developed and verified in open loop, i.e. it was not yet implemented into the model to control the aerobic phase length (Michiels, 2020).

The objective of this thesis is to further explore the feasibility of detecting the end of nitrification with off-gas analysis. The starting point is the proposed detection method which will be validated and fully implemented in a model (closed loop implementation). The benefits of using this detection strategy will be defined, and its robustness in closed loop will be tested with different influent compositions.

Additionally, this thesis will investigate if the end of denitrification in the anoxic phase can be detected by off-gas analysis, thereby expanding its potential applications.

In conclusion, the following research question is formulated for this thesis:

Can a sequencing batch reactor be controlled based on off-gas analysis?

This overall research question is addressed through four sub-questions:

1. Can the end of nitrification during the aerobic phase be detected based on the oxygen and carbon dioxide off-gas profiles?
2. What are the benefits of closed loop control of the aerobic phase length through off-gas analysis?
3. Is closed loop control of the aerobic phase length robust for a range of constant influent conditions and a dynamic influent?
4. Can the end of denitrification during the anoxic phase be detected based on off-gas analysis?

2. MATERIALS AND METHODS

2.1 System under study

To answer all research questions through model simulation, a reference case study was first defined.

2.1.1 Influent composition

To study the research questions a constant and a dynamic influent composition are required. Influent data were based on values given in BSM2 (Solon et al., 2017). BSM2 is a benchmark tool developed by the IWA task group to be able to compare developed control strategies in a reference simulation model with a defined plant-layout, influent load and evaluation criteria (Alex et al., 2008). The influent data represent a municipal wastewater inflow with minor contributions of industrial wastewater. The average constant composition was used, as well as a dynamic influent composition for 609 days. This 609-day period is proposed in BSM2 to cover a full range of seasonal variations and long-term performance trends. The composition of the constant influent and the applied range for the dynamic influent can be found in Appendix A.

2.1.2 Sequencing batch reactor cycle

BSM2 only defines a configuration for continuous wastewater treatment (Alex et al., 2018). In the search for a similar benchmark model defining an SBR configuration and its operating strategy (i.e. phase lengths in one batch cycle), the article by Pons et al. (2004) was found. This article proposes a configuration and operation strategy for SBRs while still applying the influent load and evaluation criteria of BSM1, the predecessor of BSM2. This configuration and operating strategy are based on an existing pilot-scale system used by Casellas et al. (2003) and Casellas et al. (2006) for their research on control strategies. Therefore, the SBR dimensions and operation strategy of this article were used as reference case as there was no common approach found in literature to adequately determine cycle lengths for an SBR based on influent composition. The reference case used in this thesis is the same as the one in Michiels (2020).

For the cycle length, a duration of 24 hours was considered by Casellas et al. (2006), the fixed lengths of all phases are presented in Table 2.1.

Table 2.1: Overview of the length of all phases in an SBR as applied in Casellas et al. (2006).

<i>Anaerobic phase with feeding</i>	3 hours
<i>First aerobic phase</i>	6 hours
<i>First anoxic phase with extra feeding</i>	4 hours
<i>Second aerobic phase</i>	3 hours
<i>Second anoxic phase</i>	5 hours
<i>Third aerobic phase</i>	0.5 hours
<i>Settling phase</i>	1.5 hours
<i>Draw phase</i>	0.5 hours
<i>Idle phase</i>	0.5 hours

First, the feeding phase provides the anaerobic conditions necessary for phosphorus removal. During the following aerobic phase nitrification and phosphate uptake will occur. In the anoxic phase there is additional feeding to provide sufficient COD, necessary for optimal denitrification as explained in Section 1.1. This is followed by an alternation of two aerobic phases and an anoxic phase to ensure a good effluent quality after the additional feeding. The process of settling was taken into account in the model by a fixed sludge retention time (SRT) of 30 days (Batstone et al., 2002). Assuming a negligible effect of the settling phase length on the reactor performance, the length of this phase was not considered. Hence, the cycle length was reduced to 22.5 hours in the model compared to the case study of Casellas et al. (2006). The phase cycle is ended by a draw phase and idle phase.

The considered sequencing batch reactor has a working volume of 1.32 m^3 with a surface area of 1.25 m^2 . As the initial volume is 0.66 m^3 , the feeding volume is 0.66 m^3 , equally divided over two feeding moments in the SBR cycle. The volume exchange ratio (VER) is thus equal to 50 %. During the anaerobic and anoxic phases there is no aeration (k_{La} equal to 0 d^{-1}), while for the aeration phases a constant k_{La} of 240 d^{-1} is considered. There is no active control on aeration. A schematic representation of the SBR reference cycle can be seen in Figure 2.1.

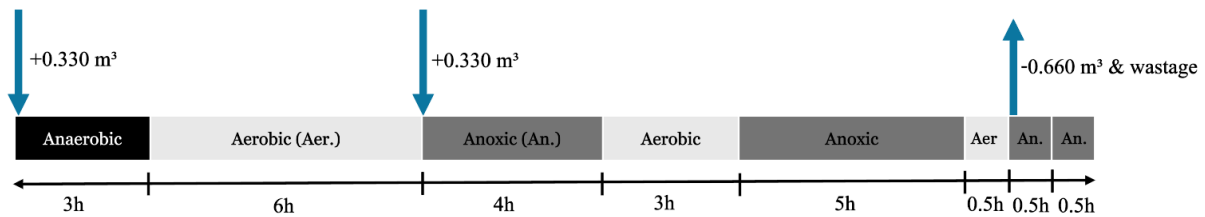


Figure 2.1: Schematic representation of the reference SBR cycle (Casellas et al., 2006). Black represents an anaerobic phase, light grey an aerobic phase and dark grey an anoxic phase. The final two cycles are the draw and idle phase, with during the draw phase also wastage of sludge flocs, adapted from Michiels (2020).

2.2 Model description

Biological behaviour during operation of the sequencing batch reactor system was simulated based on the activated sludge model ASM2d developed by Henze et al. (1999). Given the thorough analysis of off-gas oxygen and carbon dioxide concentrations in the current thesis, an accurate simulation of the off-gas phase was necessary. For precise modelling of off-gas carbon dioxide, exact pH values in the SBR system are required, which are not provided by the ASM2d model. Therefore, an extension on ASM2d by Flores-Alsina et al. (2015) was chosen: a plant-wide aqueous phase chemistry module describing pH variations and ion speciation/pairing in wastewater treatment. The full model is implemented in Matlab/Simulink.

The model has to simulate the behaviour of a sequencing batch reactor with varying volume depending on the phases of the cycle. However, the implementation by Flores-Alsina et al. (2015) represents a continuous flow reactor operating at a constant volume. Therefore, adaptations had to be made in Simulink and Matlab to obtain the desired SBR configuration. Additionally, an off-gas phase simulation was integrated into the model to capture oxygen and carbon dioxide off-gas profiles during simulation. These adaptations were carried out by Michiels (2020) in a previous thesis at the BioCo research group.

In the current thesis, additional modifications were implemented in the model to address the research questions, while maintaining the overall model structure. Therefore, an extensive explanation of the model structure can be found in Appendix B, whereas the model adaptations required for this thesis are discussed in Section 2.3. How the model was adapted from the original model to a sequencing batch reactor configuration is also described in Appendix B.

2.3 Research outline

2.3.1 Reference case: model validation and process performance

The research started by validating the model outlined in Appendix B with the defined reference case and a constant influent (Table A.1 in Appendix A). The model was run to understand its structure, analyse its results and correct any errors. Simulations of the model were performed for a duration of 150 days (160 cycles) to check if steady state was reached. Process performance was assessed by evaluating the profiles of ammonium, nitrate, phosphate and liquid oxygen during operation.

2.3.2 Detecting the end of nitrification: strategy validation

After model validation, the proposed strategy by Michiels (2020) to detect the end of nitrification by analysis of the oxygen and carbon dioxide off-gas profiles was evaluated. As a different influent was applied during simulation in this thesis and a substantial error was corrected during model validation, it was verified if the same strategy could still be applied. This was done by linking

the off-gas concentration profiles of oxygen and carbon dioxide to the nitrification process in the liquid phase. It was evaluated if similar relative changes in the off-gas profiles could be registered as shown by the proposed detection strategy. The detection strategy should be able to detect the end of nitrification, which is defined as an ammonium concentration below $1 \text{ g NH}_4^+ \cdot \text{m}^{-3}$.

2.3.3 Closed loop analysis

The validated detection strategy was implemented into the model to end the first aerobic phase after detection of the end of nitrification. Multiple adaptations were done in the model to be able to simulate a variable SBR cycle, i.e. the aerobic phase length now had a variable length instead of a fixed length of 6 hours. The model is defined to simulate in *closed loop* as the aerobic phase length is controlled by the detection strategy.

The feasibility of the detection strategy was first validated by a simulation of the closed loop model with a constant influent. The aerobic phase length and ammonium concentration at the time of detection were checked during evaluation. If these values did not comply to the definition of the end of nitrification, the detection strategy was adapted.

Subsequently, the benefits of the detection strategy to control the aerobic phase were investigated. A comparison was made between an open loop simulation (detection strategy is not implemented) and a closed loop simulation with a constant influent. Both simulations were run for 609 days. To ensure steady state during evaluation, only the last 365 days were evaluated. The open loop and closed loop simulation were compared in number of cycles during these 365 days, volume of treated wastewater, average aerobic phase length and average ammonium concentration at the end of the aerobic phase. Furthermore, the reduction in total consumed aeration energy (AEN) (kWh) was calculated. In BSM2 it is proposed to calculate the total consumed aeration energy over the entire evaluation period of 365 days (Vrecko et al., 2014):

$$AEN = \frac{C_{O_2,L,15}^*}{1.8 \cdot 1000} \int_{t_{start}}^{t_{end}} V \cdot k_{La(O_2),15}(t) dt \quad (2.1)$$

where V represents the volume of water in the reactor (m^3), $k_{La(O_2),15}$ (d^{-1}) the mass transfer coefficient of oxygen at 15°C , $C_{O_2,L,15}^*$ ($\text{g} \cdot \text{m}^{-3}$) the oxygen saturation concentration at 15°C ($8 \text{ g} \cdot \text{m}^{-3}$) and t_{start} and t_{end} the start and end time of the evaluation period, respectively. However, in the simulations of this thesis the required aeration energy remained constant during all phases, except for the shortened aerobic phase. Furthermore, at steady state the reduction in aeration energy is the same for each cycle. Therefore, only the required aeration energy over one aerobic phase was calculated and compared between a closed loop and an open loop simulation. Hence, Eq. 2.1 is reduced to (with the volume and mass transfer coefficient being constant during the aerobic phase):

$$AEN = \frac{C_{O_2,L,15}^*}{1.8 \cdot 1000} \cdot V \cdot k_{La(O_2),15} \cdot t_{aerobic \ phase} \quad (2.2)$$

After implementation and evaluation of the detection strategy in the first aerobic phase, the strategy was also implemented for the second aerobic phase. The results were briefly evaluated. The implementation was not done for the third aerobic phase, as this phase is too short.

2.3.4 Influence of influent characteristics on detection strategy robustness

2.3.4.1 Constant influent conditions

The robustness of the detection strategy was first assessed through application of different constant influent conditions. The influence of the ammonium and phosphate influent concentration was evaluated through simulations of the closed loop model, with implementation of the strategy only in the first aerobic phase. A simulation over 609 days was repeated for different combinations of ammonium and phosphate influent concentrations, and evaluation was based on the number of cycles, aerobic phase length, ammonium concentration at the end of the aerobic phase and aeration energy. Table 2.2 indicates the concentrations of ammonium and phosphate for a low, medium and high strength municipal wastewater composition (Volcke et al., 2023). To test the robustness of the strategy all possible combinations were evaluated, i.e. 9 simulations were performed.

Table 2.2: Ammonium and phosphate concentrations in municipal wastewater (in m^3) (Volcke et al., 2023).

	Low strength	Medium strength	High strength
Phosphate	4	10	15
Ammonium	20	45	75

It should be noted that the listed influent concentrations are not the concentrations experienced by the microorganisms in the SBR. The initial volume in the cycle, i.e. the volume of water that was not wasted in the previous cycle, is equal to 0.66 m^3 . During the first feeding step in the anaerobic phase 0.33 m^3 is added. The influent is thus diluted by a factor of 3. For example, if an influent with an ammonium concentration of 75 g.m^{-3} is fed, the concentration in the reactor will be equal to 25 g.m^{-3} , plus the low ammonium concentration from the previous cycle (which should be below the effluent limits). During additional feeding in the first anoxic phase, the remaining 0.33 m^3 is fed and again diluted. This was considered when evaluating the effect of the ammonium and phosphate concentration on the biological processes and the robustness of the detection strategy.

2.3.4.2 Dynamic influent conditions

The detection strategy was finally evaluated by simulating the closed loop model with a dynamic influent to assess its applicability during more realistic conditions. The strategy was only applied in the first aerobic phase of the cycle. A dynamic open loop simulation was compared to a dynamic closed loop simulation to evaluate the benefits of implementing the detection strategy.

First, a simulation was run for 300 days in open loop with a constant influent to reach steady state, as proposed in BSM2 (Alex et al., 2008). The steady state values were used as initial values in the simulations over 609 days with a dynamic influent in open and closed loop, respectively. Again, the detection strategy was evaluated for the last 365 days of the simulation and the evaluation was based on the same parameters as for the constant influent evaluation.

2.3.5 Detecting the end of denitrification: strategy development

Similar as for the detection of nitrification through analysis of the off-gas profiles of oxygen and carbon dioxide, it was investigated if this is also possible for detecting the end of denitrification.

In the reference case, no aeration occurred during the anoxic phase, hence no off-gas flow rate was present. For detection of the end of denitrification, aeration at a low flow rate was applied during the anoxic phases to be able to analyse the off-gas. By applying a $k_L a$ equal to 1 d^{-1} a lower flow rate was simulated in the model as can be seen in Eq. 2.3 (further elaborated in Appendix B):

$$Q_{in}^G = \frac{k_L a_{(O_2)}(p_{atm}^G + \rho g \frac{V}{2S})A}{0.6p_{atm}^G} \quad (2.3)$$

Nitrogen gas (N_2) is produced during denitrification (Section 1.1.2). Its off-gas concentration is affected by the process of denitrification, therefore, an off-gas flow simulation of nitrogen gas was added to the model - next to oxygen and carbon dioxide - in a similar way as described in Appendix B. Table 2.3 lists all additional parameters used for the off-gas nitrogen flow.

Table 2.3: Additional parameters used in off-gas N_2 calculation at 293 K

Parameter	Symbol	Value	Unit	Reference
Henry's law constant for N_2	H_{N_2}	0.0159	-	(Sander, 2015)
Molar mass of N_2	M_{N_2}	28	g.mole^{-1}	-
Molar fraction of N_2 in gas inflow	x_{in,N_2}^G	0.78084	-	(The Engineering Toolbox, sd)
Diffusivity of N_2	D_{N_2}	$2.01 \cdot 10^{-9}$	$\text{m}^2 \cdot \text{s}^{-1}$	(Ferrell and Himmelblau, 1967)

First, the model was run in open loop for 150 days with a constant influent to check if steady state was reached. It was evaluated if denitrification is still performed adequately with the low presence of oxygen during the anoxic phase. To develop a strategy for detecting the end of denitrification, the off-gas profiles of oxygen, carbon dioxide and nitrogen were analysed together with the profile of nitrate. Similar to the detection strategy for the end of nitrification, it was evaluated if detectable relative changes in the off-gas profiles were observed at the end of denitrification in the anoxic phase.

3. RESULTS AND DISCUSSION

This chapter presents the results of the model simulations, accompanied by their discussion. Section 3.1 validates the model for further use in this study. In Section 3.2, the focus shifts towards identifying the end of nitrification through off-gas analysis by validating an existing detection strategy. In Section 3.3 the detection strategy is implemented into the model to assess its feasibility for closed loop control of the aerobic phase. Moreover, in Section 3.4 the robustness of the detection strategy is tested by applying a dynamic influent and a range of ammonium and phosphate concentrations in the constant influent. Section 3.5 extends the application of off-gas analysis to detect the end of denitrification during the anoxic phase.

3.1 Reference case: model validation and process performance

The model simulating operation of the defined SBR system with a constant influent, as defined in Section B.1 of Appendix B, was validated through a simulation over 150 days.

When the output of the original model was briefly evaluated, it was observed that the inert particulate organic material (X_I) is extremely high after 150 days, exceeding $15\,000\text{ g}\cdot\text{m}^{-3}$, and continuously increasing after each cycle (Figure C.1 in Appendix C). This high concentration is caused by a wrong definition of the SRT in the model of Michiels (2020). Due to a mistake in units, the SRT was set at 720 days instead of the intended 30 days in the reference system. As the amount of settling and wasting of sludge was based on this SRT in the model, the amount of particulates that are removed from the reactor per cycle is almost negligible, which explains the buildup of inert particulate matter. The SRT was corrected to 30 days and the model was simulated again for 150 days. After this adaptation, the inert particulate organic material concentration reached a realistic value (see Figure C.2 in Appendix C). The fraction of X_I at an SRT of 30 days was approximately 50 % compared to the concentration of heterotrophic, autotrophic and phosphate-accumulating organisms. This fraction is confirmed in Lopez-Vazquez et al. (2020b) where similar values are reported for an SRT of 30 days.

During simulation, steady state was reached after approximately 75 days for all organisms (see Figure C.3 in Appendix C). After this check, the last cycle of the simulated 150 days was evaluated on process performance. The liquid concentration profiles of ammonium, nitrate, phosphate, pH and dissolved oxygen during this cycle can be seen in Figure 3.1.

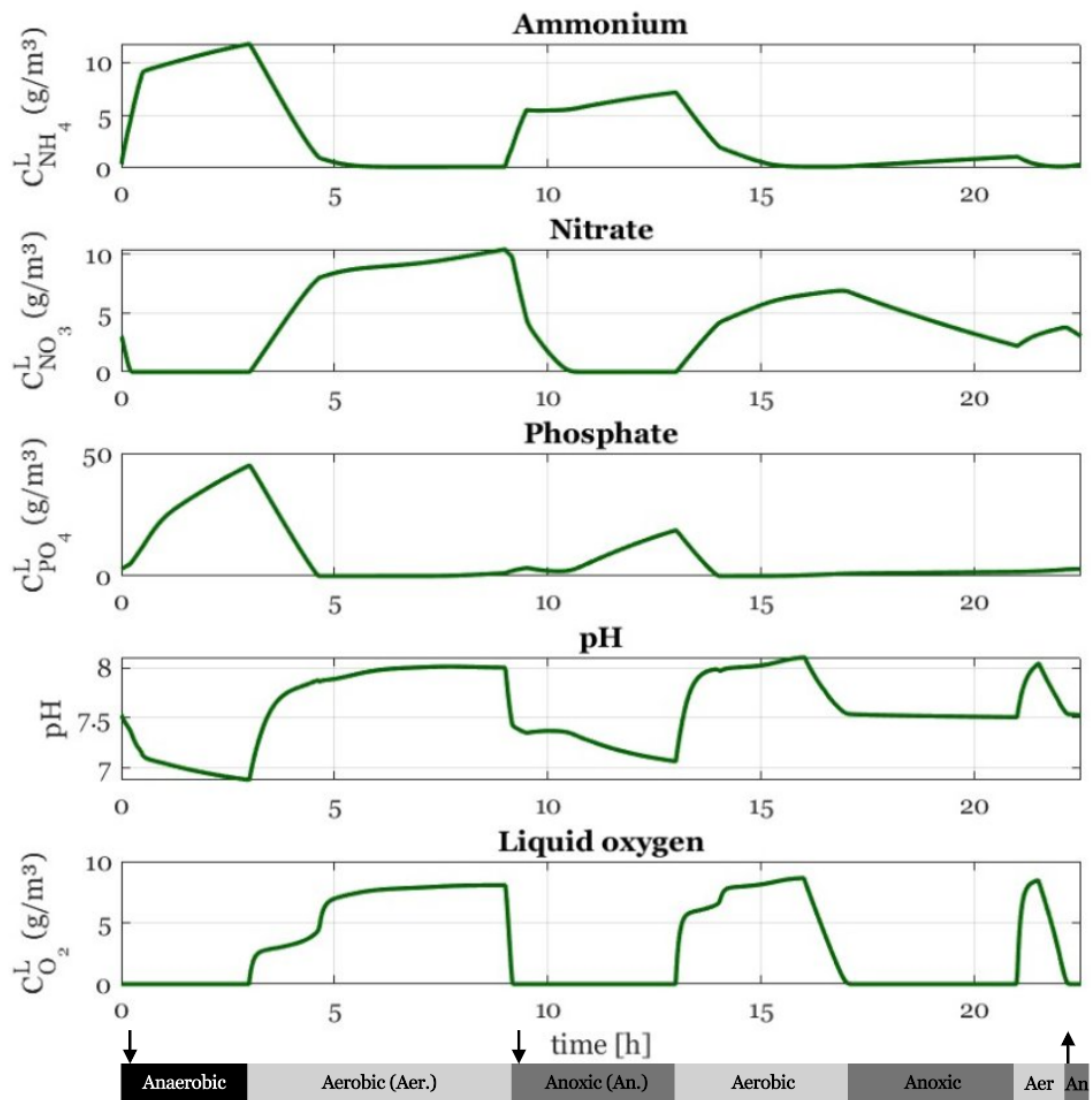


Figure 3.1: Concentration profiles of ammonium, nitrate, phosphate, pH and dissolved oxygen during the last cycle at steady state (day 150). The arrows on the bar below the plots indicate the time of (additional) feeding (\downarrow) or wasting (\uparrow).

The ammonium concentration increases during the anaerobic phase due to feeding and hydrolysis (Figure 3.1). In the aerobic phases, ammonium is removed by nitrification and converted into nitrate. In the first anoxic phase, the ammonium concentration initially increases because of additional feeding. Then it further increases by hydrolysis when anaerobic conditions occur due to the absence of nitrate after the end of denitrification.

The phosphate concentration increases in the anaerobic phase due to feeding, but primarily due to phosphate release by the PAO. During the aerobic phase phosphate is removed by uptake. It can be noted that the concentrations of phosphate are high compared to the concentrations of ammonium. This explains the absence of an ammonia valley in the pH profile during the aerobic phase, the effect of phosphate uptake on the pH is higher than the effect of nitrification. The phosphate concentration increases during the last part of the anoxic cycle due to phosphate release under anaerobic conditions due to the absence of nitrate after the end of denitrification.

The dissolved oxygen profile is zero during the anoxic and anaerobic phases, while its concentration increases during the aerobic phases. This is visible in the concentration profile due to a constant applied aeration flow rate. An inflection point is visible during the first and second aerobic phase at the end of phosphate uptake. An effect on the dissolved oxygen profile at the end of nitrification is not visible in this graph, but a limited effect can be observed when looking at the output data in detail.

The simulated concentration profiles of ammonium, nitrate, phosphate, pH and dissolved oxygen confirm the discussion of Section 1.1.4.2 in the literature review. Based on this verification and the above discussion, it can be concluded that the model is able to simulate the behaviour of an SBR adequately and can be further used for research.

3.2 Detecting the end of nitrification: strategy validation

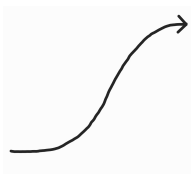
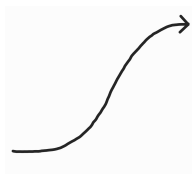
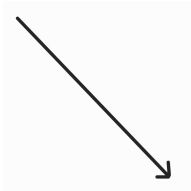
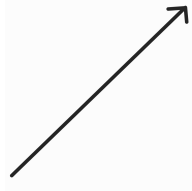
A strategy aimed at identifying the end of nitrification in the aerobic phase through off-gas analysis was proposed by Michiels (2020). This detection strategy is based on monitoring both oxygen and carbon dioxide concentrations in the off-gas. Relative changes in these off-gas concentrations at the end of nitrification could be registered and translated in a strategy to control the aerobic phase length.

Changes in the off-gas oxygen concentration reflect changes in the dissolved oxygen levels, linked through gas-liquid transfer. Similarly, off-gas carbon dioxide is influenced by the dissolved carbon dioxide concentration and pH through the bicarbonate buffer system as explained in Section 1.3. Since the end of the nitrification process has an influence on the dissolved oxygen and carbon dioxide concentrations, changes in the off-gas oxygen and carbon dioxide levels will indirectly indicate the end of the process. Mathematically linking these changes to the end of nitrification will facilitate the implementation of the strategy. An overview of these changes and their mathematical translation can be seen in the second column of Table 3.1.

At the end of nitrification, reduced oxygen consumption by microorganisms decreases oxygen uptake and oxygen transfer in the liquid phase. Consequently, less oxygen is transferred from the gas phase to the liquid phase during aeration. This leads to an increase in the off-gas oxygen concentration, occurring as an upward inflection point in the concentration profile (see Table 3.1). This inflection point will change from positive to negative in its second derivative, while transgressing zero, which can be easily detected during off-gas monitoring.

During the aerobic phase, uptake of phosphate by the PAO will occur simultaneously with nitrification. The process of phosphate uptake will thus also consume oxygen. This affects the off-gas oxygen concentration similarly as the process of nitrification, with a detectable upward inflection point in its profile at the end of the phosphate uptake process. Depending on the ammonium-to-phosphate ratio of the influent, phosphate uptake may end before or after nitrification. This could lead to an early false detection of the end of nitrification when only evaluating the oxygen off-gas profile. Therefore, differentiation between these two endpoints is needed in the detection strategy. This is possible by monitoring the carbon dioxide off-gas profile in addition to the oxygen off-gas profile. While the end of nitrification increases the pH due to a reduction in proton production, the end of phosphate uptake lowers the pH. Consequently, off-gas carbon dioxide concentrations increase at the end of phosphate uptake, but decrease at the end of nitrification. The increase and decrease translate mathematically in a positive and negative first derivative, respectively. This allows, after detecting an inflection point in the oxygen off-gas profile, to identify the end of nitrification when the first derivative of the off-gas carbon dioxide is negative. When the first derivative is positive, the oxygen increase can be attributed to the end of phosphate uptake. In Table 3.1, the last column indicates the behaviour of off-gas oxygen and carbon dioxide during the end of phosphate uptake for comparison.

Table 3.1: Relative changes in off-gas concentration profiles and mathematical translation at the end of nitrification and phosphate uptake. t indicates the current time of the SBR operation and t_{ip} indicates the time of the inflection point.

	End of nitrification	End of phosphate uptake
Off-gas oxygen	Increasing inflection point	Increasing inflection point
		
<i>Detection?</i>	$\frac{d^2 C_{O_2}^G}{dt^2}(t < t_{ip}) > 0$ and $\frac{d^2 C_{O_2}^G}{dt^2}(t_{ip}) = 0$ and $\frac{d^2 C_{O_2}^G}{dt^2}(t > t_{ip}) < 0$	$\frac{d^2 C_{O_2}^G}{dt^2}(t < t_{ip}) > 0$ and $\frac{d^2 C_{O_2}^G}{dt^2}(t_{ip}) = 0$ and $\frac{d^2 C_{O_2}^G}{dt^2}(t > t_{ip}) < 0$
Off-gas carbon dioxide	Decreasing	Increasing
		
<i>Detection?</i>	$\frac{dC_{CO_2}^G}{dt}(t) < 0$	$\frac{dC_{CO_2}^G}{dt}(t) > 0$

The detection strategy successfully identified the end of nitrification in the report of Michiels (2020). However, in the current study, a different influent was applied and the original model had to be adapted due to a wrong definition of the SRT. Therefore, it was investigated based on the results from the 150 day simulation of the adapted model, if this detection strategy is still valid for a constant influent. The concentration profiles of ammonium, phosphate, off-gas oxygen and off-gas carbon dioxide during the first aerobic phase of the reference cycle at steady state in the current study are presented in Figure 3.2.

The off-gas oxygen concentration profile only shows one clear upward inflection point, attributed to the end of phosphate uptake. Simultaneous with this inflection point, there is a limited increase in the off-gas carbon dioxide, indicated by a positive first derivative. However, the end of nitrification cannot be distinguished based on these plots. The range of the y-axis in Figure 3.2 is wide due to the significant response in the off-gas profiles after the end of phosphate uptake. However, when the range of the y-axis is considerably reduced, a response can be seen in the zoomed-in off-gas profiles which can be attributed to the end of nitrification as seen in

Figure 3.3. There is an inflection point in the off-gas oxygen concentration as confirmed via the second derivative and, simultaneously, the carbon dioxide off-gas is decreasing. This response confirms the proposed detection strategy. On Figure 3.3, the response in the off-gas due to the end of phosphate uptake cannot be clearly seen due to the smaller axis limits. Although the end of nitrification is detected at a concentration much lower than the previously proposed threshold of $1\text{g NH}_4^+ \cdot \text{m}^{-3}$, using this detection strategy shortens the length of the aerobic phase still by about an hour.

The minor response at the end of nitrification in the off-gas profiles may be attributed to the fraction of autotrophic organisms and phosphate-accumulating organisms present in the SBR during the aerobic phase. These fractions differ from the original model in Michiels (2020) due to different SRTs, as seen in Table 3.2. In the simulation of this study, the fraction of autotrophic organisms in the aerobic phase is only 2.6 % at steady state, while the fraction of phosphate-accumulating organisms exceeds 30 %. This explains why the end of phosphate uptake has a larger effect on the off-gas profiles compared to the end of nitrification as e.g. more oxygen will be simultaneously consumed during phosphate uptake. If phosphate uptake ends, this will have a larger effect on the off-gas oxygen profile. Due to the lower autotrophic fraction, this effect is smaller at the end of nitrification. The discrepancy between the fractions of autotrophic and phosphate-accumulating organisms is less pronounced in the study of Michiels (2020) as seen in Table 3.2, where the fraction of autotrophic organisms is also twice as high compared to this study. Literature on the specific fractions of active biomass during removal of organic matter, nitrogen and phosphorus in function of the SRT in an SBR is limited. However, the biomass fractions in this study were similar compared to literature data for continuous wastewater treatment. At an SRT of 30 days an autotrophic fraction below 3 % is reported when only nitrogen is removed (Ekama et al., 2023). With only phosphorus removal the fraction of phosphate-accumulating organisms is higher than 40 % (Lopez-Vazquez et al., 2020a).

Table 3.2: Fractions of active biomass (heterotrophic, autotrophic and phosphate-accumulating organisms) in the SBR during the first aerobic phase in the adapted and original model.

	Adapted model	Original model
Heterotrophic organisms	63.9%	75.7 %
Autotrophic organisms	2.6 %	5.8 %
Phosphate-accumulating organisms	33.5 %	18.5 %

Based on the studied profiles in Figures 3.2 and 3.3, it can be concluded that the detection strategy should still be able to detect the end of nitrification, even though the relative changes in the off-gas are less pronounced.

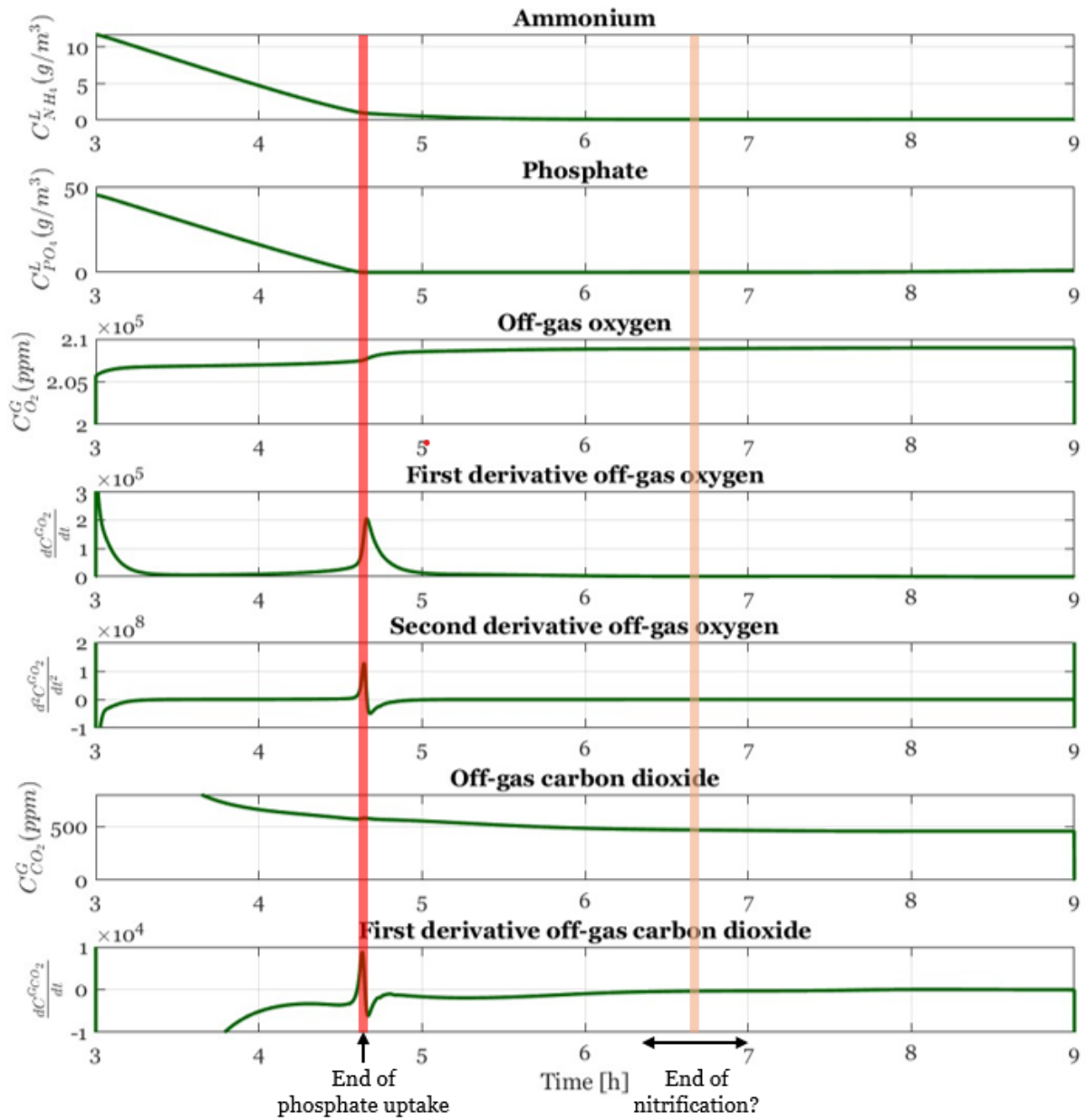


Figure 3.2: Concentration profiles of ammonium, phosphate, off-gas oxygen with its first and second derivative and off-gas carbon dioxide with its first derivative during the first aerobic phase of the last cycle (day 150). The cycle time is indicated in hours and the first aerobic phase spans hour 3 til 9 from the 22.5 hours of the cycle.

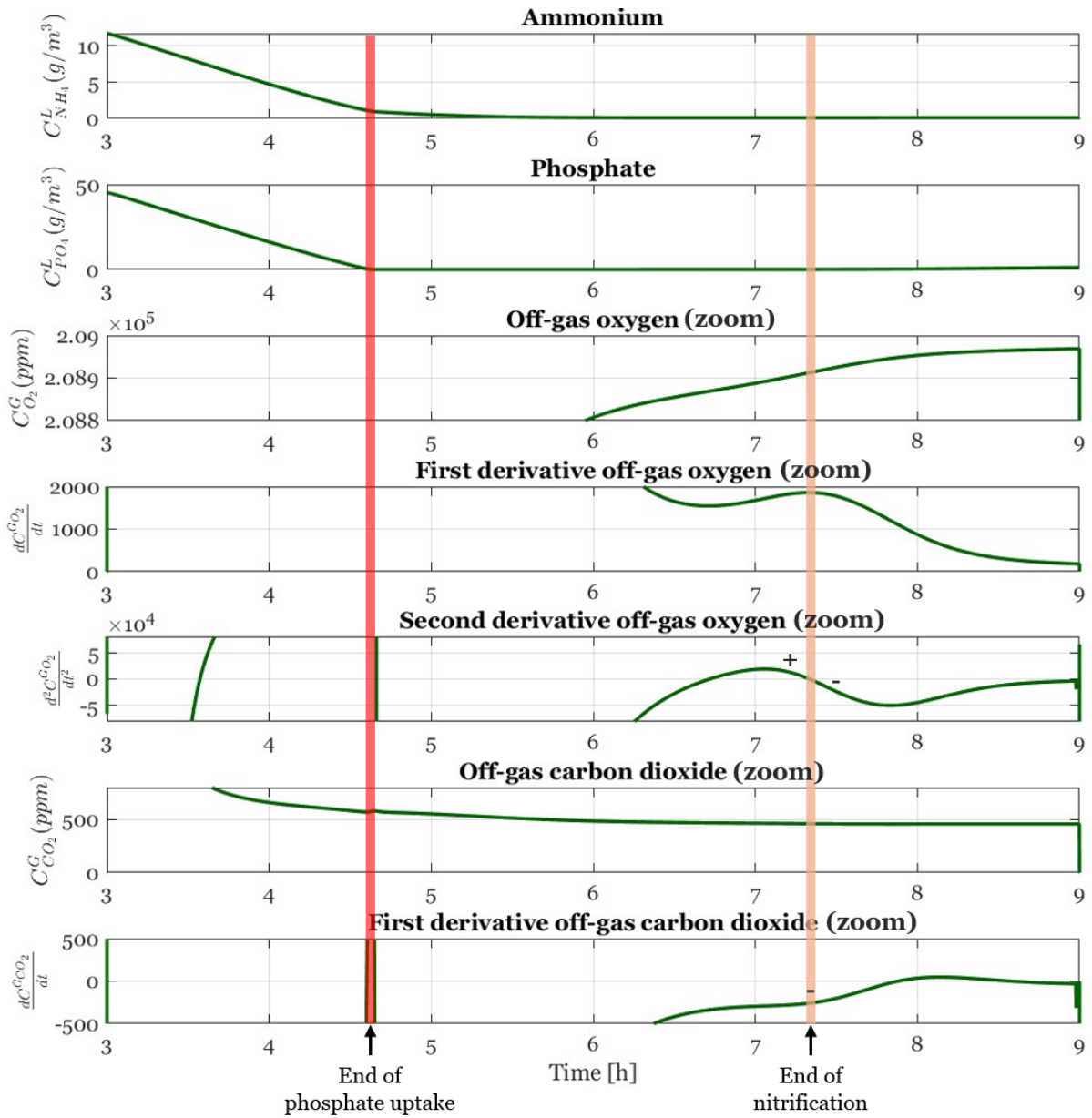


Figure 3.3: Concentration profiles of ammonium and phosphate during the first aerobic phase of the 150th cycle. The off-gas oxygen with its first and second derivative and off-gas carbon dioxide with its first derivative are **zoomed in** as compared to Figure 3.2. The cycle time is indicated in hours and the first aerobic phase spans hour 3 til 9 from the 22.5 hours of the cycle.

3.3 Closed loop analysis

3.3.1 Closed loop implementation and strategy adaptation

The detection strategy was implemented into the model to control the length of the first aerobic phase. A flowchart on how to understand and implement this detection strategy can be found in Appendix C Section C.2. With this implementation, the reactor operation switches from the aerobic phase to the anoxic phase upon detection of the end of nitrification. First, the feasibility of the strategy was investigated with a constant influent in a 150-day simulation of the closed loop model.

After approximately 100 days, steady state was reached (See Figure C.5 in Appendix C). Figure 3.4 shows the corresponding concentration profiles of ammonium, nitrate, phosphate, pH and dissolved oxygen during the last cycle. The first aerobic phase is ended after about 1 hour. However, at this moment, the ammonium concentration amounts to $5.2 \text{ g NH}_4^+ \cdot \text{m}^{-3}$, which is considerably above the defined threshold of $1 \text{ g NH}_4^+ \cdot \text{m}^{-3}$. Aeration is in fact ended before the end of nitrification, which is not desired. Visually on Figure 3.4, it appears that the first aerobic phase ended at the end of phosphate uptake. After evaluating the model output in more detail, it was concluded that this is indeed the case. Hence, the current strategy resulted in a false positive detection of the end of nitrification.

The implemented detection strategy relies on the simultaneous detection of an inflection point in the off-gas oxygen profile and a decrease in the carbon dioxide off-gas linked to the end of nitrification. A false positive detection at the end of phosphate uptake and consequently early end of the aerobic phase implies that, together with an upward inflection point in the off-gas oxygen profile, a decrease in the carbon dioxide off-gas is occurring. The expected simultaneous increase of the carbon dioxide off-gas concentration at the end of phosphate uptake did not occur (Table 3.1).

The output data of the carbon dioxide off-gas concentration were evaluated in detail to explain this unexpected behaviour. It was observed that a few time steps before the occurrence of the upward inflection point in the off-gas oxygen, the carbon dioxide concentration was increasing. As seen in Figure 3.2, the carbon dioxide concentration is constantly decreasing, with a limited increase over a short time period at the end of phosphate uptake. This increase occurred between a phosphate concentration of $0.86 \text{ g} \cdot \text{m}^{-3}$ and $0.006 \text{ g} \cdot \text{m}^{-3}$. At a concentration lower than $0.006 \text{ g} \cdot \text{m}^{-3}$ the carbon dioxide off-gas concentration decreased again. The upward inflection point in the off-gas oxygen profile occurred at a concentration lower than $0.006 \text{ g} \cdot \text{m}^{-3}$, i.e. $0.0046 \text{ g} \cdot \text{m}^{-3}$. This explains the false positive detection of the end of nitrification since the effect of the end of phosphate uptake on the oxygen and carbon dioxide off-gas concentrations did not occur simultaneously.

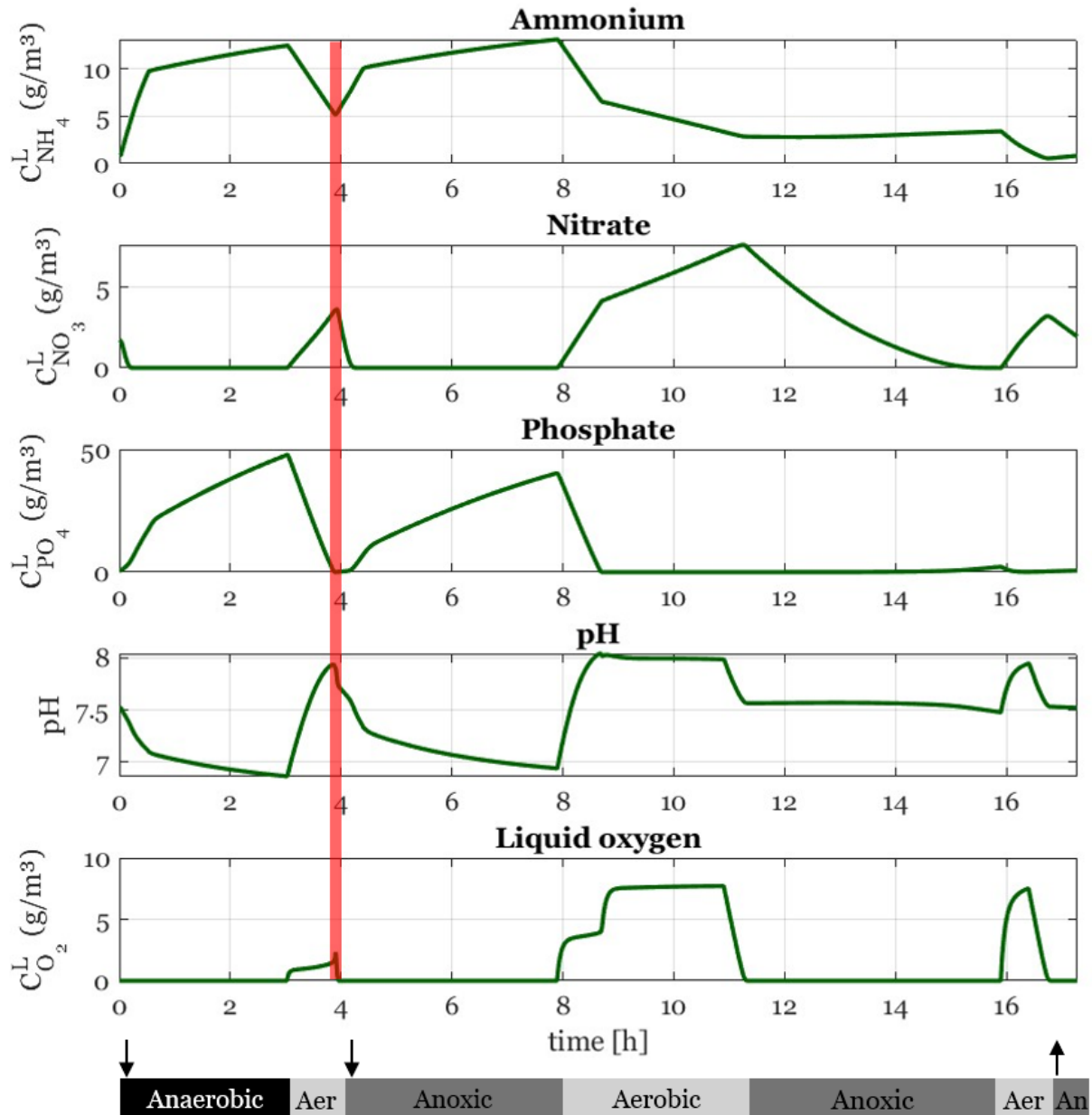


Figure 3.4: Concentration profiles of ammonium, nitrate, phosphate, pH and dissolved oxygen during the last cycle of the constant closed loop scenario (day 150). The cycle time is indicated in hours and the arrows on the bar below the plots indicate when (additional) feeding or wasting occurs. The red line indicates when the aerobic phase is ended due to detection.

The proposed detection strategy failed to detect the end of nitrification in a closed loop implementation. A new strategy was proposed where the simultaneous detection of changes in the off-gas oxygen and carbon dioxide profile is not necessary. The new strategy is able to remember if an increase in carbon dioxide occurred in a time period before detecting an upward inflection point in the off-gas oxygen concentration. In that way, the end of phosphate uptake can still be differentiated from the end of nitrification. The new detection strategy is depicted in Figure 3.5 in combination with a more detailed explanation on how to interpret the strategy.

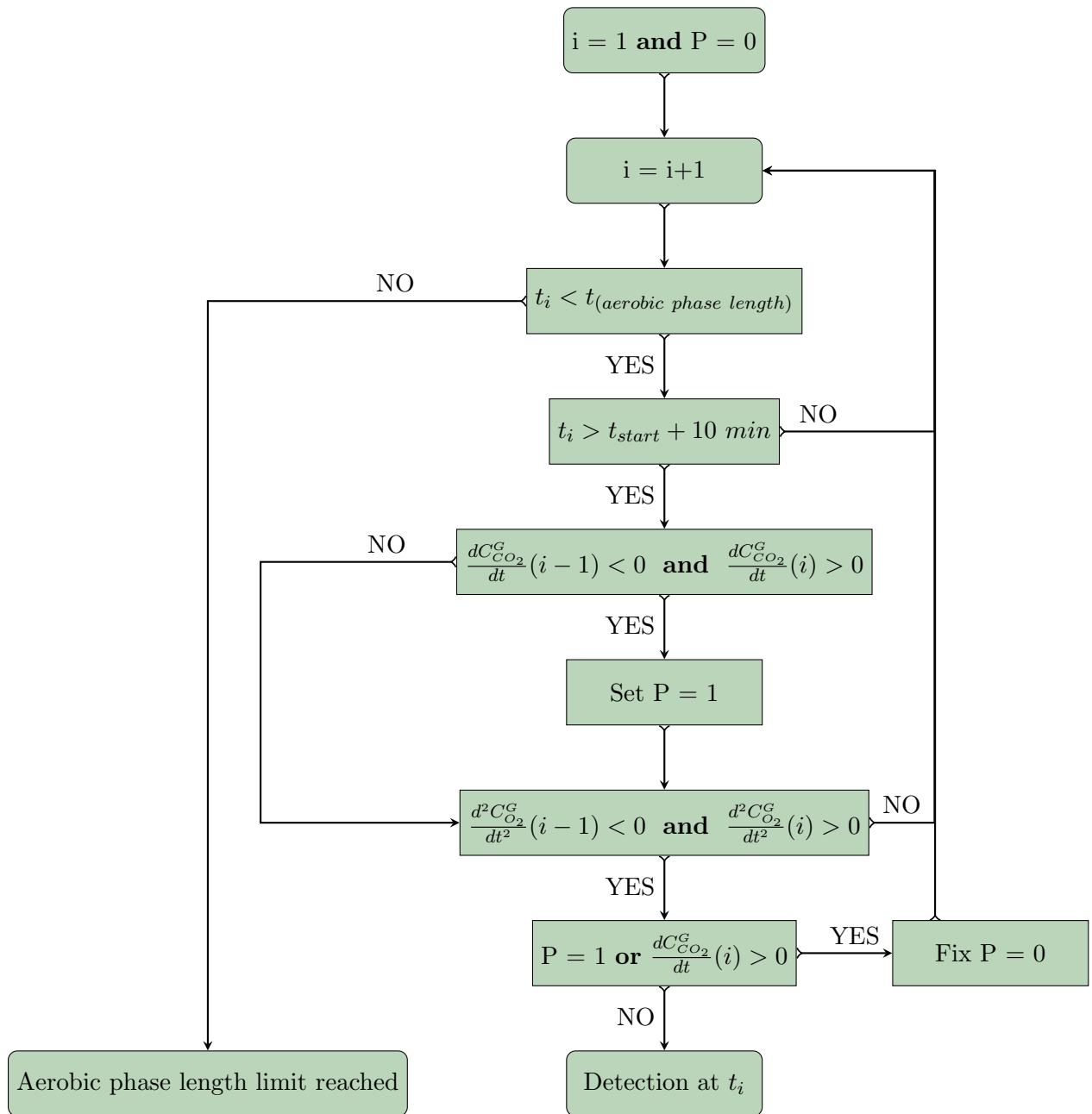


Figure 3.5: Flowchart of the new detection strategy.

Interpretation of the detection strategy flowchart

1. **Initialization:** The process starts with setting i to 1 and P to 0.
2. **Incrementing i :** i is then incremented by 1.
3. **Time check:** It is verified if the current time, t_i , is less than the specified length of the aerobic phase (6 hours).
4. **Time check (Cont.):** If the time condition is met, it checks if the current time, t_i , is greater than the start time plus 10 minutes to avoid the unstable behaviour of the off-gas flow at the start of aeration.
5. **Carbon dioxide concentration check:** If both time conditions are met, it checks if the first derivative of the carbon dioxide concentration ($\frac{dC_{CO_2}^G}{dt}$) was negative at the previous time step ($i - 1$) and positive at the current time step (i).
6. **Fixing P :** If the carbon dioxide condition is met, it fixes P to 1. This step facilitates the strategy to remember that the carbon dioxide off-gas concentration was increasing for a time period.
7. **Oxygen concentration check:** After the carbon dioxide concentration check, it checks whether the second derivative of the oxygen concentration ($\frac{d^2C_{O_2}^G}{dt^2}$) was negative at the previous time step ($i - 1$) and positive at the current time step (i). This is the mathematical translation of an inflection point in the oxygen off-gas profile.
8. **Carbon dioxide concentration check (Cont.):** If the oxygen condition is met, it is verified if P is still 1 or the first derivative of carbon dioxide ($\frac{dC_{CO_2}^G}{dt}$) is positive at time step (i).
9. **Detection:** If the conditions are met, it proceeds to "Detection at t_i ". The end of nitrification is detected and the aerobic phase is ended.
10. **Fixing P :** If the conditions for detection are not met, it fixes P back to 0.
11. **Looping back:** In the case of no detection, it loops back to increment the i variable and repeats the process until the end of nitrification is detected or the maximum length of the aerobic phase is reached.

The new detection strategy was implemented into the model and run for 150 days. As shown in Figure 3.6, the ammonium concentration is now well below the threshold of $1 \text{ g NH}_4^+ \cdot \text{m}^{-3}$ when the aerobic phase is ended. The adapted detection strategy is now able to detect the end of nitrification and subsequently end the aerobic phase.

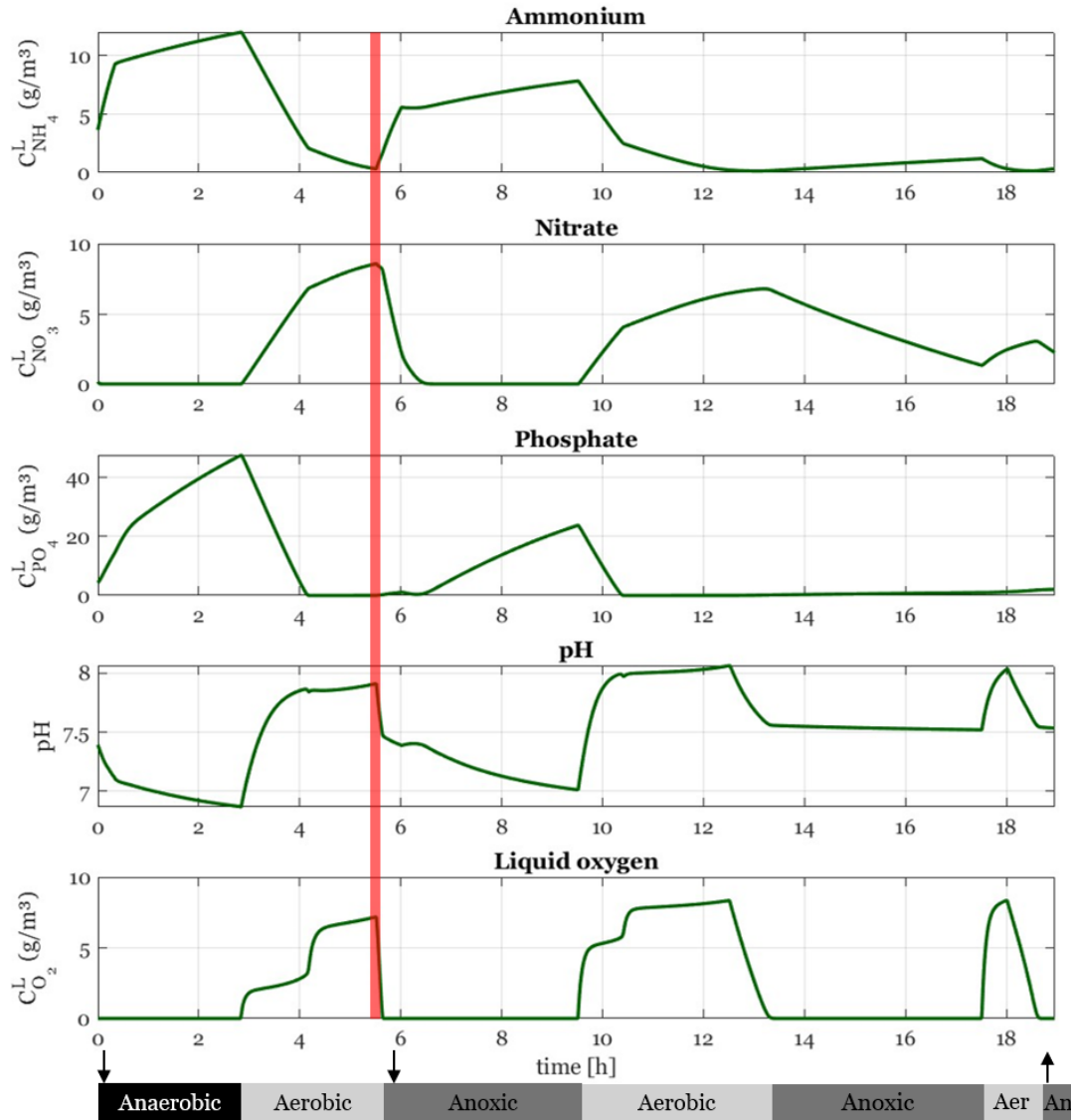


Figure 3.6: Concentration profiles of ammonium, nitrate, phosphate, pH and dissolved oxygen during the last cycle of the constant closed loop scenario with the new detection strategy. The cycle time is indicated in hours and the arrows on the bar below the plots indicate when (additional) feeding or wasting occurs. The red line indicates when the aerobic phase is ended upon detection.

3.3.2 Open loop versus closed loop: benefits

The operational advantages of applying the detection strategy were evaluated through a simulation of the closed loop model and a simulation of the open loop model where the aerobic phase length is not controlled (i.e. length is fixed to six hours). A constant influent was applied for 609 days. The last 365 days of both simulations were compared in number of cycles, average aerobic phase

length, average ammonium concentration at the end of nitrification and required aeration energy. An overview of this comparison can be seen in Table 3.3.

Table 3.3: Comparison open and closed loop simulations with a constant influent over 365 days.

	Open loop scenario	Closed loop scenario
Number of cycles	389	431
Volume treated water	513.5 m ³	568.9 m ³
Average length first aerobic phase	6 h	2h 38 min
Average ammonium concentration	0.11 g.m ⁻³	0.31 g.m ⁻³
Aeration energy in 1st aerobic phase	0.18 kWh	0.08 kWh

The closed loop simulation (Figure 3.6) showed a clear difference from the open loop simulation (Figure 3.1). Over the evaluated 365 days, 42 additional SBR cycles could be run, increasing the volume of treated wastewater by 55.4 m³. The first aerobic phase was reduced on average to 2 hours and 38 minutes, a decrease of almost 56 % compared to the defined 6 hours in the reference case. Although the ammonium concentration at the detection point was slightly higher compared to the open loop scenario, it remained well below the threshold of 1 g NH₄⁺ · m⁻³. The required aeration energy during the first aerobic phase showed a similar reduction as the average length of the aerobic phase as the equation for calculating the aeration energy assumed that the aeration energy is linearly dependent on the length of the aerobic phase. Since aeration energy is a considerable part of the cost during wastewater treatment the reduction of its demand is a huge benefit of the detection strategy.

In general, the newly adapted detection strategy is able to detect the end of nitrification with a constant influent composition and has several benefits as proven by the comparison of the open loop and closed loop simulations.

3.4 Influence of influent characteristics on detection strategy robustness

3.4.1 Constant influent conditions

The effect of the ammonium and phosphate influent concentration on the detection strategy was investigated by simulating the closed loop model with different constant influents. An influent concentration range of 20 - 75 g.m⁻³ for ammonium and 4 - 15 g.m⁻³ for phosphate was applied. The number of cycles, aerobic phase length, ammonium concentration at detection and required aeration energy of each closed loop simulation are presented with bar plots in Figure 3.7.

First, it was checked if the ammonium concentration at the end of the aerobic phase is below the defined threshold of $1 \text{ g NH}_4^+ \cdot \text{m}^{-3}$. As depicted in Figure 3.7a, only for a combination of the highest ammonium concentration ($75 \text{ g} \cdot \text{m}^{-3}$) and lowest phosphate concentration ($4 \text{ g} \cdot \text{m}^{-3}$), the end concentration is too high. Here, the detection strategy failed. After assessing the model output, it became evident that this originated from a false positive detection at the end of phosphate uptake.

To assess this false positive detection, the output of the closed loop model simulation with these specific influent conditions was further evaluated. It could be seen that during the first aerobic phase the carbon dioxide off-gas concentration is constantly increasing before detection (see Figure C.6 in Appendix C). This could be due to a high rate of nitrification compared to the rate of phosphate uptake as the autotrophic organisms are exposed to a high concentration of ammonium in the reactor¹. Nitrification produces protons and thus has a decreasing effect on the pH, this results in an increase of the carbon dioxide off-gas concentration.

The original detection strategy was adapted in Section 3.3.1 based on the assumption that the carbon dioxide concentration is constantly decreasing in the aerobic phase with only an increase at the end of phosphate uptake. The ammonium concentration and phosphate concentration were then equal to $25.2 \text{ g} \cdot \text{m}^{-3}$ and $5.7 \text{ g} \cdot \text{m}^{-3}$, respectively (Appendix B). With a significantly higher ammonium concentration of $75 \text{ g} \cdot \text{m}^{-3}$ and a low phosphate concentration, the carbon dioxide off-gas profile is constantly increasing. It is evident that the detection strategy is not robust for this different behaviour. Adapting the detection strategy to accommodate these influent conditions has to be researched in an extension of this thesis.

Combinations of $75 \text{ g} \cdot \text{m}^{-3}$ ammonium with a phosphate influent concentration of $10 \text{ g} \cdot \text{m}^{-3}$ and $15 \text{ g} \cdot \text{m}^{-3}$ also showed a continuous increase of the carbon dioxide off-gas concentration. However, as the end of phosphate uptake occurred after the end of nitrification due to the higher phosphate concentration present in the reactor, the false positive detection did not occur. All combinations with a $20 \text{ g} \cdot \text{m}^{-3}$ and $45 \text{ g} \cdot \text{m}^{-3}$ influent ammonium concentration showed a decreasing trend of the carbon dioxide off-gas concentration, here the detection strategy was feasible.

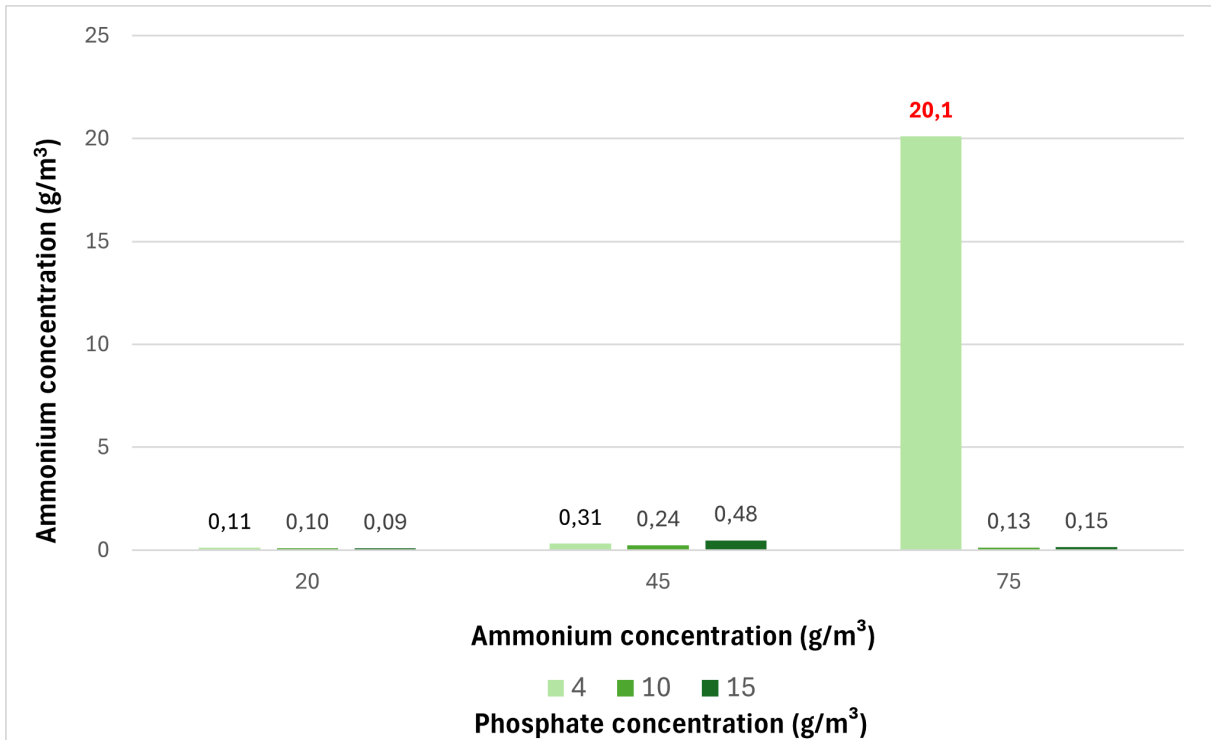
The robustness of the detection strategy was further evaluated for all influent conditions which resulted in a correct detection. The average aerobic phase length revealed a general trend towards phase length reduction across most combinations (Figure 3.7b). However, for the combination of $4 \text{ g} \cdot \text{m}^{-3}$ of phosphate and $20 \text{ g} \cdot \text{m}^{-3}$ of ammonium in the influent, no decrease was observed as the average length of the aerobic phase in this scenario is 6 hours, equal to the maximum length of the first aerobic phase. However, the output data showed that the nitrification threshold of $1 \text{ g NH}_4^+ \cdot \text{m}^{-3}$ was already reached before these six hours, indicating that the detection strategy is not able to detect the end of nitrification at these low strength influent concentrations. Further analysis attributed this failure to the absence of an inflection point in the off-gas oxygen profile. At these low concentrations, there seems to be a lower concentration of autotrophic organisms in the SBR which results in a less pronounced effect in the off-gas, as explained in Section 3.2. Nevertheless, the complete absence of such an inflection point at a phosphate concentration of

¹Ammonium concentration in reactor is about $25 \text{ g} \cdot \text{m}^{-3}$ due to dilution of the influent as explained in Section 2.3.4.1 of Materials and Methods

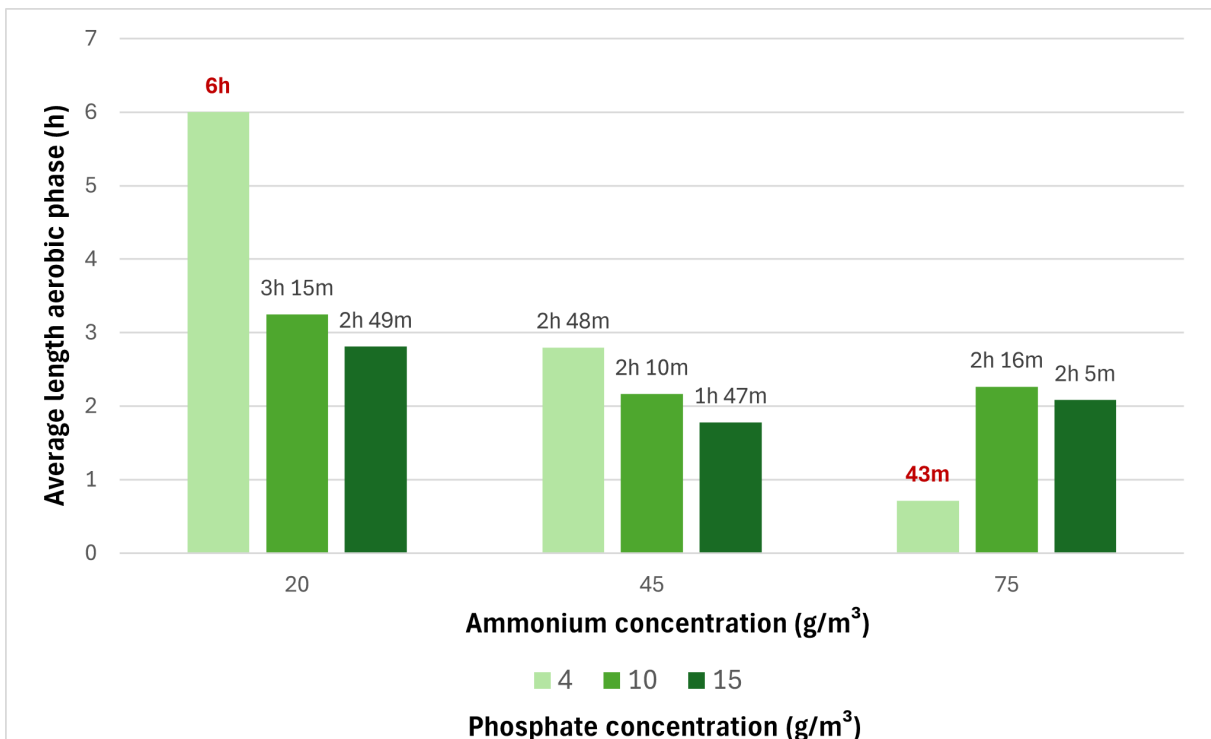
4 g.m⁻³ remains unexplained by the model output as at a higher phosphate concentration the detection strategy is still feasible.

Furthermore, the increase in number of cycles during these 365 days and the reduction in required aeration energy during the first aerobic phase were assessed (Figures 3.7c and 3.7d). Both scenarios where the detection strategy was proven not to be feasible were not taken into account. Overall, there is a significant increase in number of cycles between an ammonium influent concentration of 20 g.m⁻³ and 45 g.m⁻³. A higher ammonium concentration resulted in a considerable increase in the concentration of autotrophic organisms, which increases the nitrification rate. This leads to an earlier end of nitrification, hence an earlier detection in the aerobic phase and a shorter cycle. When changing the ammonium influent concentration from 45 g.m⁻³ to 75 g.m⁻³, the effect on the number of cycles is limited. The phosphate concentration also has a positive effect on the cycle increase, but less pronounced. The required aeration energy confirms the previous trend: there is a significant reduction of the required aeration energy between an ammonium concentration of 20 g.m⁻³ and 45 g.m⁻³.

Overall, for most combinations of the ammonium and phosphate concentration, the detection strategy was still able to detect the end of nitrification and shorten the total cycle time. However, at the highest ammonium concentration (75 g.m⁻³) the detection strategy is not feasible if the end of phosphate uptake occurs before the end of nitrification, resulting in a false positive detection. Furthermore, at a combination of the lowest ammonium (20 g.m⁻³) and lowest phosphate (4 g.m⁻³) influent concentration the end of nitrification could not be detected. The detection strategy is thus not fully robust for the full range of applied ammonium and phosphate influent concentrations.

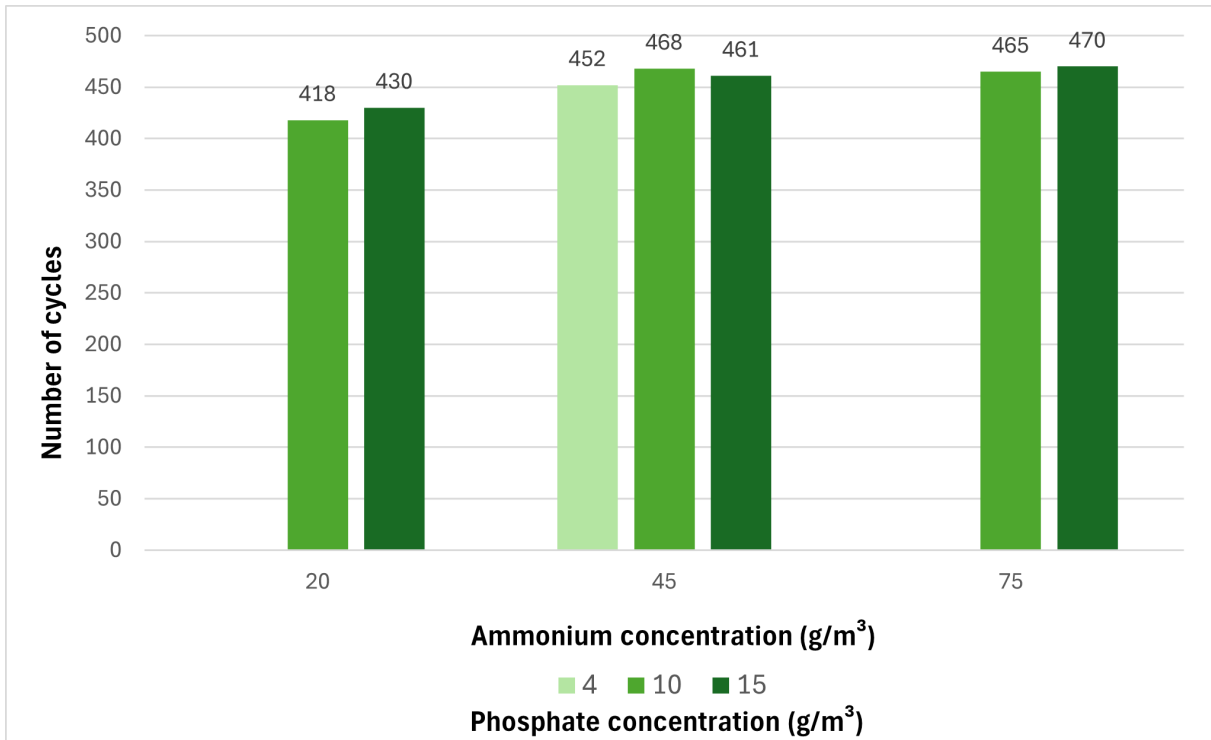


(a) Ammonium concentration at the end of the aerobic phase.

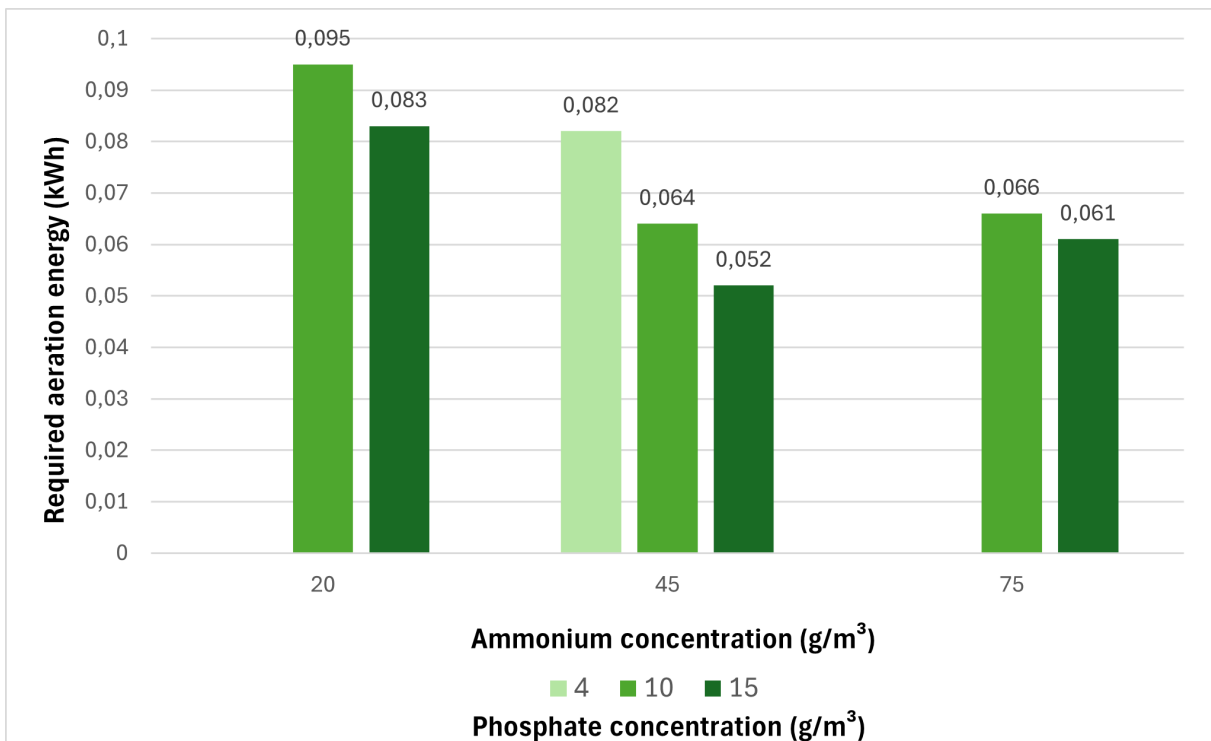


(b) Average length of the aerobic phase.

Figure 3.7: Bar plots showing the average final ammonium concentration and the average aerobic phase length in function of the ammonium and phosphate concentration in the influent.



(c) Number of cycles during evaluated 365 days.



(d) Required aeration energy during the aerobic phase.

Figure 3.7: Bar plots showing the number of cycles and aeration energy requirement in function of the ammonium and phosphate concentration in the influent.

Further evaluation of the detection strategy involved its implementation in the second aerobic phase to assess the possibility of detecting nitrification in both the first and second aerobic phase. Once again, simulations were done for every combination of ammonium and phosphate in the influent. Table C.1 in Appendix C presents the results of these simulations.

At an ammonium concentration of 20 g.m^{-3} no distinguishable change is observed by implementing the detection strategy in the second aerobic phase, which is linked to the lower nitrification rate at this ammonium concentration. The end of nitrification is not reached within 3 hours, there is no earlier end of the aerobic phase. For ammonium influent concentrations of 45 g.m^{-3} and 75 g.m^{-3} , a higher nitrification rate is expected, resulting in an earlier end of the second aerobic phase and an increase of the total number of cycles compared to its implementation only in the first aerobic phase. However, only for the combination of 45 g.m^{-3} ammonium and 10 g.m^{-3} phosphate, the number of cycles increased. For the other combinations the duration of the first aerobic phase length was even prolonged compared to previous evaluation, while the second aerobic phase length was slightly reduced. Overall, the earlier end of the second aerobic phases, negatively affected the length of the first aerobic phase.

Implementation of the detection strategy in the second aerobic phase did not increase the number of cycles, except for one specific combination.

3.4.2 Dynamic influent conditions

The final purpose of this research would be to implement the detection strategy based on off-gas analysis in practice. The detection strategy was tested with a dynamic influent composition to approach reality. The influent composition was retrieved from BSM2 (Solon et al., 2017), which provides values for a changing influent every 15 minutes over a period of 609 days. The detection strategy was only implemented in the first aerobic phase. After simulation, the results were evaluated over the last 365 days as seen in Table 3.4.

Table 3.4: Evaluation dynamic influent scenario over 365 days.

	Dynamic influent scenario
Number of cycles	503
Volume treated water	618.7 m^3
Average length first aerobic phase	<i>0h 42 min</i>
Maximum length first aerobic phase	<i>5h 4 min</i>
Maximum length first aerobic phase	<i>0h 16 min</i>
Average ammonium concentration	15.6 g.m^{-3}
Maximum ammonium concentration	34.6 g.m^{-3}
Minimum ammonium concentration	0.08 g.m^{-3}

During the last 365 days of the dynamic influent simulation, a high number of cycles are obtained, leading to a high volume of treated wastewater. However, when evaluating the average ammonium concentration at the point of detection this is above the threshold of $1 \text{ g NH}_4^+ \cdot \text{m}^{-3}$. In fact, only 22 cycles out of the simulated 503 cycles have an ammonium concentration lower than $1 \text{ g NH}_4^+ \cdot \text{m}^{-3}$ at the point of detection. It can be concluded that the detection strategy is failing with a dynamic influent by detecting the end of nitrification too early. This early detection, which is sometimes even after 20 minutes into the first aerobic phase, can be attributed to the occurrence of an early inflection point in the off-gas oxygen profile. At the point of this inflection point, the carbon dioxide concentration is decreasing. This leads to the fulfillment of the detection conditions, which results in ending the first aerobic phase. The early inflection point cannot be linked to the end of nitrification, nor the end of phosphate uptake. There are thus changes in the off-gas profiles during the first aerobic phase with a dynamic influent that were not present in the previous simulations with a constant influent. It is hypothesized that this could be due to the system not being in steady state with a dynamic influent. The biological reactions have to constantly adapt to the changing conditions of the influent which also leads to a more changing off-gas composition. This changing off-gas composition results in a less robust detection and in this case failing of the detection strategy.

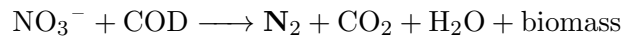
An implementation in practice with a more dynamic influent seems, based on this evaluation, not feasible. More research would be needed to explain the reason of the early occurring inflection point in the off-gas better. Furthermore, the detection strategy has to be adapted to differentiate the inflection point in the oxygen off-gas profile linked to the end of nitrification in a robust way.

3.5 Detecting the end of denitrification: strategy development

To extend the potential applications of off-gas analysis for controlling a sequencing batch reactor, it was investigated if a strategy could be developed to control the anoxic phase length based on off-gas measurements. This involved linking changes in the off-gas to the end of denitrification, similar to the strategy to detect the end of nitrification in previous sections. While controlling the anoxic phase length does not reduce the aeration energy (as no aeration is required during the anoxic phase), it can reduce cycle time, allowing a higher volume of wastewater to be treated within the same time period.

The open loop model was adapted by implementing a small aeration flow during the anoxic phase to be able to measure an off-gas flow and a simulation of the nitrogen gas concentration in the off-gas was added (Section 2.3.5 in Materials and Methods). This open loop model was simulated for 150 days with a constant influent composition (defined in Appendix A), reaching a steady state after 75 days (Figure C.7 in Appendix C). It was verified that the low aeration gas flow during the anoxic phase had minimal influence on the denitrification process by evaluating the last cycle at steady state (Figure C.8 in Appendix C). Due to the low applied k_La , the dissolved oxygen concentration was very low (about $0.004 \text{ g}\cdot\text{m}^{-3}$) in the first anoxic phase, having a negligible effect on denitrification.

To develop a detection strategy, the nitrate and off-gas concentration profiles during the last cycle of the 150 days were evaluated (Figure 3.8). In addition to oxygen and carbon dioxide, nitrogen gas, produced during denitrification by the heterotrophic organisms, was evaluated:



Changes in the nitrogen off-gas profile could thus potentially be linked to the end of denitrification.

The oxygen off-gas concentration in Figure 3.8 decreases in the anoxic phases. In the limited gas flow distributed to the SBR during the anoxic phases, there is mass transfer of oxygen gas to the liquid phase. As heterotrophic organisms prefer oxygen above nitrate as an electron acceptor, oxygen will be consumed first. However, as indicated before, the presence of dissolved oxygen is very limited due to the low gas flow rate, so it does not affect denitrification considerably. The oxygen off-gas concentration decreases due to this continuous consumption, but this is not related to the process of denitrification and will not respond to changes in this biological process. Thus, oxygen cannot be used to detect the end of denitrification with off-gas analysis.

Carbon dioxide and nitrogen gas are produced during denitrification, with visual changes in their profiles during the anoxic phases (Figure 3.8). At the start of the first anoxic phase, carbon dioxide off-gas increases due to the additional feeding step which reduces the pH of the SBR system. During denitrification the increase in carbon dioxide is limited, but at the end of denitrification the increase is more pronounced due to the occurrence of anaerobic conditions when all nitrate is removed. Anaerobic conditions lead to a decrease in the pH of the system which will affect the carbon dioxide concentration in the off-gas. The nitrogen off-gas

concentration decreases briefly during additional feeding but continuously increases during the remainder of denitrification while reaching a plateau at the end of denitrification.

To link changes in the off-gas carbon dioxide and nitrogen to the end of denitrification, their profiles were studied in detail during the first anoxic cycle in Figure 3.9. Similar as for the detection strategy of nitrification, it was determined if these changes can be mathematically translated to set up a detection strategy. As an easy mathematical translation is a derivative, the derivatives of off-gas carbon dioxide and nitrogen gas (until the third derivative) were plotted in Figure 3.9.

When the profiles of off-gas carbon dioxide and nitrogen were analysed, there is a response in both their profiles close to the end of denitrification, indicated by their derivatives (highlighted by the red area on Figure 3.9). The carbon dioxide off-gas has a local maximum in the second derivative and a sign change from positive to negative in the third derivative. The nitrogen off-gas has a local minimum in the second derivative and a sign change from negative to positive in the third derivative at the end of denitrification. As it is easiest to measure a sign change in a detection strategy, monitoring of the third derivative to detect the end of denitrification would be most suitable.

The third derivative can be defined as the rate of change of the acceleration of a function. Table C.2 in Appendix C gives an interpretation of the meaning of the first, second and third derivative if clarification is needed. Off-gas carbon dioxide increases during denitrification with an increasing acceleration (always faster). It reached a maximum acceleration at the end of denitrification, thereafter, the acceleration rate of the increase of carbon dioxide concentration slowed down. The fast increase in carbon dioxide at the end of denitrification can be linked to this maximum acceleration. This behaviour at the end of denitrification can be seen as a local maximum in the second derivative and a change from positive to negative in the third derivative. For the off-gas nitrogen concentration a similar interpretation can be made. During denitrification the nitrogen gas increases with a decreasing acceleration (always slower) to reach a minimum at the end of denitrification. This leads to a local minimum in the second derivative of the nitrogen gas concentration and a sign change from negative to positive in the third derivative.

Based on this evaluation, monitoring the third derivative of the carbon dioxide and nitrogen off-gas profiles seems to enable detection of denitrification, as a first step towards the development of a detection strategy. Further assessment is necessary to ensure that monitoring carbon dioxide and nitrogen off-gas is sufficient for integration into a detection strategy, as some concerns can be raised. The highly unstable behaviour during the first hour of the anoxic phase - as observed in Figure 3.9 - has to be dealt with in a possible detection strategy. Furthermore, more research has to be done into the effect of different applied influent compositions on the off-gas profiles of carbon dioxide and nitrogen gas. Finally, measurements could be less straightforward compared to the aerobic phases due to the very low gas flow rate applied during the anoxic phase and the necessity to monitor nitrogen gas, which is not common. The applicability of this detection strategy could be affected by the accuracy of these measurements.

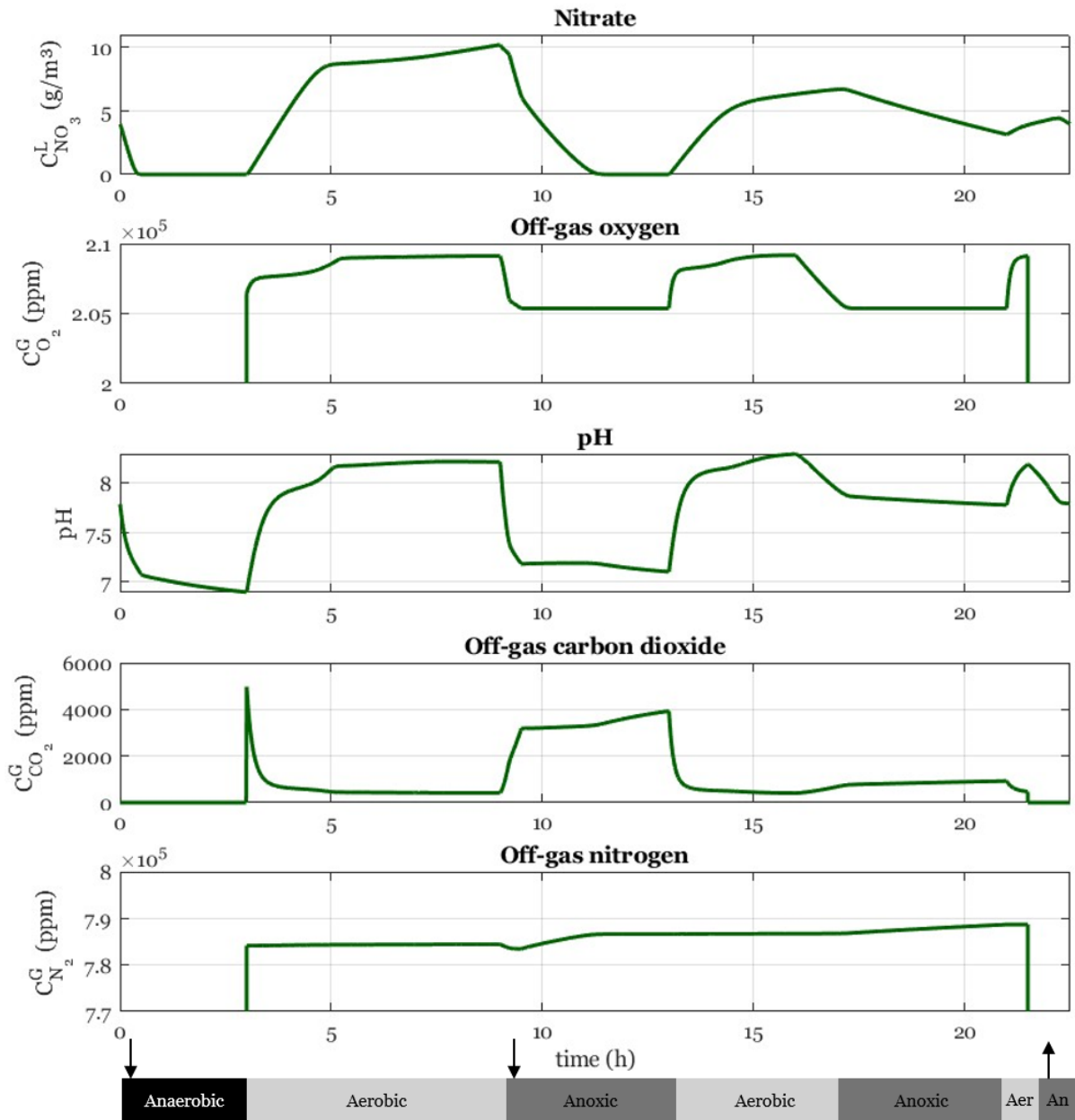


Figure 3.8: Nitrate and off-gas (O₂, CO₂ and N₂) concentration profiles during the last cycle of a 150 day open loop simulation.

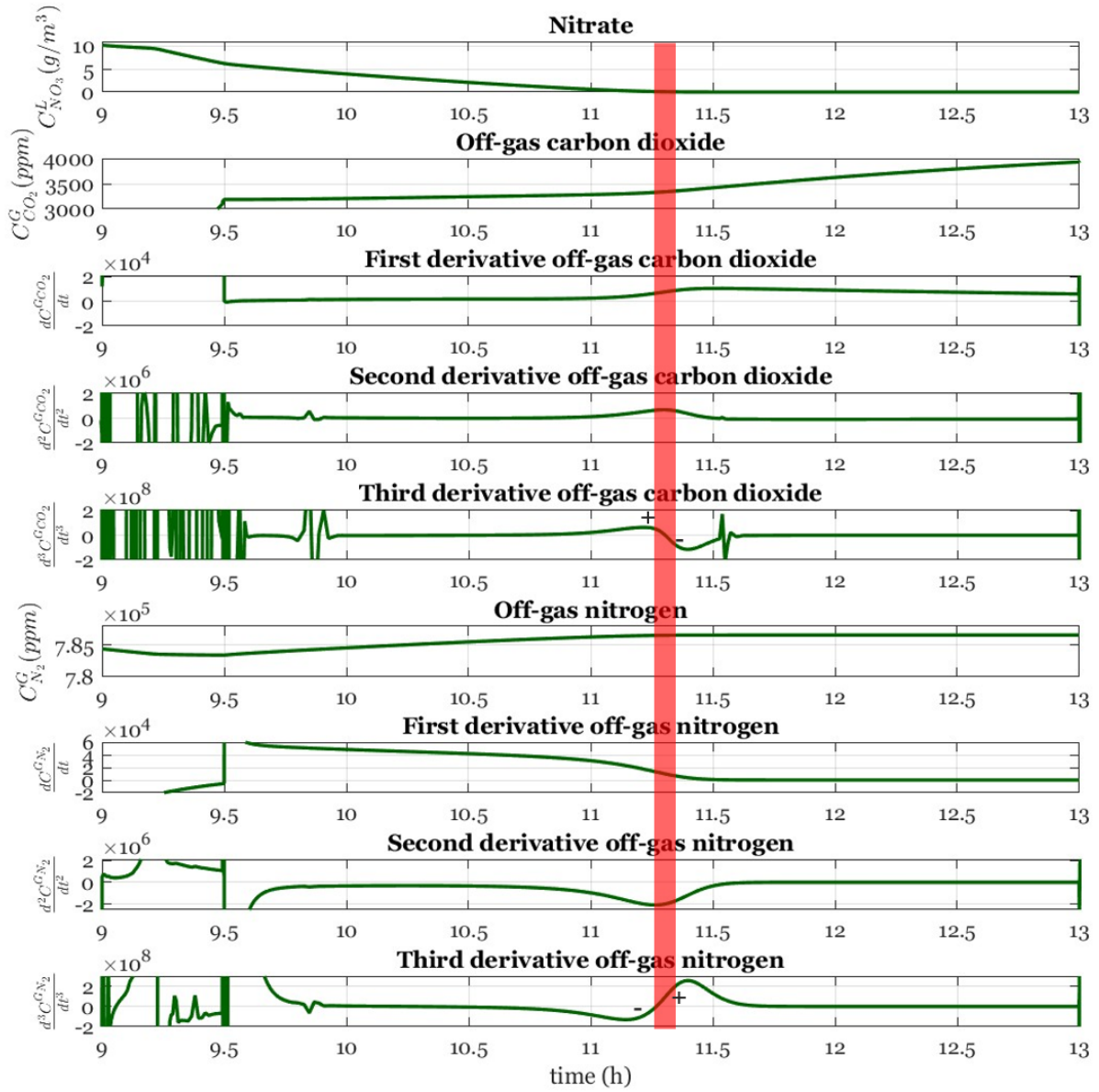


Figure 3.9: Nitrate and off-gas (CO_2 and N_2) concentration profiles with their derivatives during the first anoxic phase (hour 9 - 13) of the last cycle of a 150 day open loop simulation. The red line indicates the end of denitrification.

4. CONCLUSIONS AND PERSPECTIVES

In biological wastewater treatment effective monitoring and control during operation are of high importance to minimize treatment time and avoid excessive energy consumption. In aerobic systems, control is focused on optimizing aeration since it contributes significantly (up to 75 %) to the energy use (Rosso et al., 2008). Any reduction in aeration supply results in substantial operational cost savings.

During wastewater treatment in sequencing batch reactors, aeration control is primarily based on identifying the end of nitrification, during which oxygen is consumed. As this type of reactor operates in a transient state, parameters such as ammonium concentration, phosphate concentration, pH and ORP can be measured in the liquid phase to guide process decisions.

Concentrations in the off-gas could, aside from liquid-phase concentrations, indirectly reflect biological processes, offering a potential complement to or substitute for liquid phase control. Additionally, off-gas measurements require less maintenance, are cheaper and often more representative for the whole reactor.

In this thesis, the potential of off-gas analysis for process control in a sequencing batch reactor was investigated through simulations in Matlab/Simulink. The feasibility of detecting the end of nitrification in the aerobic phase was tested starting from a previously proposed detection strategy (Michiels, 2020). The detection strategy was validated, adapted and implemented in the model to end the aerobic phase. The robustness of the strategy was tested through application of a range of constant influents and a dynamic influent. Additionally, the end of denitrification in the anoxic phase was linked to the off-gas concentrations in order to develop a detection strategy.

Four specific research questions were addressed in this thesis. They are answered in what follows, drawing conclusions and indicating perspectives for research as well as practical implications.

1. Can the end of nitrification during the aerobic phase be detected based on the oxygen and carbon dioxide off-gas profiles?

In order to answer this question, an available model was first validated to simulate the behaviour of an SBR for a constant influent composition, revealing a mistake in the value of the sludge retention time (SRT), which was subsequently corrected. It was confirmed that relative changes in the off-gas oxygen and carbon dioxide concentration could be linked to the end of the nitrification process. A proposed detection strategy based on this correlation by Michiels (2020)

was implemented into the model (defined closed loop model) to check if the aerobic phase length could be controlled based on detecting the end of nitrification through off-gas analysis. The detection strategy was adapted to cope with non-simultaneous changes in the oxygen and carbon dioxide off-gas profiles at the end of phosphate uptake. The adapted closed loop detection strategy was able to detect the end of nitrification during the aerobic phase based on the oxygen and carbon dioxide off-gas profiles.

2. What are the benefits of closed loop control of the aerobic phase length through off-gas analysis?

The benefits of closed loop control were determined through steady state simulation considering a constant influent composition. By applying closed loop control through off-gas analysis, both time and energy could be saved. The average length of the aerobic phase reduced by 56 %, which contributed to an increase of treated wastewater over the evaluated period of 365 days by almost 10 %. The required aeration energy during the aerobic phase was also reduced by 56 %.

3. Is closed loop control of the aerobic phase length robust for a range of constant influent conditions and a dynamic influent?

The detection strategy used for closed loop control of the aerobic phase length needs improvement to be robust over the full range of constant influent conditions. An influent with a high ammonium concentration and low phosphate concentration resulted in a different behaviour of the carbon dioxide off-gas concentration (continuous increase during the aerobic phase) which was not taken into account in the detection strategy. Furthermore, a false negative detection with an influent of a low ammonium and phosphate concentration could not be accounted for. The detection strategy was also not yet robust for a dynamic influent as there were false positive detections due to early changes in the off-gas oxygen profile.

Further development of the detection strategy is required to allow detection of the end of nitrification with a constantly increasing carbon dioxide off-gas concentration. Furthermore, the detection strategy should be able to cope with the more variable off-gas behaviour during treatment of a dynamic influent.

It could be of interest to simultaneously start experiments of off-gas monitoring in practice to verify if the off-gas oxygen and carbon dioxide profiles correspond with the modelled profiles. Practical off-gas measurements could provide insight into the variable behaviour of the off-gas and help adapt the detection strategy from another perspective.

4. Can the end of denitrification during the anoxic phase be detected based on off-gas analysis?

A correlation was observed between the end of denitrification and the off-gas carbon dioxide and nitrogen concentrations. In the third derivative of the off-gas profiles of both compounds, a sign change occurred, facilitating detection during monitoring of the off-gas. These findings could be used to further develop a robust detection strategy during the anoxic phase. Furthermore, several concerns about the feasibility of measuring the off-gas during the anoxic phase were raised which must be addressed in future research.

Overall, in this thesis several aspects about the control of a sequencing batch reactor based on off-gas analysis were investigated. It can be concluded that the possibilities for controlling the aerobic and anoxic phase length through off-gas analysis are promising. However, further research into detection strategy development and robustness is necessary.

Finally, the potential of off-gas analysis for process control could be broadened to other systems in the wastewater treatment sector such as continuous flow reactors to monitor the aerobic and anoxic parts or reactors with aerobic granular sludge to monitor the simultaneous processes of nitrification and denitrification.

Acknowledgment of the use of Generative Artificial Intelligence

I would like to acknowledge the use of the generative artificial intelligence tool ChatGPT (OpenAI, 2023) during the writing process of this thesis, specifically for proofreading or rephrasing certain sections. No new information was sourced from ChatGPT. Its usage was limited to improving the structure of the text, using the following commands: 'Rephrase in a scientific context' or 'Rephrase if necessary, but keep my writing style'. The proposed text by ChatGPT was not copied but used to improve or correct language of parts in the report.

BIBLIOGRAPHY

- Adav, S. S., Lee, D.-J., Show, K.-Y., and Tay, J.-H. (2008). Aerobic granular sludge: recent advances. *Biotechnology advances*, 26(5):411–423.
- Al-Ghusain, I. A., Huang, J., Hao, O. J., and Lim, B. S. (1994). Using pH as a real-time control parameter for wastewater treatment and sludge digestion processes. *Water Science and Technology*, 30(4):159.
- Al-Rekabi, W. S., Qiang, H., and Qiang, W. W. (2007). Review on sequencing batch reactors. *Pakistan Journal of nutrition*, 6(1):11–19.
- Alattabi, A. W., Harris, C., Alkhaddar, R., Alzeyadi, A., and Abdulredha, M. (2017). Online monitoring of a sequencing batch reactor treating domestic wastewater. *Procedia engineering*, 196:800–807.
- Alex, J., Benedetti, L., Copp, J. B., Gernaey, K. V., Jeppsson, U., Nopens, I., Pons, M. N., Rieger, L., Rosen, C., Steyer, J. P., et al. (2008). Benchmark simulation model no. 1 (BSM1). *Report by the IWA Taskgroup on benchmarking of control strategies for WWTPs*, 1.
- Alex, J., Benedetti, L., Copp, J. B., Gernaey, K. V., Jeppsson, U., Nopens, I., Pons, M. N., Rosen, C., Steyer, J. P., and Vanrolleghem, P. (2018). Benchmark simulation model no. 2 (BSM2). *Report by the IWA Taskgroup on benchmarking of control strategies for WWTPs*, 1.
- Alleman, J. E. and Prakasam, T. B. S. (1983). Reflections on seven decades of activated sludge history. *Journal (Water Pollution Control Federation)*, pages 436–443.
- Amaral, A., Gillot, S., Garrido-Baserba, M., Filali, A., Karpinska, A. M., Plósz, B. G., De Groot, C., Bellandi, G., Nopens, I., Takács, I., et al. (2019). Modelling gas–liquid mass transfer in wastewater treatment: when current knowledge needs to encounter engineering practice and vice versa. *Water science and Technology*, 80(4):607–619.
- Amerlinck, Y., Bellandi, G., Amaral, A., Weijers, S., and Nopens, I. (2016). Detailed off-gas measurements for improved modelling of the aeration performance at the WWTP of Eindhoven. *Water Science and Technology*, 74(1):203–211.
- Andreottola, G., Foladori, P., and Ragazzi, M. (2001). On-line control of a SBR system for nitrogen removal from industrial wastewater. *Water science and Technology*, 43(3):93–100.
- Arora, M. L., Barth, E. F., and Umphres, M. B. (1985). Technology evaluation of sequencing batch reactors. *Journal (Water Pollution Control Federation)*, pages 867–875.
- Artan, N., Wilderer, P., Orhon, D., Morgenroth, E., and Özgür, N. (2001). The mechanism and design of sequencing batch reactor systems for nutrient removal - the state of the art. *Water Science and Technology*, 43(3):53–60.

-
- Baeten, J. E., van Dijk, E. J. H., Pronk, M., van Loosdrecht, M. C. M., and Volcke, E. I. P. (2021). Potential of off-gas analyses for sequentially operated reactors demonstrated on full-scale aerobic granular sludge technology. *Science of The Total Environment*, 787:147651.
- Baeten, J. E., van Loosdrecht, M. C. M., and Volcke, E. I. P. (2020). When and why do gradients of the gas phase composition and pressure affect liquid-gas transfer? *Water Research*, 178:115844.
- Batstone, D. J., Keller, J., Angelidaki, I., Kalyuzhnyi, S., Pavlostathis, S. G., Rozzi, A., Sanders, W. T. M., Siegrist, H. a., and Vavilin, V. A. (2002). The IWA anaerobic digestion model no 1 (adm1). *Water Science and Technology*, 45(10):65–73.
- Bozorg-Haddad, O., Delpasand, M., and Loáiciga, H. A. (2021). 10 - water quality, hygiene, and health. In Bozorg-Haddad, O., editor, *Economical, Political, and Social Issues in Water Resources*, pages 217–257. Elsevier.
- Bukhtiyarova, M. V., Nuzhdin, A. L., and Bukhtiyarova, G. A. (2023). Comparative study of batch and continuous flow reactors in selective hydrogenation of functional groups in organic compounds: What is more effective? *International Journal of Molecular Sciences*, 24(18):14136.
- Campos, J. L., Valenzuela-Heredia, D., Pedrouso, A., Val del Río, A., Belmonte, M., Mosquera-Corral, A., et al. (2016). Greenhouse gases emissions from wastewater treatment plants: minimization, treatment, and prevention. *Journal of Chemistry*, 2016.
- Casellas, M., Dagot, C., and Baudu, M. (2006). Set up and assessment of a control strategy in a SBR in order to enhance nitrogen and phosphorus removal. *Process Biochemistry*, 41(9):1994–2001.
- Casellas, M., Dagot, C., Stelmach, S., Pons, M.-N., and Baudu, M. (2003). Setting-up a control simulation strategy for a sequencing batch reactor (SBR): application to municipal wastewater. *Water science and technology*, 47(1):297–302.
- Cassidy, D. P., Efendiev, S., and White, D. M. (2000). A comparison of CSTR and SBR bioslurry reactor performance. *Water Research*, 34(18):4333–4342.
- Chandran, K., Volcke, E. I. P., and van Loosdrecht, M. C. M. (2016). Off-gas emission tests. In van Loosdrecht, M. C. M., Nielsen, P. H., Lopez-Vazquez, C. M., and Brdjanovic, D., editors, *Experimental Methods in Wastewater Treatment*, pages 177–200. IWA Publishing.
- Chen, G., van Loosdrecht, M. C. M., Ekama, G. A., and Damir, B. (2020). Wastewater treatment development. In Chen, G., van Loosdrecht, M. C. M., Ekama, G. A., and Damir, B., editors, *Biological Wastewater Treatment: Principles, Modelling and Design*, pages 1–10. IWA Publishing, 2 edition.
- Comeau, Y., Rabionwitz, B., Hall, K. J., and Oldham, W. K. (1987). Phosphate release and uptake in enhanced biological phosphorus removal from wastewater. *Journal (Water Pollution Control Federation)*, pages 707–715.

- Contreras, E. M. (2007). Carbon dioxide stripping in bubbled columns. *Industrial & engineering chemistry research*, 46(19):6332–6337.
- Daelman, M. R., van Voorthuizen, E. M., van Dongen, U. G., Volcke, E. I., and van Loosdrecht, M. C. (2012). Methane emission during municipal wastewater treatment. *Water research*, 46(11):3657–3670.
- De Bruin, L. M. M., De Kreuk, M. K., Van Der Roest, H. F. R., Uijterlinde, C., and van Loosdrecht, M. C. M. (2004). Aerobic granular sludge technology: an alternative to activated sludge? *Water Science and Technology*, 49(11-12):1–7.
- De heyder, B., Vanrolleghem, P., Van Langenhove, H., and Verstraete, W. (1997). Kinetic characterization of mass transfer limited biodegradation of a low water soluble gas in batch experiments—necessity for multiresponse fitting. *Biotechnology and bioengineering*, 55(3):511–519.
- Doran, P. M. (2013). Mass transfer. In *Bioprocess engineering principles*, pages 379 – 444. Elsevier.
- Dries, J. (2016). Dynamic control of nutrient-removal from industrial wastewater in a sequencing batch reactor, using common and low-cost online sensors. *Water Science and Technology*, 73(4):740–745.
- Dutta, A. and Sarkar, S. (2015). Sequencing batch reactor for wastewater treatment: recent advances. *Current Pollution Reports*, 1:177–190.
- Dutta, B. K. (2007). *Principles of mass transfer and separation processes*. PHI Learning Pvt. Ltd.
- Ekama, G. A. and Wentzel, M. C. (2020). Organic matter removal. In Chen, G., van Loosdrecht, M. C. M., Ekama, G. A., and Damir, B., editors, *Biological Wastewater Treatment: Principles, Modelling and Design*, pages 111–160. IWA Publishing, 2 edition.
- Ekama, G. A., Wentzel, M. C., and van Loosdrecht, M. C. M. (2023). Nitrogen removal. In Chen, G., van Loosdrecht, M. C. M., Ekama, G. A., and Damir, B., editors, *Biological Wastewater Treatment: Principles, Modelling and Design*, pages 161 – 238. IWA Publishing, 2 edition.
- Eloy water (2022). Biological wastewater treatment plant airoxy. <https://www.elaywater.com/solutions/small-communities-commercial-and-industrial/sbr>. Accessed November 11, 2023.
- Encyclopaedia Britannica (2023). Universal gas constant. <https://www.britannica.com/science/universal-gas-constant/additional-info#historyt>. Accessed February 25, 2024.
- EPA (1999). Wastewater technology fact sheet - sequencing batch reactors. https://www3.epa.gov/npdes/pubs/sbr_new.pdf. Accessed October 15, 2023.
- Fatone, F., Battistoni, P., Bolzonella, D., Pavan, P., and Cecchia, F. (2008). Long-term experience with an automatic process control for nitrogen removal in membrane bioreactors. *Desalination*, 227(1-3):72–84.

-
- Ferrell, R. T. and Himmelblau, D. M. (1967). Diffusion coefficients of nitrogen and oxygen in water. *Journal of chemical and engineering data*, 12(1):111–115.
- Flores-Alsina, X., Kazadi Mbamba, C., Solon, K., Vrecko, D., Tait, S., Batstone, D. J., Jeppsson, U., and Gernaey, K. V. (2015). A plant-wide aqueous phase chemistry module describing pH variations and ion speciation/pairing in wastewater treatment process models. *Water Research*, 85:255–265.
- Fox, S. and Clifford, E. (2018). Detecting the end of nitrification in small and decentralized wastewater treatment systems using low-resource real-time control methods. *Journal of Environmental Engineering*, 144(8):04018069.
- Frahm, B., Blank, H.-C., Cornand, P., Oelßner, W., Guth, U., Lane, P., Munack, A., Johannsen, K., and Pörtner, R. (2002). Determination of dissolved CO₂ concentration and CO₂ production rate of mammalian cell suspension culture based on off-gas measurement. *Journal of Biotechnology*, 99(2):133–148.
- Freitas, F., Temudo, M. F., Carvalho, G., Oehmen, A., and Reis, M. A. M. (2009). Robustness of sludge enriched with short SBR cycles for biological nutrient removal. *Bioresource technology*, 100(6):1969–1976.
- Garcia-Ochoa, F., Gomez, E., Santos, V. E., and Merchuk, J. C. (2010). Oxygen uptake rate in microbial processes: an overview. *Biochemical engineering journal*, 49(3):289–307.
- Gillot, S. and Héduit, A. (2008). Prediction of alpha factor values for fine pore aeration systems. *Water Science and Technology*, 57(8):1265–1269.
- Grady Jr, C. P. L., Daigger, G. T., Love, N. G., and Filipe, C. D. M. (2011). *Biological wastewater treatment*. CRC press.
- Groves, K. P., Daigger, G. T., Simpkin, T. J., Redmon, D. T., and Ewing, L. (1992). Evaluation of oxygen transfer efficiency and alpha-factor on a variety of diffused aeration systems. *Water environment research*, 64(5):691–698.
- Guo, J., Yang, Q., Peng, Y., Yang, A., and Wang, S. (2007). Biological nitrogen removal with real-time control using step-feed SBR technology. *Enzyme and Microbial Technology*, 40(6):1564–1569.
- Gupta, D. and Singh, S. K. (2012). Greenhouse gas emissions from wastewater treatment plants: a case study of noida. *Journal of Water Sustainability*, 2(2):131–139.
- Hellinga, C., Vanroileghem, P., Van Loosdrecht, M. C. M., and Heijnen, J. J. (1996). The potential of off-gas analyses for monitoring wastewater treatment plants. *Water Science and Technology*, 33(1):13–23.
- Henze, M., Gujer, W., Mino, T., Matsuo, T., Wentzel, M. C., v R Marais, G., and Van Loosdrecht, M. C. M. (1999). Activated sludge model no.2d, asm2d. *Water Science and Technology*, 39(1):165–182. Modelling and microbiology of activated sludge processes.
- Henze, M., Gujer, W., Mino, T., and Van Loosdrecht, M. (2006). Activated sludge models ASM1, ASM2, ASM2d and ASM3.

- Hill, G. A. (2006). Measurement of overall volumetric mass transfer coefficients for carbon dioxide in a well-mixed reactor using a pH probe. *Industrial & engineering chemistry research*, 45(16):5796–5800.
- Hong, S., Choi, I., Lim, B. J., and Kim, H. (2012). A DO-and pH-based early warning system of nitrification inhibition for biological nitrogen removal processes. *Sensors*, 12(12):16334–16352.
- Husemann, U., Kaiser, S. C., Kauling, J., Kuhlmann, W., Moller, J., Sieblist, C., Tscheschke, B., and Werner, S. (2021). *Recommendations for process engineering characterisation of single-use bioreactors and mixing systems by using experimental methods - supplement to the 2nd edition: Volumetric mass transfer coefficient of CO₂*. Dechema.
- IPCC (2021). Climate change 2021 the Physical Science basis - Working Group I Contribution to the Sixth Assessment Report of the Intergovernmental Panel on Climate Change. https://report.ipcc.ch/ar6/wg1/IPCC_AR6_WGI_FullReport.pdf. Accessed April 3, 2024.
- Irvine, R. L. and Busch, A. W. (1979). Sequencing batch biological reactors: an overview. *Journal (Water Pollution Control Federation)*, pages 235–243.
- Irvine, R. L., Ketchum, L. H., Breyfogle, R., and Barth, E. F. (1983). Municipal application of sequencing batch treatment. *Journal (Water Pollution Control Federation)*, pages 484–488.
- Jamnongwong, M., Loubiere, K., Dietrich, N., and Hébrard, G. (2010). Experimental study of oxygen diffusion coefficients in clean water containing salt, glucose or surfactant: Consequences on the liquid-side mass transfer coefficients. *Chemical Engineering Journal*, 165(3):758–768.
- Kalff, J. (2002). Inorganic carbon and pH. In *Limnology - Inland Water Ecosystems*, pages 218 – 226. Prentice Hall.
- Khan Academy (2023). What are inflection points? <https://www.khanacademy.org/math/ap-calculus-ab/ab-diff-analytical-applications-new/ab-5-6b/a/inflection-points-review>. Accessed November 3, 2023.
- Khoo, C. G., Lam, M. K., and Lee, K. T. (2016). Pilot-scale semi-continuous cultivation of microalgae *chlorella vulgaris* in bubble column photobioreactor (BC-PBR): Hydrodynamics and gas–liquid mass transfer study. *Algal Research*, 15:65–76.
- Kim, J.-H., Chen, M., Kishida, N., and Sudo, R. (2004). Integrated real-time control strategy for nitrogen removal in swine wastewater treatment using sequencing batch reactors. *Water Research*, 38(14-15):3340–3348.
- Kim, K.-S., Yoo, J.-S., Kim, S., Lee, H. J., Ahn, K.-H., and Kim, I. S. (2007). Relationship between the electric conductivity and phosphorus concentration variations in an enhanced biological nutrient removal process. *Water science and Technology*, 55(1-2):203–208.
- Koutsoukous, X. D. and Antsaklis, P. J. (2000). Chapter 3 - computational issues in intelligent control: Discrete-event and hybrid systems. In Sinha, N. K. and Gupta, M. M., editors, *Soft Computing and Intelligent Systems*, Academic Press Series in Engineering, pages 39–69. Academic Press, San Diego.

-
- Kurrer, C. and Lipcaneanu, N. (2023). Environment policy: general principles and basic framework. <https://www.europarl.europa.eu/factsheets/en/sheet/71/environment-policy-general-principles-and-basic-framework#:~:text=Origins%20and%20development&text=The%20Single%20European%20Act%20of,rational%20use%20of%20natural%20resources>. Accessed September 10, 2023.
- Leu, S.-Y., Libra, J. A., and Stenstrom, M. K. (2010). Monitoring off-gas O₂/CO₂ to predict nitrification performance in activated sludge processes. *Water research*, 44(11):3434–3444.
- Leu, S.-Y., Rosso, D., Larson, L. E., and Stenstrom, M. K. (2009). Real-time aeration efficiency monitoring in the activated sludge process and methods to reduce energy consumption and operating costs. *Water Environment Research*, 81(12):2471–2481.
- Lewis, W. K. and Whitman, W. G. (1924). Principles of gas absorption. *Industrial & Engineering Chemistry*, 16(12):1215–1220.
- Li, J., Ni, Y., Peng, Y., Gu, G., Lu, J., Wei, S., Cheng, G., and Ou, C. (2008). On-line controlling system for nitrogen and phosphorus removal of municipal wastewater in a sequencing batch reactor (SBR). *Frontiers of Environmental Science & Engineering in China*, 2:99–102.
- Li, S., Mu, J., Du, Y., and Wu, Z. (2019). Study and application of real-time control strategy based on DO and ORP in nitrification–denitrification SBR start-up. *Environmental technology*.
- Li, Z., Yuan, L., Sun, G., Lv, J., and Zhang, Y. (2021). Experimental determination of CO₂ diffusion coefficient in a brine-saturated core simulating reservoir condition. *Energies*, 14(3):540.
- Lijklema, L. (1969). Factors affecting pH change in alkaline waste water treatment—i. *Water Research*, 3(12):913–930.
- Lijklema, L. (1971). Factors affecting pH change in alkaline wastewater treatment—ii carbon dioxide production. *Water research*, 5(4):123–142.
- Lin, Y.-F. and Jing, S.-R. (2001). Characterization of denitrification and nitrification in a step-feed alternating anoxic–oxic sequencing batch reactor. *Water Environment Research*, 73(5):526–533.
- Liu, S., Daigger, G. T., Liu, B., Zhao, W., and Liu, J. (2020). Enhanced performance of simultaneous carbon, nitrogen and phosphorus removal from municipal wastewater in an anaerobic-aerobic-anoxic sequencing batch reactor (aoa-SBR) system by alternating the cycle times. *Bioresour. Technol.*, 301:122750.
- Lofrano, G. and Brown, J. (2010). Wastewater management through the ages: A history of mankind. *Science of the Total Environment*, 408(22):5254–5264.
- Lopez-Vazquez, C. M., Wentzel, M. C., Comeau, Y., Ekama, G. A., van Loosdrecht, M. C. M., Brdjanovic, D., and Oehmen, A. (2020a). Enhanced biological phosphorus removal. In Chen, G., van Loosdrecht, M. C. M., Ekama, G. A., and Damir, B., editors, *Biological Wastewater Treatment: Principles, Modelling and Design*, pages 239 – 326. IWA Publishing, 2 edition.

- Lopez-Vazquez, C. M., Wentzel, M. C., Comeau, Y., Ekama, G. A., van Loosdrecht, M. C. M., Brdjanovic, D., and Oehmen, A. (2020b). Enhanced biological phosphorus removal - 6.10 influence of operational factors on full scale EBP WWTP. In Chen, G., van Loosdrecht, M. C. M., Ekama, G. A., and Damir, B., editors, *Biological Wastewater Treatment: Principles, Modelling and Design*, pages 302 – 304. IWA Publishing, 2 edition.
- Ma, Y., Peng, Y., and Wang, S. (2006). New automatic control strategies for sludge recycling and wastage for the optimum operation of predenitrification processes. *Journal of Chemical Technology & Biotechnology: International Research in Process, Environmental & Clean Technology*, 81(1):41–47.
- Mace, S. and Mata-Alvarez, J. (2002). Utilization of SBR technology for wastewater treatment: an overview. *Industrial & engineering chemistry research*, 41(23):5539–5553.
- Manesis, S., Sapidis, D. J., and King, R. E. (1998). Intelligent control of wastewater treatment plants. *Artificial Intelligence in Engineering*, 12(3):275–281.
- Mears, L., Stocks, S. M., Sin, G., and Gernaey, K. V. (2017). A review of control strategies for manipulating the feed rate in fed-batch fermentation processes. *Journal of biotechnology*, 245:34–46.
- Meijer, S. C. F. (2004). Theoretical and practical aspects of modelling activated sludge processes. *Delft, The Netherlands: Delft University of Technology*.
- Metcalf & Eddy, Abu-Orf, M., Bowden, G., Burton, F. L., Pfrang, W., Stensel, H. D., Tchobanoglous, G., Tsuchihashi, R., and (Firm), A. (2014). *Wastewater engineering: treatment and resource recovery*. McGraw Hill Education.
- Mettler Toledo (sd). Continuous stirred tank reactors (CSTRs) - flow technology for chemical and biological syntheses. https://www.mt.com/be/nl/home/applications/L1_AutoChem_Applications/L2_ReactionAnalysis/continuous-stirred-tank-reactor-cstr.html. Accessed November 9, 2023.
- Miao, L., Wang, K., Wang, S., Zhu, R., Li, B., Peng, Y., and Weng, D. (2014). Advanced nitrogen removal from landfill leachate using real-time controlled three-stage sequence batch reactor (SBR) system. *Bioresource Technology*, 159:258–265.
- Michiels, W. (2020). What bubbles can tell about water–control of wastewater treatment basins using off-gas analyses.
- Mino, T., Van Loosdrecht, M., and Heijnen, J. (1998). Microbiology and biochemistry of the enhanced biological phosphate removal process. *Water research*, 32(11):3193–3207.
- Mirbagheri, S. A., SM, S. Y., Rafeidehkordi, N., and Vakilian, R. (2017). Comparison of CAS, MBR, SBR, and biolak treatment systems in removal of BOD and COD from municipal wastewater—case study: Ekbatan wastewater treatment plant. In *15th International Conference on Environmental Science and Technology, Rhodes, Greece*, volume 31, pages 1–5.
- Morgenroth, E. and Wilderer, P. A. (1998). Sequencing batch reactor technology: concepts, design and experiences (abridged). *Water and Environment Journal*, 12(5):314–320.

-
- Morrison, F. A. (2021). Diffusion and mass transfer ii. https://pages.mtu.edu/~fmorriso/cm3120/lectures/2021_CM3120_module4_22lectureV.pdf. Accessed November 16, 2023.
- Mueller, J., Boyle, W. C., and Popel, H. J. (2002). Principles. In *Aeration: Principles and Practice, Volume 11*. CRC press.
- Muzaffar, W. M. B. W., Aznah, A., and Halim, H. (2022). Energy efficiency and nutrient removal performance: comparison between several types of activated sludge process. In *IOP Conference Series: Earth and Environmental Science*, volume 1091, page 012056. IOP Publishing.
- Myers, D. N. (2019). Chapter 10 - innovations in monitoring with water-quality sensors with case studies on floods, hurricanes, and harmful algal blooms. In Ahuja, S., editor, *Evaluating Water Quality to Prevent Future Disasters*, volume 11 of *Separation Science and Technology*, pages 219–283. Academic Press.
- Nathanson, J. A. and Ambulkar, A. (2023). wastewater treatment. <https://www.britannica.com/technology/wastewater-treatment>. Accessed September 8, 2023.
- Newhart, K. B., Marks, C. A., Rauch-Williams, T., Cath, T. Y., and Hering, A. S. (2020). Hybrid statistical-machine learning ammonia forecasting in continuous activated sludge treatment for improved process control. *Journal of Water Process Engineering*, 37:101389.
- Ochoa, F. G. and Gómez, E. (2009). Bioreactor scale up and oxygen transfer rate in microbial processes: An overview. *Biotech. Adv.*, 27:153–176.
- Olsson, G., Nielsen, M. K., Yuan, Z., Lynggaard-Jensen, A., and Steyer, J.-P. (2005). *Instrumentation, Control and Automation in Wastewater Systems*. IWA Publishing.
- Orhon, D. (2015). Evolution of the activated sludge process: the first 50 years. *Journal of Chemical Technology & Biotechnology*, 90(4):608–640.
- Patziger, M., Günthert, F. W., Jardin, N., Kainz, H., and Londong, J. (2016). On the design and operation of primary settling tanks in state of the art wastewater treatment and water resources recovery. *Water Science and Technology*, 74(9):2060–2067.
- Paul, E., Plisson-Saune, S., Mauret, M., and Cantet, J. (1998). Process state evaluation of alternating oxic-anoxic activated sludge using ORP, pH and DO. *Water Science and Technology*, 38(3):299–306.
- Pavšelj, N., Hvala, N., Kocijan, J., Roš, M., Šubelj, M., Mušič, G., and Strmčnik, S. (2001). Experimental design of an optimal phase duration control strategy used in batch biological wastewater treatment. *ISA Transactions*, 40(1):41–56.
- Pitman, A. R. (1991). Design considerations for nutrient removal activated sludge plants. *Water Science and Technology*, 23(4-6):781–790.
- Pittoors, E., Guo, Y., and WH Van Hulle, S. (2014). Modeling dissolved oxygen concentration for optimizing aeration systems and reducing oxygen consumption in activated sludge processes: a review. *Chemical Engineering Communications*, 201(8):983–1002.

- Plisson-Saune, S., Capdeville, B., Mauret, M., Deguin, A., and Baptiste, P. (1996). Real-time control of nitrogen removal using three ORP bending-points: signification, control strategy and results. *Water Science and Technology*, 33(1):275–280.
- Pons, M.-N., Casellas, M., and Dagot, C. (2004). Definition of a benchmark protocol for sequencing batch reactors (B-SBR). *IFAC Proceedings Volumes*, 37(3):439–444.
- Pratt, S., Yuan, Z., Gapes, D., Dorigo, M., Zeng, R. J., and Keller, J. (2003). Development of a novel titration and off-gas analysis (TOGA) sensor for study of biological processes in wastewater treatment systems. *Biotechnology and bioengineering*, 81(4):482–495.
- Pronk, M., De Kreuk, M. K., De Bruin, B., Kamminga, P., Kleerebezem, R. v., and Van Loosdrecht, M. C. M. (2015). Full scale performance of the aerobic granular sludge process for sewage treatment. *Water research*, 84:207–217.
- Pronk, M., van Dijk, E. J. H., and van Loosdrecht, M. C. M. (2020). Aerobic granular sludge. In Chen, G., van Loosdrecht, M. C. M., Ekama, G. A., and Damir, B., editors, *Biological Wastewater Treatment: Principles, Modelling and Design*, pages 497–522. IWA Publishing, 2 edition.
- Puig, S., Vives, M. T., Corominas, L., Balaguer, M. D., and Colprim, J. (2004). Wastewater nitrogen removal in SBRs, applying a step-feed strategy: from lab-scale to pilot-plant operation. *Water Science and Technology*, 50(10):89–96.
- Puig Broch, S. (2008). *Operation and control of SBR processes for enhanced biological nutrient removal from wastewater*. Universitat de Girona.
- Rania, R. and Singha, S. (2020). Green chemistry and its applications in hospital wastewater and its treatment. *Green Chemistry and Water Remediation: Research and Applications*, page 271.
- Redmon, D., Boyle, W. C., and Ewing, L. (1983). Oxygen transfer efficiency measurements in mixed liquor using off-gas techniques. *Journal (Water Pollution Control Federation)*, pages 1338–1347.
- Rosso, D., Larson, L. E., and Stenstrom, M. K. (2008). Aeration of large-scale municipal wastewater treatment plants: state of the art. *Water Science and Technology*, 57(7):973–978.
- Rosso, D., Stenstrom, M. K., and Garrido-Baserba, M. (2018). Aeration fundamentals, performance and monitoring. In Rosso, D., editor, *Aeration, Mixing and Energy: Bubbles and Sparks*, pages 31–71. IWA Publishing.
- Rosso, D., Stenstrom, M. K., and Garrido-Baserba, M. (2020). Aeration and mixing. In Chen, G., van Loosdrecht, M. C. M., Ekama, G. A., and Damir, B., editors, *Biological Wastewater Treatment: Principles, Modelling and Design*, pages 419 – 474. IWA Publishing, 2 edition.
- Sander, R. (2015). Compilation of henry’s law constants (version 4.0) for water as solvent. *Atmospheric Chemistry and Physics*, 15(8):4399–4981.
- Schilling, W., Andersson, B., Nyberg, U., Aspegren, H., Rauch, W., and Harremoës, P. (1996). Real time control of wastewater systems. *Journal of hydraulic research*, 34(6):785–797.

-
- Schleypen, P., Michel, I., and Siewert, H. (1997). Sequencing batch reactors with continuous inflow for small communities in rural areas in Bavaria. *Water Science and Technology*, 35(1):269–276.
- Schuchardt, A., Libra, J., Sahlmann, C., Handschag, J., Wiesmann, U., and Gnirss, R. (2005). Potential of our and otr measurements for identification of activated sludge removal processes in aerated basins. *Water science and Technology*, 52(12):141–149.
- Schwarz, M., Trippel, J., Engelhart, M., and Wagner, M. (2022). Determination of alpha factors for monitoring of aeration systems with the ex situ off-gas method: experience from practical application and estimation of measurement uncertainty. *Environmental Science and Pollution Research*, 29(58):87950–87968.
- Shammas, N. K. and Wang, L. K. (2009). SBR systems for biological nutrient removal. *Advanced biological treatment processes*, pages 157–183.
- Singh, M. and Srivastava, R. K. (2011). Sequencing batch reactor technology for biological wastewater treatment: a review. *Asia-pacific journal of chemical engineering*, 6(1):3–13.
- Solon, K., Flores-Alsina, X., Mbamba, C. K., Ikumi, D., Volcke, E., Vaneeckhaute, C., Ekama, G., Vanrolleghem, P., Batstone, D. J., Gernaey, K. V., et al. (2017). Plant-wide modelling of phosphorus transformations in wastewater treatment systems: Impacts of control and operational strategies. *Water Research*, 113:97–110.
- Spagni, A., Buday, J., Ratini, P., and Bortone, G. (2001). Experimental considerations on monitoring ORP, pH, conductivity and dissolved oxygen in nitrogen and phosphorus biological removal processes. *Water Science and Technology*, 43(11):197–204.
- Spanjers, H. and Vanrolleghem, P. A. (2020). Respirometry. In van Loosdrecht, M. C. M., Nielsen, P. H., Lopez-Vazques, C. M., and Damir, B., editors, *Experimental Methods in Wastewater Treatment*, pages 133 – 176. IWA Publishing, 1 edition.
- Spérandio, M. and Paul, E. (1997). Determination of carbon dioxide evolution rate using on-line gas analysis during dynamic biodegradation experiments. *Biotechnology and bioengineering*, 53(3):243–252.
- Stenstrom, M. K. and Gilbert, R. G. (1981). Effects of alpha, beta and theta factor upon the design, specification and operation of aeration systems. *Water Research*, 15(6):643–654.
- Strubbe, L., van Dijk, E. J. H., Deenekamp, P. J. M., van Loosdrecht, M. C. M., and Volcke, E. I. P. (2023). Oxygen transfer efficiency in an aerobic granular sludge reactor: Dynamics and influencing factors of alpha. *Chemical Engineering Journal*, 452:139548.
- Taylor, R. and Krishna, R. (1993). *Multicomponent mass transfer*, volume 2. John Wiley & Sons.
- The Engineering Toolbox (s.d.). Air - composition and molecular weight. https://www.engineeringtoolbox.com/air-composition-d_212.html. Accessed February 25, 2024.
- Treyball, R. E. (1980). *Mass Transfer Operations*. McGraw Hill Book Company.

- Vilanova, R., Katebi, M., and Wahab, N. (2011). N-removal on wastewater treatment plants: A process control approach. *Journal of Water Resource and Protection*, 2011(3):1–11.
- Villadsen, J., Nielsen, J., and Lidén, G. (2011). Gas-liquid mass transfer. In *Bioreaction engineering principles*, pages 459 – 496. Springer Science & Business Media.
- Vivienne, H. (2023). Urban wastewater treatment - updating EU rules. [https://www.europarl.europa.eu/RegData/etudes/BRIE/2023/739370/EPRS_BRI\(2023\)739370_EN.pdf](https://www.europarl.europa.eu/RegData/etudes/BRIE/2023/739370/EPRS_BRI(2023)739370_EN.pdf). Accessed October 14, 2023.
- Volcke, E. I. P., Kimberly, S., Y, C., and M, H. (2023). Wastewater characteristics. In Chen, G., van Loosdrecht, M. C. M., Ekama, G. A., and Damir, B., editors, *Biological Wastewater Treatment: Principles, Modelling and Design*, pages 77 – 110. IWA Publishing, 2 edition.
- Von Sperling, M. (2002). Relationship between first-order decay coefficients in ponds, for plug flow, CSTR and dispersed flow regimes. *Water science and Technology*, 45(1):17–24.
- Vrecko, D., Volcke, E. I. P., Jeppsson, U., Gernaey, K. V., Copp, J. B., and A, V. P. (2014). Evaluation criteria. In Gernaey, K. V., Jeppsson, U., Vanrolleghem, P. A., and Copp, J. B., editors, *Benchmarking of Control Strategies for Wastewater Treatment Plants*, pages 59 – 74. IWA Publishing, 1 edition.
- Wang, Y., Cheng, Y., Liu, H., Guo, Q., Dai, C., Zhao, M., and Liu, D. (2023). A review on applications of artificial intelligence in wastewater treatment. *Sustainability*, 15(18):13557.
- Weissenbacher, N., Lenz, K., Mahnik, S. N., Wett, B., and Fuerhacker, M. (2007). Determination of activated sludge biological activity using model corrected CO₂ off-gas data. *Water research*, 41(7):1587–1595.
- Wilén, B.-M., Liébana, R., Persson, F., Modin, O., and Hermansson, M. (2018). The mechanisms of granulation of activated sludge in wastewater treatment, its optimization, and impact on effluent quality. *Applied microbiology and biotechnology*, 102:5005–5020.
- Won, S. and Ra, C. (2011). Biological nitrogen removal with a real-time control strategy using moving slope changes of ph (mv)-and orp-time profiles. *Water Research*, 45(1):171–178.
- Xing, W., Yin, M., Lv, Q., Hu, Y., Liu, C., and Zhang, J. (2014). Oxygen solubility, diffusion coefficient, and solution viscosity. In *Rotating electrode methods and oxygen reduction electrocatalysts*, pages 1–31. Elsevier.
- Yang, Q., Gu, S., Peng, Y., Wang, S., and Liu, X. (2010). Progress in the development of control strategies for the SBR process. *Clean–Soil, Air, Water*, 38(8):732–749.
- Yoshida, H., Mønster, J., and Scheutz, C. (2014). Plant-integrated measurement of greenhouse gas emissions from a municipal wastewater treatment plant. *Water research*, 61:108–118.
- Yuan, Z., Oehmen, A., and Ingildsen, P. (2002). Control of nitrate recirculation flow in predenitrification systems. *Water Science and Technology*, 45(4-5):29–36.
- Yuan, Z., Pratt, S., and Batstone, D. J. (2012). Phosphorus recovery from wastewater through microbial processes. *Current opinion in biotechnology*, 23(6):878–883.

Zanetti, L., Frison, N., Nota, E., Tomizioli, M., Bolzonella, D., and Fatone, F. (2012). Progress in real-time control applied to biological nitrogen removal from wastewater. a short-review. *Desalination*, 286:1–7.

APPENDIX A

INFLUENT COMPOSITION

Table A.1: Constant influent composition defined in BSM2 (Solon et al., 2017).

State variable	Symbol	Value	Units
Dissolved oxygen	S_{O_2}	0	g O ₂ .m ⁻³
Fermentable, readily biodegradable organic substrate	S_F	69.9	g COD.m ⁻³
Fermentation products (acetate)	S_A	57.5	g COD.m ⁻³
Inert soluble organic material	S_I	26.6	g COD.m ⁻³
Ammonium plus ammonia nitrogen	S_{NH_4}	25.2	g N.m ⁻³
Dinitrogen	S_{N_2}	0	g N.m ⁻³
Nitrate plus nitrite nitrogen	S_{NO_3}	0	g N.m ⁻³
Inorganic soluble phosphorus (phosphate)	S_{PO_4}	5.7	g P.m ⁻³
Total inorganic carbon	S_{TIC}	84	g C.m ⁻³
Inert particulate organic material	X_I	94.1	g COD.m ⁻³
Slowly biodegradable substrate	X_S	369.9	g COD.m ⁻³
Heterothropic organisms	X_H	51.5	g COD.m ⁻³
Phosphate accumulating organisms	X_{PAO}	0	g COD.m ⁻³
Polyphosphate	X_{PP}	0	g P.m ⁻³
Cell internal storage product of PAO	X_{PHA}	0	g COD.m ⁻³
Nitrifying organisms	X_{AUT}	0	g COD.m ⁻³
Total suspended solids	X_{TSS}	374.7	g TSS.m ⁻³
Potassium	S_K	20	g K.m ⁻³
Magnesium	S_{Mg}	30	g Mg.m ⁻³

Table A.2: Range of the dynamic influent composition over 609 days defined in BSM2 (Solon et al., 2017).

State variable	Symbol	Value	Units
Dissolved oxygen	S_{O_2}	0	g O ₂ .m ⁻³
Fermentable, readily biodegradable organic substrate	S_F	0.6 - 183.3	g COD.m ⁻³
Fermentation products (acetate)	S_A	0.5 - 150.4	g COD.m ⁻³
Inert soluble organic material	S_I	2.1 - 41.1	g COD.m ⁻³
Ammonium plus ammonia nitrogen	S_{NH_4}	0.8 - 58.7	g N.m ⁻³
Dinitrogen	S_{N_2}	0	g N.m ⁻³
Nitrate plus nitrite nitrogen	S_{NO_3}	0	g N.m ⁻³
Inorganic soluble phosphorus (phosphate)	S_{PO_4}	0.2 - 14.9	g P.m ⁻³
Total inorganic carbon	S_{TIC}	84	g C.m ⁻³
Inert particulate organic material	X_I	4.9 - 201.3	g COD.m ⁻³
Slowly biodegradable substrate	X_S	20.5 - 776.5	g COD.m ⁻³
Heterothropic organisms	X_H	2.4 - 107.8	g COD.m ⁻³
Phosphate accumulating organisms	X_{PAO}	0	g COD.m ⁻³
Polyphosphate	X_{PP}	0	g P.m ⁻³
Cell internal storage product of PAO	X_{PHA}	0	g COD.m ⁻³
Nitrifying organisms	X_{AUT}	0	g COD.m ⁻³
Total suspended solids	X_{TSS}	29.9 - 787.8	g TSS.m ⁻³
Potassium	S_K	20	g K.m ⁻³
Magnesium	S_{Mg}	30	g Mg.m ⁻³

APPENDIX B

MODEL DESCRIPTION

B.1 Model structure

The model used to describe the operation of the considered sequencing batch reactor is presented below. Its structure is based on Henze et al. (1999), Flores-Alsina et al. (2015) and Michiels (2020).

B.1.1 Biochemical processes

The biochemical processes in the sequencing batch reactor are described by the activated sludge model ASM2d by Henze et al. (1999). This is a mathematical model which allows for dynamic simulation of biological COD, nitrogen and phosphorus removal with the influent composition as main input. Several fractions of biomass are considered: the ordinary heterotrophic organisms for COD removal and denitrification, the phosphate accumulating organisms for COD removal, denitrification and phosphate uptake and the ammonium oxidizing bacteria for nitrification. To represent the model in an efficient way, matrix notation is mostly used where index i indicates the state variables and index j the processes. The full matrix notation of this model can be found in the reference work of Henze et al. (1999).

19 components are considered as state variables in the model, listed in Table B.1 (Henze et al., 2006). Soluble components (e.g. ammonium, phosphate or magnesium) are indicated by S , while particulate components (e.g. biomass fractions or poly-phosphate) are indicated by X . In comparison to the original ASM2d model some adaptations were made to be able to interface with the speciation model (Section B.1.2) (Flores-Alsina et al., 2015): alkalinity S_{ALK} is replaced by total inorganic carbon S_{TIC} , the process of chemical precipitation (represented by states X_{MeOH} and X_{MeP}) is neglected and potassium (S_K) and magnesium (S_{Mg}) are explicitly added (Flores-Alsina et al., 2015). Additionally, the volume is added as a 20th state variable, as the volume in an SBR changes over time (Michiels, 2020). The initial values of all state variables applied during simulation can be found in Table B.2.

Table B.1: Overview of state variables in all biochemical processes.

State variable		Units	Reference
Dissolved oxygen	S_{O_2}	g O ₂ .m ⁻³	(Henze et al., 1999)
Fermentable, readily biodegradable organic substrate	S_F	g COD.m ⁻³	(Henze et al., 1999)
Fermentation products (acetate)	S_A	g COD.m ⁻³	(Henze et al., 1999)
Inert soluble organic material	S_I	g COD.m ⁻³	(Henze et al., 1999)
Ammonium plus ammonia nitrogen	S_{NH_4}	g N.m ⁻³	(Henze et al., 1999)
Dinitrogen	S_{N_2}	g N.m ⁻³	(Henze et al., 1999)
Nitrate and nitrite nitrogen	S_{NO_3}	g N.m ⁻³	(Henze et al., 1999)
Inorganic soluble phosphorus (phosphate)	S_{PO_4}	g P.m ⁻³	(Henze et al., 1999)
Total inorganic carbon	S_{TIC}	g C.m ⁻³	(Flores-Alsina et al., 2015)
Inert particulate organic material	X_I	g COD.m ⁻³	(Henze et al., 1999)
Slowly biodegradable substrate	X_S	g COD.m ⁻³	(Henze et al., 1999)
Heterotrophic organisms	X_H	g COD.m ⁻³	(Henze et al., 1999)
Phosphate accumulating organisms	X_{PAO}	g COD.m ⁻³	(Henze et al., 1999)
Polyphosphate	X_{PP}	g P.m ⁻³	(Henze et al., 1999)
Cell internal storage product of PAO	X_{PHA}	g COD.m ⁻³	(Henze et al., 1999)
Nitrifying organisms	X_{AUT}	g COD.m ⁻³	(Henze et al., 1999)
Total suspended solids	X_{TSS}	g TSS.m ⁻³	(Henze et al., 1999)
Potassium	S_K	g K.m ⁻³	(Flores-Alsina et al., 2015)
Magnesium	S_{Mg}	g Mg.m ⁻³	(Flores-Alsina et al., 2015)
Volume	V	m ³	(Michiels, 2020)

Table B.2: Initial values of state variables during simulation (Flores-Alsina et al., 2015).

State variable	Symbol	Value	Units
Dissolved oxygen	S_{O_2}	0	$\text{g O}_2 \cdot \text{m}^{-3}$
Fermentable, readily biodegradable organic substrate	S_F	2	$\text{g COD} \cdot \text{m}^{-3}$
Fermentation products (acetate)	S_A	5	$\text{g COD} \cdot \text{m}^{-3}$
Inert soluble organic material	S_I	30	$\text{g COD} \cdot \text{m}^{-3}$
Ammonium plus ammonia nitrogen	S_{NH_4}	22	$\text{g N} \cdot \text{m}^{-3}$
Dinitrogen	S_{N_2}	21	$\text{g N} \cdot \text{m}^{-3}$
Nitrate plus nitrite nitrogen	S_{NO_3}	0.001	$\text{g N} \cdot \text{m}^{-3}$
Inorganic soluble phosphorus (phosphate)	S_{PO_4}	11	$\text{g P} \cdot \text{m}^{-3}$
Total inorganic carbon	S_{TIC}	84	$\text{g C} \cdot \text{m}^{-3}$
Inert particulate organic material	X_I	1800	$\text{g COD} \cdot \text{m}^{-3}$
Slowly biodegradable substrate	X_S	150	$\text{g COD} \cdot \text{m}^{-3}$
Heterothropic organisms	X_H	1900	$\text{g COD} \cdot \text{m}^{-3}$
Phosphate accumulating organisms	X_{PAO}	250	$\text{g COD} \cdot \text{m}^{-3}$
Polyphosphate	X_{PP}	70	$\text{g P} \cdot \text{m}^{-3}$
Cell internal storage product of PAO	X_{PHA}	7	$\text{g COD} \cdot \text{m}^{-3}$
Nitrifying organisms	X_{AUT}	125	$\text{g COD} \cdot \text{m}^{-3}$
Total suspended solids	X_{TSS}	3700	$\text{g TSS} \cdot \text{m}^{-3}$
Potassium	S_K	100	$\text{g K} \cdot \text{m}^{-3}$
Magnesium	S_{Mg}	100	$\text{g Mg} \cdot \text{m}^{-3}$
Volume	V	0.660	g m^3

All state variables are involved in multiple processes in the reactor: 19 biochemical processes are considered in ASM2d. These processes can be found in Table B.3. Mathematical expressions of their respective process rates ρ_j can be found in the reference work of Henze et al. (1999). To calculate the overall reaction rate of one state variable A, all applicable processes where compound A is involved are considered with their respective process rate (ρ_j) and the stoichiometric coefficient ($v_{i,j}$) of state variable A. The overall reaction rate r_A ($\text{g} \cdot \text{h}^{-1} \cdot \text{m}^{-3}$) is calculated by reaction B.1:

$$r_A = \sum_j v_{A,j} \cdot \rho_j \quad (\text{B.1})$$

The overall reaction rate of state variable A is thus the sum of the products of the individual process rates with their respective stoichiometric coefficient.

Table B.3: Overview of considered biochemical processes in ASM2d model (Henze et al., 2006)

<i>Hydrolysis processes</i>
Aerobic hydrolysis
Anoxic hydrolysis
Anaerobic hydrolysis
<i>By heterotrophic organisms: X_H</i>
Growth on fermentable substrates, S_F
Growth on fermentation products, S_A
Denitrification with fermentable substrates, S_F
Denitrification with fermentation products, S_A
Fermentation
Lysis
<i>By phosphorus-accumulating organisms: X_{PAO}</i>
Storage of X_{PHA}
Aerobic storage of X_{PP}
Anoxic storage of X_{PP}
Aerobic growth on X_{PHA}
Anoxic growth on X_{PP}
Lysis of X_{PAO}
Lysis of X_{PP}
Lysis of x_{PHA}
<i>By autotrophic organisms: X_{AUT}</i>
Aerobic growth of X_{AUT}
Lysis of X_{AUT}

Based on the principle of mass balances, the values of the state variables over time can be calculated. A distinction is made between soluble and particulate state variables.

Mass balance for soluble state variable A

$$\frac{d(V \cdot S_A)}{dt} = (Q_{in}^L \cdot S_{A,in} - Q_{out}^L \cdot S_{A,out}) + r_A \cdot V + m_A^{L-G} \quad (\text{B.2})$$

With V the liquid volume in the bioreactor (m^3), S_A the concentration of state variable A in the bioreactor ($g \cdot m^{-3}$), Q_{in}^L and Q_{out}^L the influent and effluent flow rate, respectively ($m^3 \cdot h^{-1}$),

$S_{A,in}$ and $S_{A,out}$ the concentration of state variable A in the influent and effluent, respectively ($g \cdot m^{-3}$) and m_A^{L-G} the gas-liquid mass transfer rate of state variable A ($g \cdot h^{-1}$).

Only for soluble components that are transferable to the gas phase the last term of Eq. B.2 is considered.

Mass balance for particulate state variable B

During filling and reaction phase

$$\frac{d(V \cdot X_B)}{dt} = Q_{in}^L \cdot X_{B,in} + r_B \cdot V \quad (B.3)$$

During draw phase

$$\frac{d(V \cdot X_B)}{dt} = Q_{in}^L \cdot X_{B,in} - \frac{V \cdot X_{B,out}}{SRT} \cdot \frac{t_{tot}}{t_w} + r_B \cdot V \quad (B.4)$$

With SRT (h) the chosen sludge retention time, t_{tot} (h) the total length of one cycle and t_w (h) the length of the draw phase. The length of the settling phase is not considered, as the predefined SRT takes this settling already into account (Batstone et al., 2002).

As the volume is also a state variable in this model, a mass balance is considered with influent flow rate Q_{in}^L and effluent flow rate Q_{out}^L to calculate the changing volume:

$$\frac{dV}{dt} = Q_{in}^L - Q_{out}^L \quad (B.5)$$

The code for the ASM2d model was initially implemented as a C-file by Gernaey (2004) and further modified by Flores-Alsina et al. (2015) to complement the additional speciation model.

B.1.2 Speciation

The overall purpose of the whole model is to link the oxygen and carbon dioxide off-gas profile with the liquid phase biological processes. As the off-gas carbon dioxide concentration is dependent on the bicarbonate buffer system as described in Section 1.2.3, the speciation of total inorganic carbon in the liquid phase has to be known. By calculating pH variations and ion speciation/pairing this is possible. The code of the speciation model was written in a C-file by Flores-Alsina et al. (2015) and has as input the output of the ASM2d model. The aqueous phase of the sequencing batch reactor is here characterized by a set of chemical entities: 120 species are considered which all can be formulated by a linear combination of 19 components. These 19 components account for the total molar content of the aqueous phase. For an overview of these 19 components and 120 species and how these are linked by linear combination, one is referred to Flores-Alsina et al. (2015).

To calculate the concentration of all species over time, mass balances for the species and components and a charge balance are considered. In those mass balances chemical activity

corrections are made and temperature dependence is included. These differential equations result in a nonlinear algebraic system which is solved by a multi-dimensional version of the Newton-Rhapson method.

This speciation model is especially useful to calculate the fraction of total inorganic carbon that is present as H_2CO_3^* (free carbon dioxide ($\text{CO}_{2\text{aq}}$) and carbonic acid (H_2CO_3)). This concentration will be further used in the off-gas calculations to determine the carbon dioxide off-gas concentration.

B.1.3 Off-gas

Based on the dissolved oxygen concentration (S_{O_2}) and the dissolved carbon dioxide concentration (H_2CO_3^*), the oxygen and carbon dioxide off-gas concentrations over time are calculated. These calculations are based on the gas-liquid mass transfer principles as described in Section 1.2. However, instead of applying the formulas of the two-film theory (Lewis and Whitman, 1924), a more complex formula is used to calculate the gas-liquid mass transfer rate m^{L-G} ($g \cdot m^{-3} \cdot h^{-1}$) of oxygen or carbon dioxide which takes into account the mean pressure and mean composition of the gas phase over the reactor height (Baeten et al., 2020). Eq. B.6 was stated in Baeten et al. (2020) as a good balance between complexity and accuracy for poorly soluble gases like oxygen.

$$m^{L-G} = k_L a \left[\frac{H \frac{(p_{atm}^G + \rho g \frac{V}{2S})M}{RT} x_{in}^G - C^L}{1 + \frac{k_L a H (p_{atm}^G + \rho g \frac{V}{2S}) V}{2 p_{atm}^G Q_{in}^G}} \right] V \quad (\text{B.6})$$

With $k_L a$ the mass transfer coefficient (h^{-1}), H Henry's law constant for oxygen or carbon dioxide, p_{atm}^G the atmospheric pressure (Pa), ρ the density of water ($kg \cdot m^{-3}$), g the gravitational acceleration ($m \cdot s^{-1}$), S the cross-sectional area of the reactor (m^2), M_A the molar mass of oxygen or carbon dioxide ($g \cdot mole^{-1}$), R the universal gas constant ($J \cdot mole^{-1} \cdot K^{-1}$), T the temperature (K), $x_{in,A}^G$ the molar fraction of oxygen or carbon dioxide in the gas flow rate and C^L the concentration of dissolved oxygen or carbon dioxide ($g \cdot m^{-3}$).

The average gas flow rate Q_{in}^G is calculated empirically as a function of the oxygen mass transfer coefficient $k_L a_{(O_2)}$ (Baeten et al., 2020):

$$Q_{in}^G = \frac{k_L a_{(O_2)} (p_{atm}^G + \rho g \frac{V}{2A}) A}{0.6 p_{atm}^G} \quad (\text{B.7})$$

Also the carbon dioxide mass transfer coefficient $k_L a_{(CO_2)}$ is correlated to $k_L a_{(O_2)}$ (De heyder et al., 1997):

$$k_L a_{(CO_2)} = k_L a_{(O_2)} \sqrt{\frac{D_{CO_2}}{D_{O_2}}} \quad (\text{B.8})$$

With D_{CO_2} and D_{O_2} the diffusivities of carbon dioxide and oxygen, respectively ($m^2 \cdot s^{-1}$).

B. Model description

Based on the calculated gas-liquid mass transfer rates of oxygen and carbon dioxide and their mass balances in the gas phase considering no accumulation, the off-gas oxygen and carbon dioxide concentrations could be calculated:

$$\frac{d(V^G \cdot C_i^G)}{dt} = Q^G(C_{i,in}^G - C_{i,out}^G) - m_i^{L-G} = 0 \quad (\text{B.9})$$

$$C_{i,out}^G = C_{i,in}^G - \frac{m_i^{L-G}}{Q^G} \quad (\text{B.10})$$

With index i representing oxygen or carbon dioxide.

The values of the used parameters in the above off-gas calculations can be found in Table B.4. The mass transfer coefficients and volume are variable over time and thus not listed in the table.

Table B.4: Parameters used in off-gas calculations at 293 K

Parameter	Symbol	Value	Unit	Reference
Henry's law constant for oxygen	H_{O_2}	0.0297	-	(Sander, 2015)
Henry's law constant for carbon dioxide	H_{CO_2}	0.818	-	(Sander, 2015)
Atmospheric pressure	p_{atm}^G	101325	Pa	-
Density of water	ρ	1000	kg.m ⁻³	-
Gravitational acceleration	g	9.81	m.s ⁻¹	-
Cross sectional area of the reactor	S	1	m ²	-
Molar mass of oxygen	M_{O_2}	32	g.mole ⁻¹	-
Molar mass of carbon dioxide	M_{CO_2}	44	g.mole ⁻¹	-
Universal gas constant	R	8.314	J.mole ⁻¹ .K ⁻¹	(Encyclopaedia Britannica, 2023)
Molar fraction of oxygen in gas inflow	x_{in,O_2}^G	0.20946	-	(The Engineering Toolbox, sd)
Molar fraction of carbon dioxide in gas inflow	x_{in,CO_2}^G	$3.3 \cdot 10^{-4}$	-	(The Engineering Toolbox, sd)
Diffusivity of oxygen	D_{O_2}	$2.2 \cdot 10^{-9}$	m ² .s ⁻¹	(Ferrell and Himmelblau, 1967)
Diffusivity of carbon dioxide	D_{CO_2}	$1.92 \cdot 10^{-9}$	m ² .s ⁻¹	(Ferrell and Himmelblau, 1967)

B.2 Adaptations on the original model

B.2.1 Original model

The original model is a Matlab/Simulink implementation of a pH module within BSM1 by Flores-Alsina et al. (2015) downloaded from GitHub. The original model represents a continuous configuration with a settler and recycling streams. Furthermore, for this thesis the files associated with ASM2d were chosen.

C-files ¹

- `asm2d.c` - s-function for Simulink model (biological part).
- `combiner_asm2d.c` - function which combines two separate streams into one based on loads.
- `hyddelay_asm2d.c` - a special delay function to avoid algebraic loops.
- `settler1d_asm2d.c` - file for a 10-layer one dimensional settler model.
- `UQ_speciation_DAE.c` - s-function for Simulink model (speciation part).

Initialisation files

- `init_asm2d.m` - initial values of the state variables and parameter definition (biological part).
- `settler1dinit_asm2d.m` - initial values of the state variables in the settler.
- `speciation_init.m` - initial values of the state variables and parameter definition (speciation part).
- `benchmarkinit_asm2d.m` - runs all initialisation files and defines dummy variables of model.

Input data

- `CONSTINFLUENT_asm2d.mat` - constant value influent file (average values).
- `DRYINFLUENT_asm2d.mat` - dynamic influent file for dry weather data for 14 days (15 minute samples).
- `LTINFLUENT_asm2d.mat` - full dynamic data for 609 days (15 minute samples).
- `RAININFLUENT_asm2d.mat` - dynamic influent file for rain weather data for 14 days (15 minute samples).
- `STORMINFLUENT_asm2d.mat` - dynamic influent file for storm weather data for 14 days (15 minute samples)

¹These C-files must be compiled in Matlab by the mex command: `mexall_asm2d.m`

Simulink models

- benchmark_asm2d.slx - simulate the plant without active control using dynamic input data.
- benchmarkLT_asm2d.slx - simulate the plant without active control using full long term dynamic input data.
- benchmarkss_asm2d.slx - simulate the plant without active control using constant input data.

B.2.2 Adapted model by Michiels (2020)

The adapted model differs primarily in configuration: a batch configuration without separate settler or recycling streams. Due to this batch configuration, the volume varies over time. Secondly, off-gas simulation was added to the model.

Used C-files from original model

- asm2d.c - s-function for Simulink model (biological part)
- UQ_speciation_DAE.c - s-function for Simulink model (speciation part)

Used initialisation files from original model

- speciation_init.m - initial values of the state variables and parameter definition (speciation part)
- benchmarkinit_asm2d.m - runs all initialisation files and defines dummy variables of model

Simulink model

Adaptation of this simulink model was necessary to an SBR configuration. The Simulink model was simplified by only modelling one bioreactor and excluding the settler block and recycling streams. The content of the bioreactor block remained similar with asm2d.c and UQ_speciation_DAE.c to simulate biological behaviour and speciation. Additional input information regarding influent flow rate, aeration and wasting was added as this varies in an SBR, along with the inclusion of an off-gas simulation.

B.3 How to run the model?

1. Run the mex command to be able to use all C-files in Matlab.
2. Define all input data (influent, cycle times, flowrate, aeration, wasting etc.)
3. Run benchmarkinit_asm2d to load initial values of all state variables and parameters.
4. Run the correct model.
5. Process obtained data to desired formats or graphs.

APPENDIX C

RESULTS AND DISCUSSION: EXTRA FIGURES

C.1 Reference case: model validation and process performance

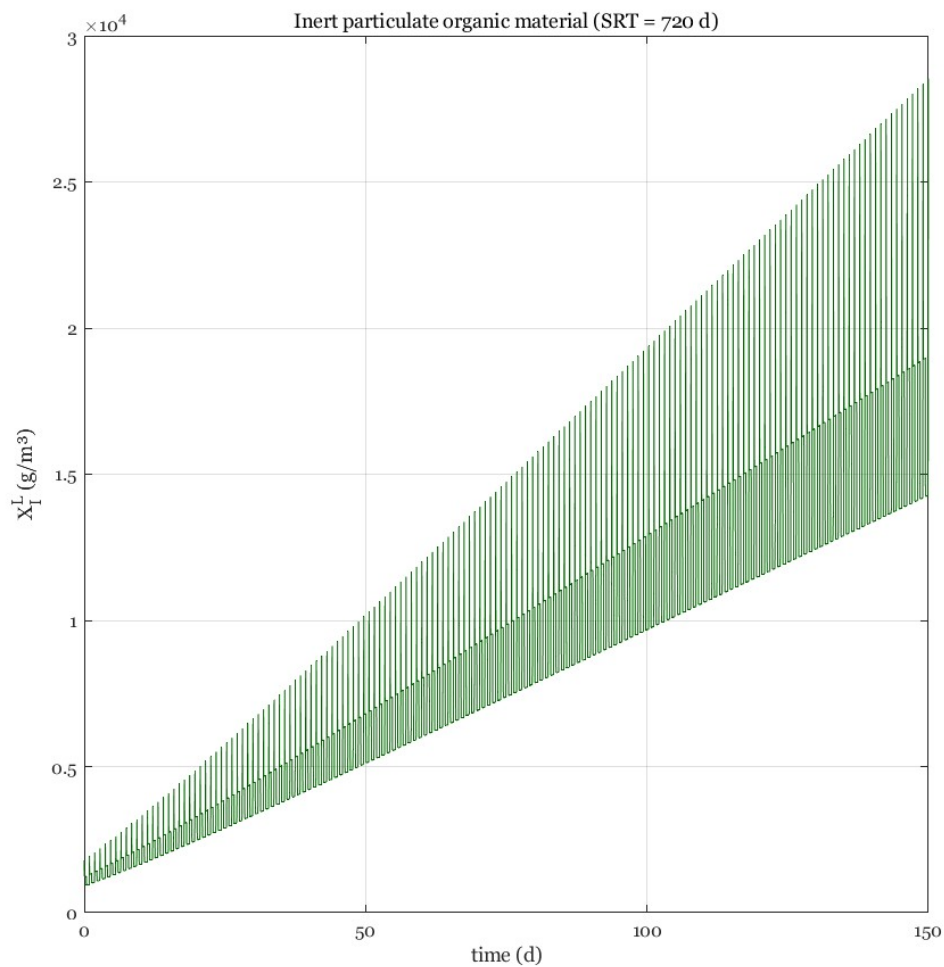


Figure C.1: Profile of inert particulate organic matter during 150-day simulation of the original model (SRT = 720 days). The concentration exceeds $15\,000\text{ g}\cdot\text{m}^{-3}$ at day 150 and continues to increase.

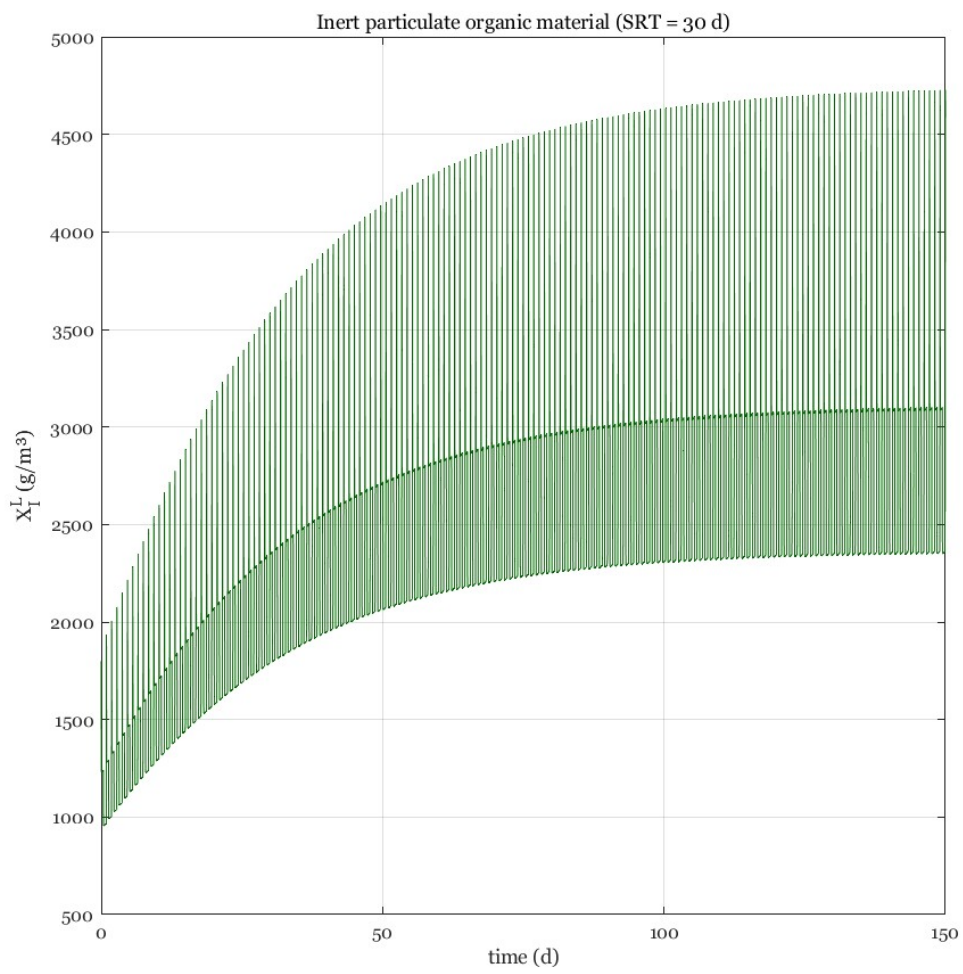


Figure C.2: Profile of inert particulate organic matter during 150-day simulation of the adapted model (SRT = 30 days).

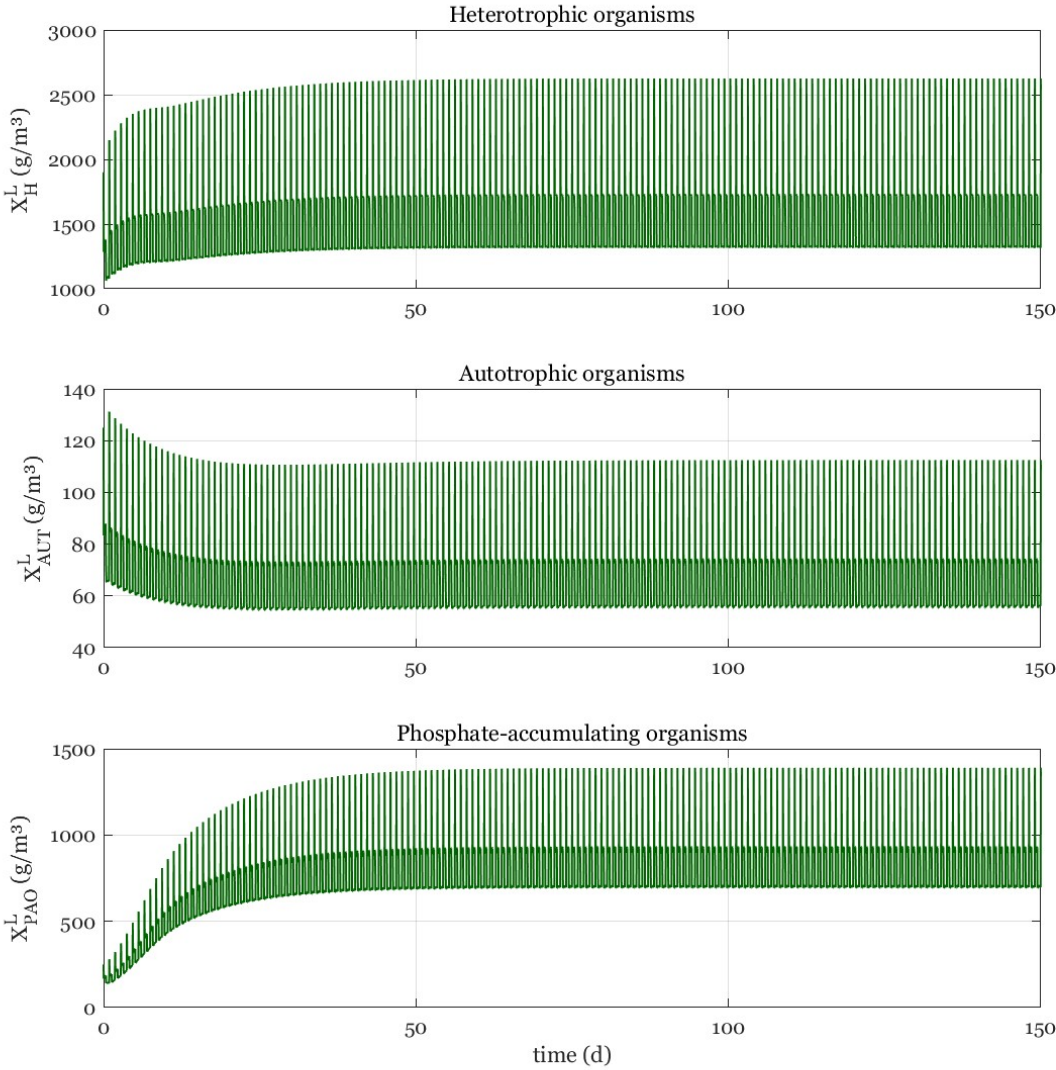


Figure C.3: Biomass concentration profiles over 150 day simulation with constant influent input at defined initial values. Steady state was reached after approximately 100 days.

C.2 Closed loop analysis

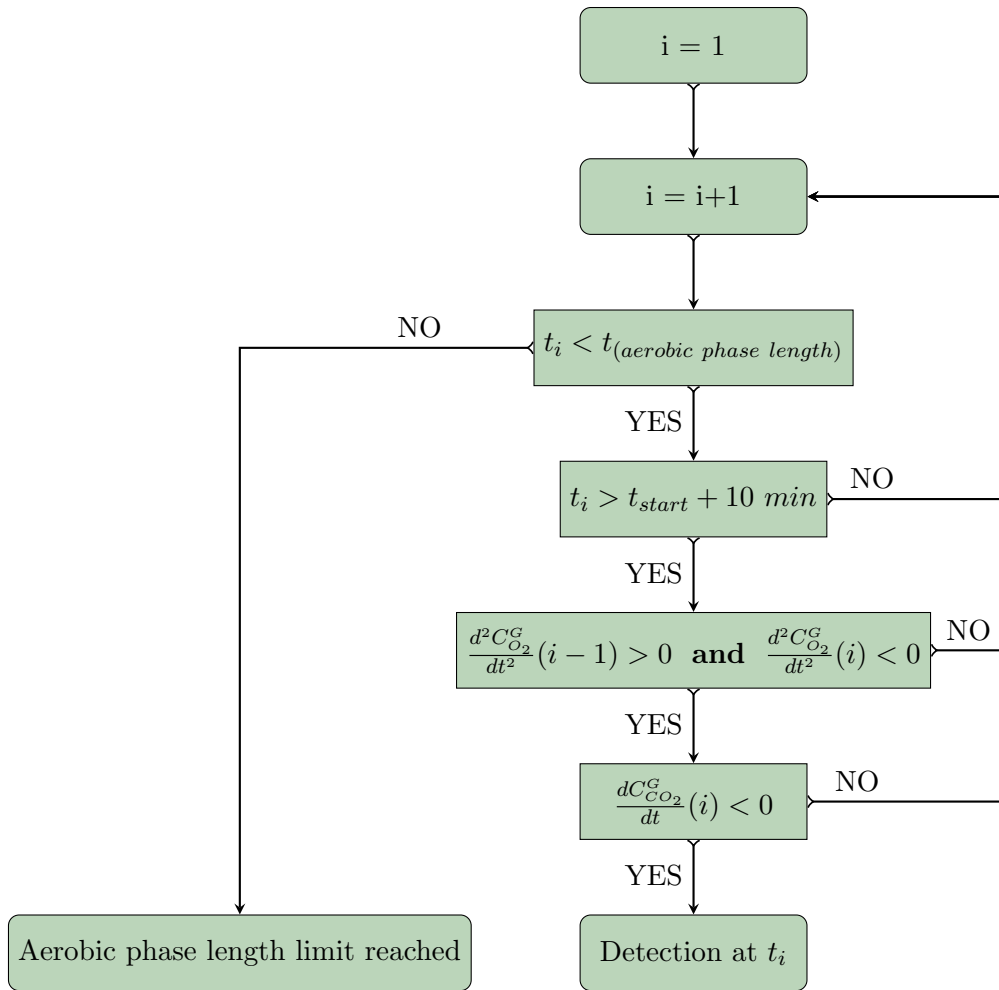


Figure C.4: Flow chart explaining how to implement the detection strategy in the model as developed by Michiels (2020). It takes into account some variability in the off-gas at the beginning of aeration (10 minutes). How to interpret this flow chart is discussed below.

1. **Initialization:** The process starts with setting i to 1.
2. **Incrementing i :** i is then incremented by 1.
3. **Time Check:** It is verified if the current time, t_i , is less than the specified length of the aerobic phase.
4. **Time Check (Cont.):** If the time condition is met, it checks if the current time, t_i , is greater than the start time plus 10 minutes to avoid the unstable behaviour of the off-gas flow at the start of aeration.
5. **Oxygen Concentration Check:** If both time conditions are met, it checks whether the second derivative of the oxygen concentration ($\frac{d^2 C_{O_2}^G}{dt^2}$) was positive at the previous time step ($i - 1$) and negative at the current time step (i). This is the mathematical translation of an inflection point in the oxygen off-gas profile.

6. **Carbon Dioxide Concentration Check:** If the oxygen condition is met, it checks if the first derivative of the carbon dioxide concentration ($\frac{dC_{CO_2}^G}{dt}$) is negative at the current time step (i). This is the mathematical translation of a decreasing carbon dioxide profile.
7. **Detection:** If all conditions are met, it proceeds to "Detection at t_i ".
8. **Looping Back:** When there is no detection, it loops back to increment the i variable and repeats the process.

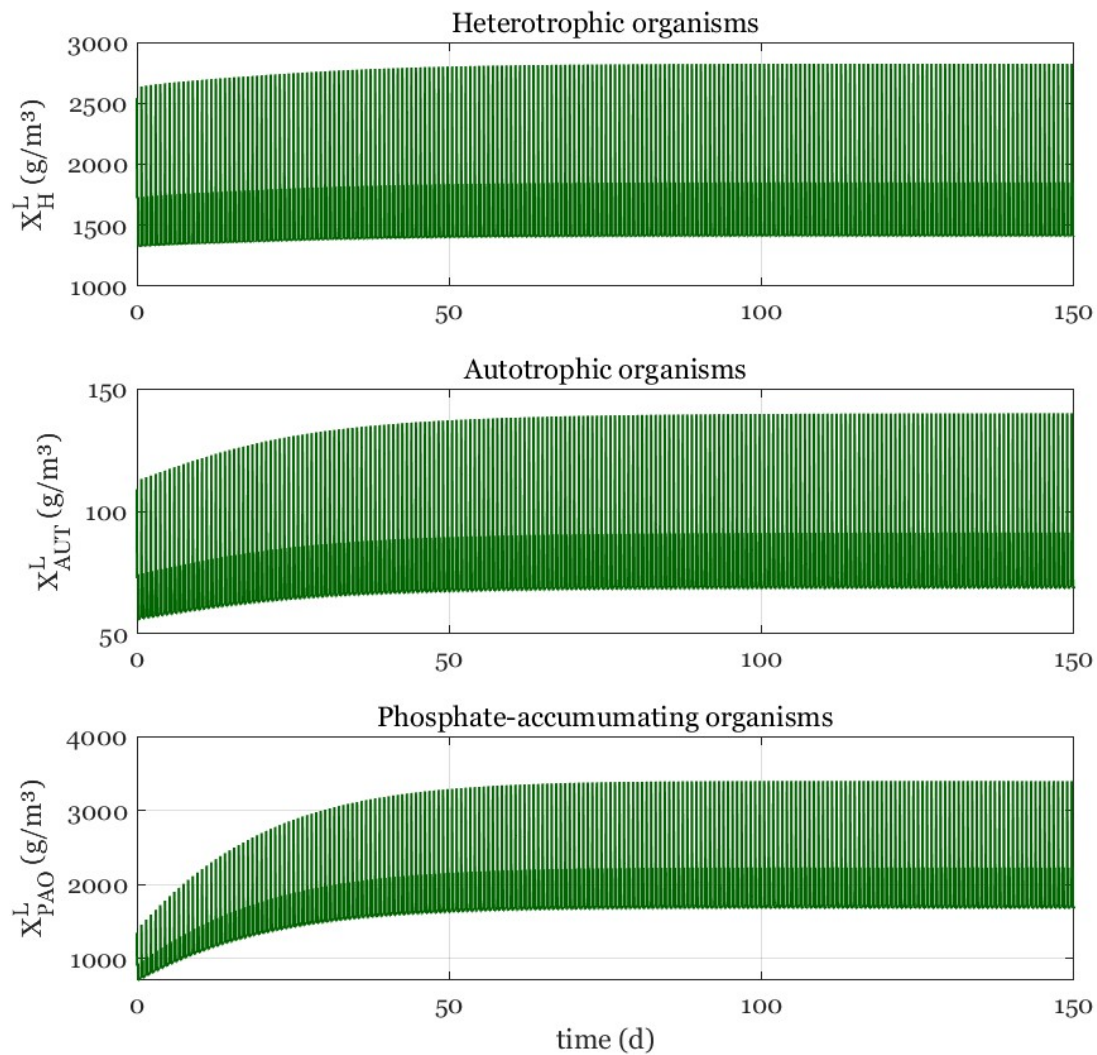


Figure C.5: Biomass concentration profiles over 150 day simulation of the closed loop model with constant influent input. Steady state was reached after approximately 100 days.

C.3 Influence of influent characteristics on detection strategy robustness

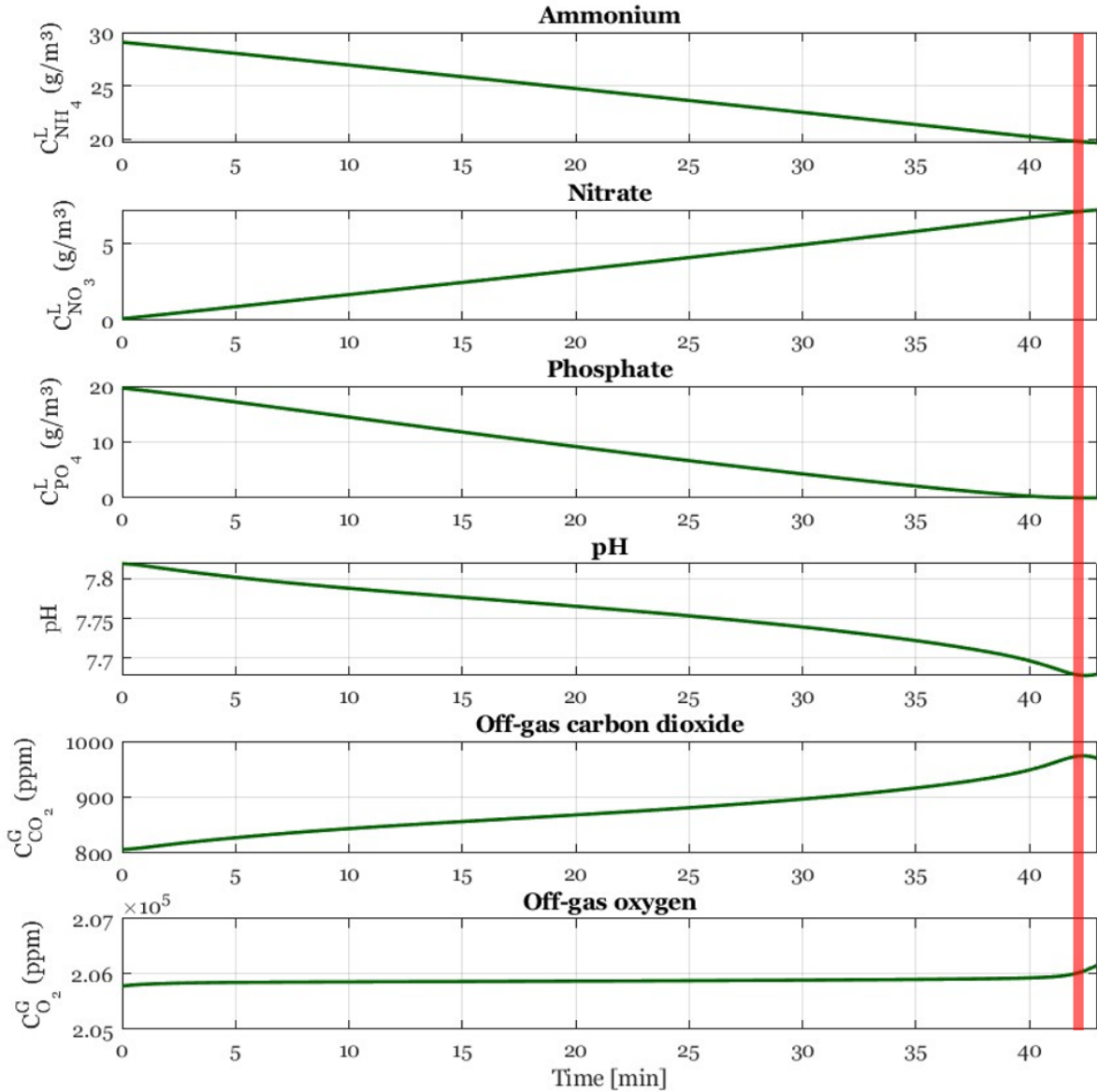


Figure C.6: Profiles of ammonium, phosphate, nitrate, pH, off-gas oxygen and off-gas carbon dioxide during the aerobic phase of the closed loop simulation with an ammonium concentration of $75 \text{ g}\cdot\text{m}^{-3}$ and a phosphate concentration of $4 \text{ g}\cdot\text{m}^{-3}$. The off-gas carbon dioxide concentration is constantly increasing which lead to a false positive detection with the implemented detection strategy.

Table C.1: Overview of the influence of different ammonium and phosphate concentrations in a constant influent for closed-loop control of the first aerobic phase AND second aerobic phase.

Number of cycles						
	N = 20 g.m ⁻³		N = 45 g.m ⁻³		N = 75 g.m ⁻³	
P = 4 g.m ⁻³	388		452		501	
P = 10 g.m ⁻³	418		494		466	
P = 15 g.m ⁻³	430		462		468	

Average aerobic length						
	N = 20 g.m ⁻³		N = 45 g.m ⁻³		N = 75 g.m ⁻³	
	Phase 1	Phase 2	Phase 1	Phase 2	Phase 1	Phase 2
P = 4 g.m ⁻³	6 h	3 h	2 h 48 min	3 h	2 h 53 min	1 h 2 min
P = 10 g.m ⁻³	3 h 15 min	3 h	2 h 16 min	1 h 53 min	3 h 41 min	1 h 36 min
P = 15 g.m ⁻³	2 h 49 min	3 h	2 h 1 min	1 h 38 min	3 h 16 min	1 h 53 min

Average final ammonium concentration						
	N = 20 g.m ⁻³		N = 45 g.m ⁻³		N = 75 g.m ⁻³	
	Phase 1	Phase 2	Phase 1	Phase 2	Phase 1	Phase 2
P = 4 g.m ⁻³	0.11 g.m ⁻³	0.26 g.m ⁻³	0.31 g.m ⁻³	0.08 g.m ⁻³	0.27 g.m ⁻³	5.54 g.m ⁻³
P = 10 g.m ⁻³	0.11 g.m ⁻³	0.13 g.m ⁻³	0.22 g.m ⁻³	0.27 g.m ⁻³	0.11 g.m ⁻³	2.81 g.m ⁻³
P = 15 g.m ⁻³	0.18 g.m ⁻³	0.11 g.m ⁻³	0.21 g.m ⁻³	0.28 g.m ⁻³	0.11 g.m ⁻³	0.25 g.m ⁻³

C.4 Detecting the end of denitrification: strategy development

Table C.2: Overview of how to interpret sign of first, second and third derivative.

	Positive (+)	Negative (-)
First derivative	Increasing function	Decreasing function
Second derivative	Function with a positive acceleration	Function with a negative acceleration
Third derivative	Function with an increasing acceleration	Function with a decreasing acceleration

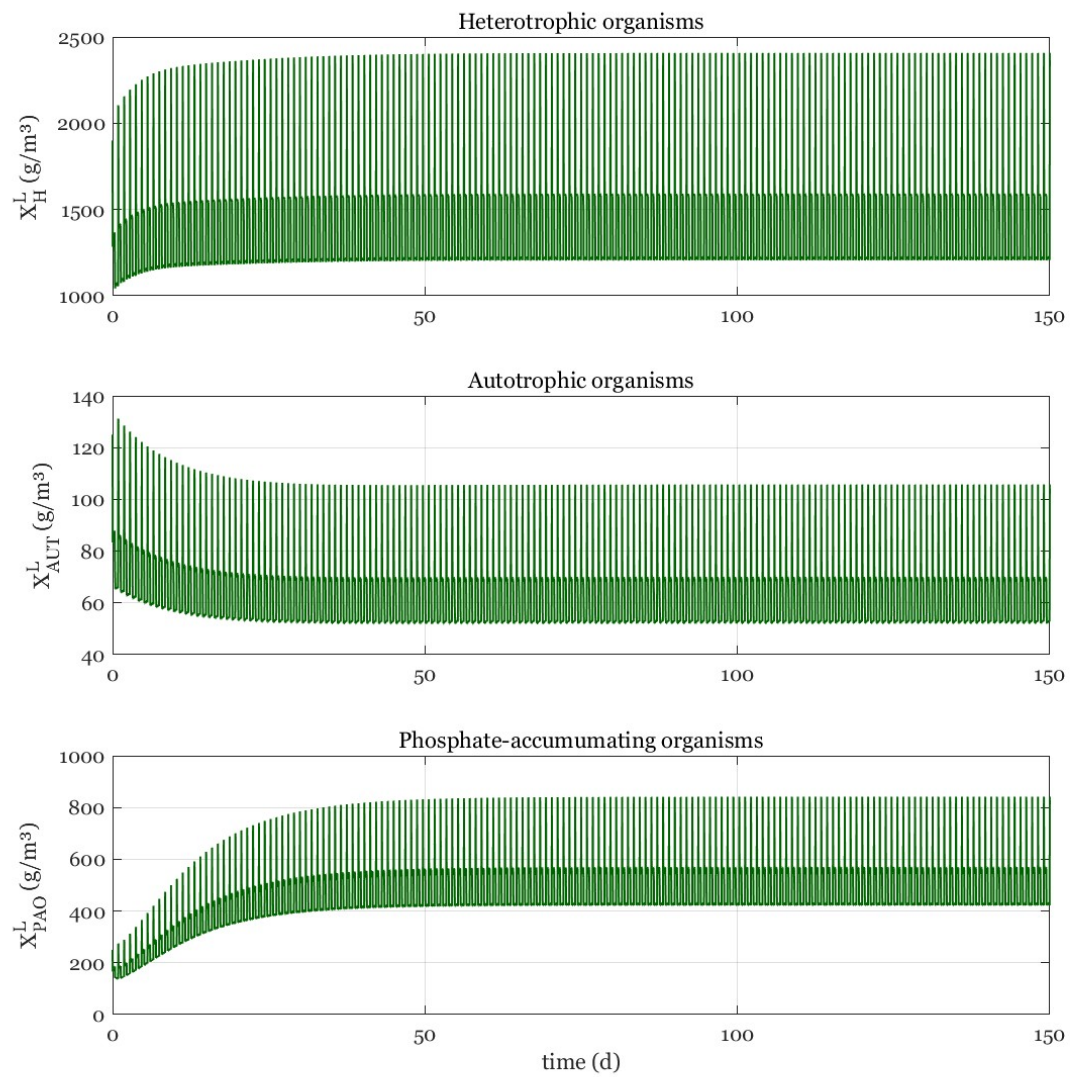


Figure C.7: Biomass concentration profiles over 150 day simulation for the open loop model to investigate the application of off-gas analysis to detect the end of denitrification.

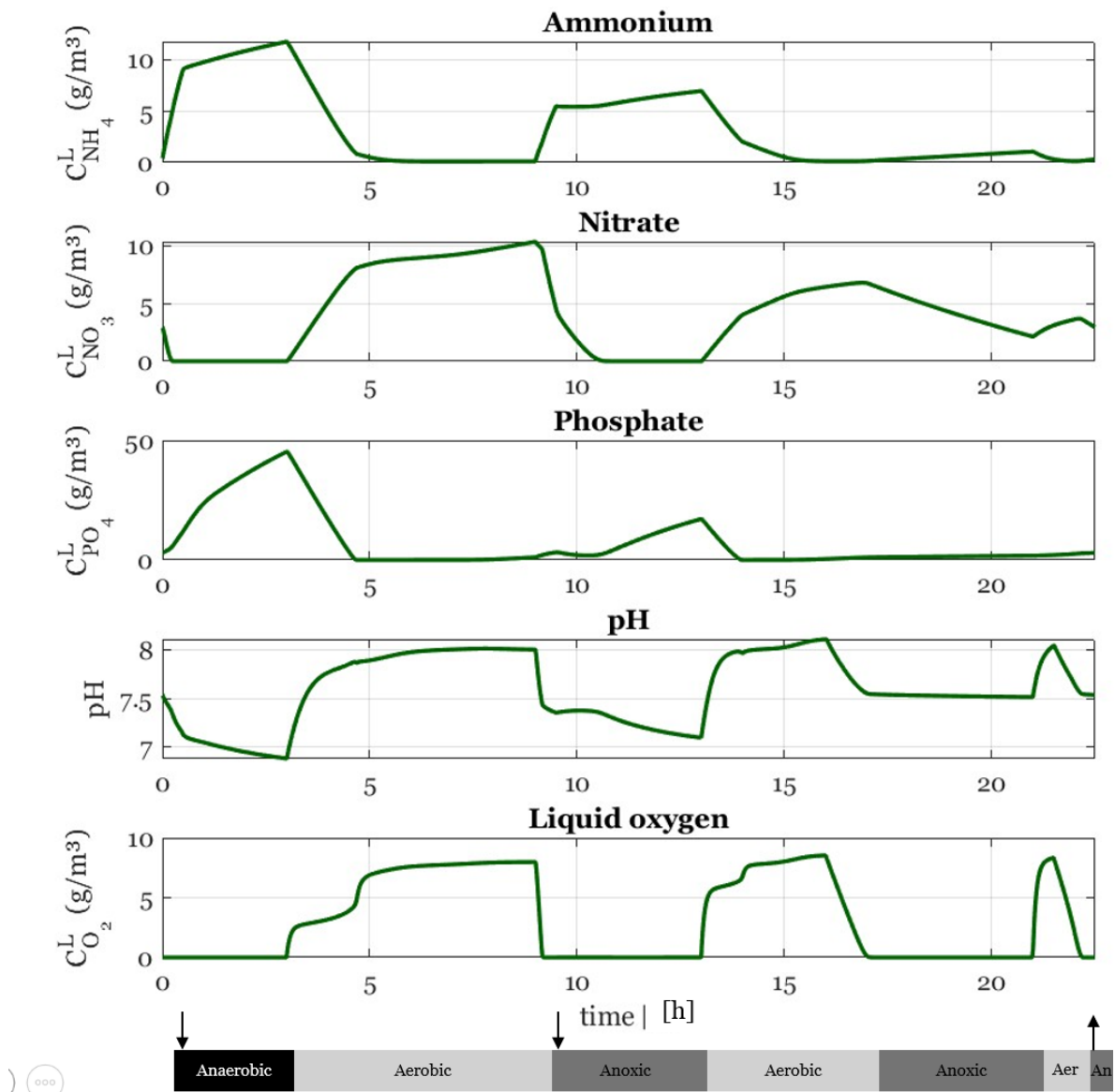


Figure C.8: Concentration profiles of ammonium, nitrate, phosphate, pH and dissolved oxygen during the last cycle of the denitrification simulation (day 150). Denitrification during the anoxic phase is still feasible.